Nano Today 69 (2026) 103033

Contents lists available at ScienceDirect

Nano Today

journal homepage: www.elsevier.com/locate/nanotoday

Review

Point-of-care testing for early diagnosis and population screening of Alzheimer's disease: Recent advances and perspectives

Md. Ahasan Ahamed [a,b,1,2], Bingyuan Guo [a,*,1,3], Muhammad Asad Ullah Khalid [a,4], Tathagata Pal [a,5], Feng Guo [a,6], Weihua Guan [a,*,7,8]

[a] Department of Intelligent Systems Engineering, Indiana University, Bloomington, IN 47408, United States
[b] Department of Electrical Engineering, Pennsylvania State University, University Park, PA, 16802, United States

ARTICLE INFO

Keywords:
Point-of-care testing
Alzheimer's disease
Early diagnosis
Population screening
AT(N) framework
Biomarkers
Aptamer
Immunoassay
Optical sensing
Electrochemical sensing
Electronic sensing
Single-molecule sensing

ABSTRACT

Alzheimer's disease (AD) is a neurodegenerative disorder that profoundly impairs quality of life and imposes substantial societal and economic burdens through rising healthcare and long-term care costs, lost productivity, and caregiver strain, while also representing a leading cause of mortality among older adults. Although disease-modifying therapies are not yet available, accumulating evidence supports identifying biological risk during the preclinical and prodromal stages to enable earlier clinical decision-making and enrich trial enrollment. Point-of-care testing (POCT) is a scalable approach to expanding access to biomarker-based detection by reducing travel and mobility barriers and enabling timely assessment in routine care settings. However, a central challenge is that early-stage AD detection at the point of care (POC) must balance analytical sensitivity and specificity with accessibility, rapid turnaround, low cost, and compatibility with routine clinical workflows. Here, we first review AD pathobiology and established diagnostic approaches within the AT(N) framework, and then highlight recent advances in POCT strategies targeting AD-related biomarkers across clinically relevant sample types. We further identify the dominant technical and translational gaps that currently limit clinical adoption. Finally, we highlight near-term opportunities in multiplexing, integrated sample-to-answer-out design, and workflow-aligned performance benchmarks to accelerate the clinical translation of POCT platforms for early AD detection.

1. Introduction

Alzheimer's disease (AD) is one of the most prevalent and clinically challenging neurodegenerative disorders worldwide [1]. In 2024, it affects nearly 7 million Americans aged 65 and older, and as populations continue to age, U.S. care costs are expected to exceed $1 trillion annually by 2050 [2]. Globally, AD cases are projected to rise to 78 million by 2030 and 153 million by 2050, placing an immense socioeconomic and healthcare burden on societies [3]. Although the precise etiology of AD remains elusive, extensive evidence implicates amyloid-β (Aβ) misfolding, tau hyperphosphorylation, and their abnormal aggregation as key drivers of neuronal injury and death, ultimately leading to irreversible cognitive decline [4]. As a progressive and currently incurable condition, existing therapeutic strategies for AD are limited to symptomatic relief and modest delays in disease progression [5]. However, increasing evidence indicates that neuronal and synaptic dysfunction during the earliest stages of AD precedes irreversible neurodegeneration and may remain partially reversible [6]. In this context, identifying individuals at risk and intervening during this critical window could significantly slow disease progression, improve patient

* Corresponding authors.
E-mail addresses: bingguo@iu.edu (B. Guo), guanw@iu.edu (W. Guan).
[1] These authors contributed equally.
[2] Orcid: 0009-0006-9962-2994.
[3] Orcid: 0009-0008-0314-0961.
[4] Orcid: 0000-0001-5926-1764.
[5] Orcid: 0000-0002-2473-6974.
[6] Orcid: 0000-0001-9103-3235.
[7] Leader contact.
[8] Orcid: 0000-0002-8435-9672.

https://doi.org/10.1016/j.nantod.2026.103033
Received 19 January 2026; Received in revised form 28 February 2026; Accepted 12 March 2026

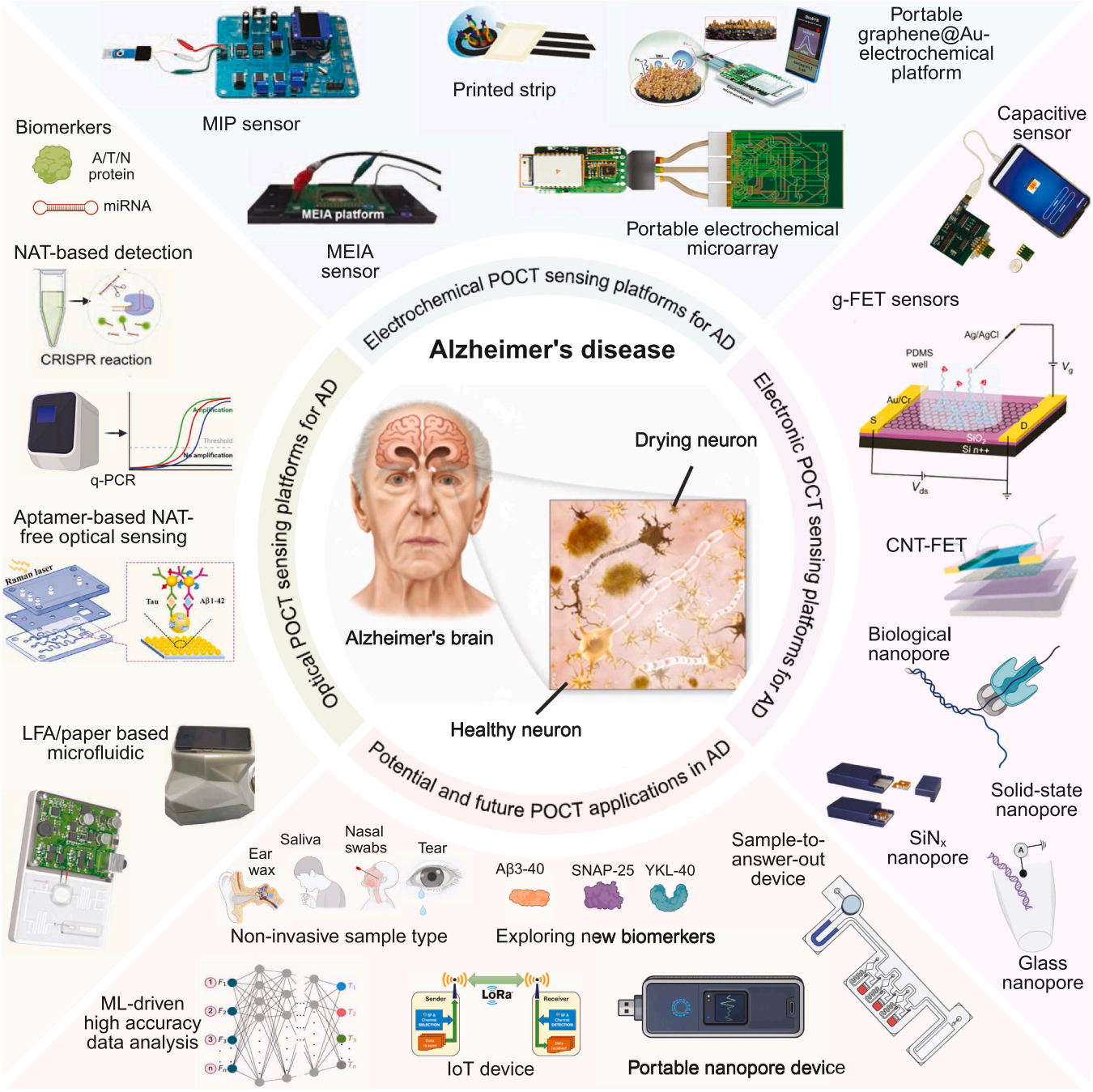

Fig. 1. Schematic overview of POCT strategies for AD, centered on key neuropathology and organized by major sensing modalities. The outer panels summarize representative platforms for optical, electrochemical, and electronic readouts, as well as potential steps to translate them into POCT platforms. (Created with BioRender.com).

outcomes, and reduce the overwhelming burden on families and healthcare systems [7]. Nevertheless, early-stage AD often remains clinically silent; by the time patients exhibit noticeable symptoms, the optimal intervention window has usually closed, rendering timely treatment exceedingly challenging [8]. To address this, developing more accessible and scalable tools for early AD diagnosis and screening has become a central goal in both clinical practice and research.

Currently, numerous early diagnostic methods for AD have been developed, mainly including genetic testing [9], cognitive and neuropsychological assessment [10], neuroimaging techniques [11], and body fluid biomarker analysis [12]. Genetic testing is particularly effective for detecting familial AD cases, but it provides limited predictive value for sporadic AD, which constitutes the vast majority of cases. Cognitive assessments are non-invasive and cost-effective, yet they typically lack sufficient sensitivity to detect impairments at the preclinical stage. Neuroimaging techniques, including magnetic resonance imaging (MRI) and positron emission tomography (PET), provide high-resolution insights into structural and functional brain changes, though they are often expensive and available only at specialized medical centers. Body fluid biomarker analysis, such as the measurement of Aβ and tau proteins in cerebrospinal fluid (CSF), can provide direct evidence of pathological changes but typically requires lumbar puncture (spinal tap). Collectively, these approaches provide complementary information, but their use for broad screening remains limited by cost, accessibility,

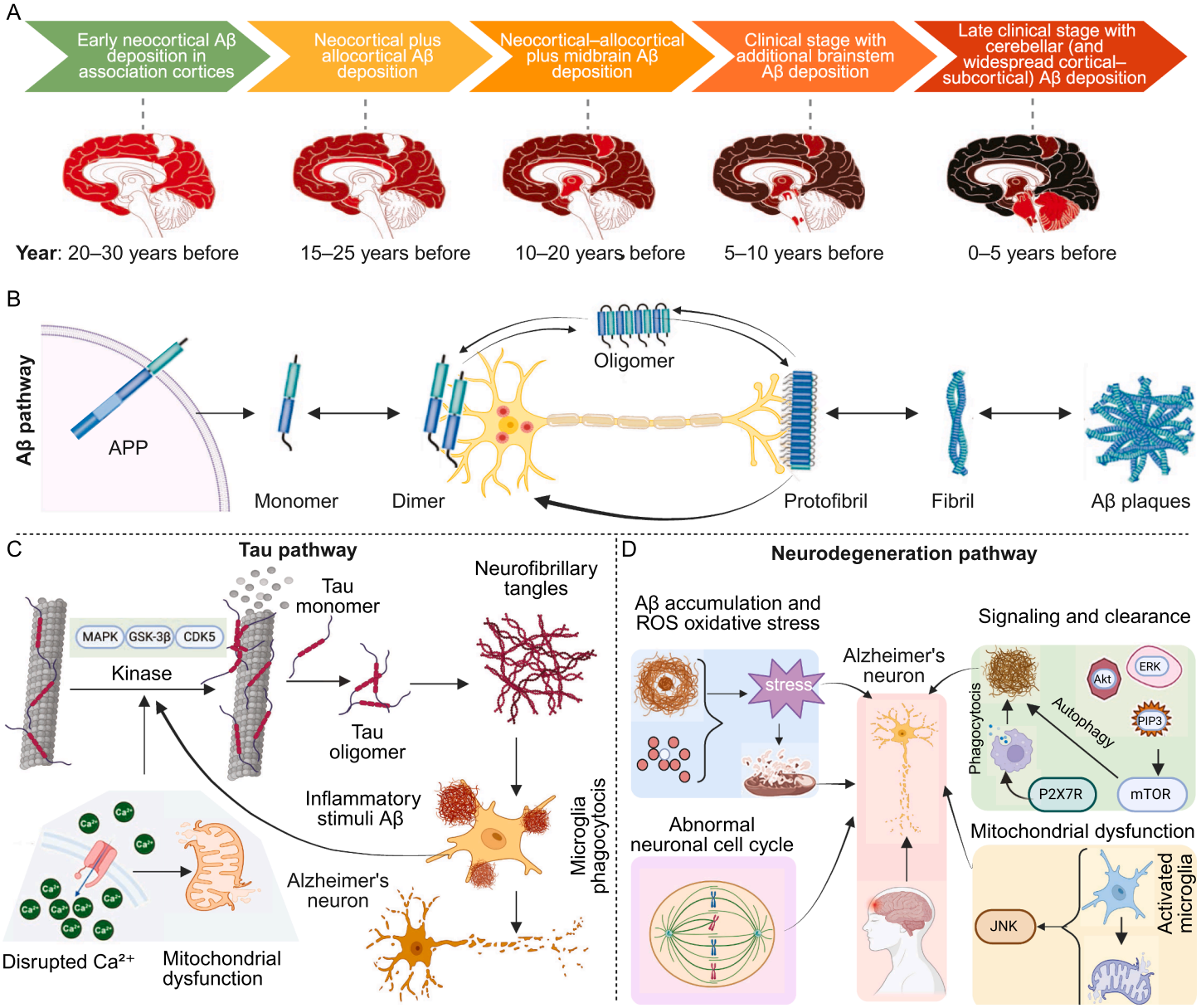

Fig. 2. AD progression timeline and pathway. A Spatiotemporal timeline of Aβ deposition. Traditional neuropathological phases of Aβ spread, from early neocortical deposition in association cortices 20–30 years before dementia, through allocortical and midbrain involvement, to brainstem and finally cerebellar and widespread cortical-subcortical deposition within 0–5 years of clinical onset. Adapted from Ref. [14] under the Creative Commons CC BY 4.0 license. **B** Aβ pathway. Amyloid precursor protein is cleaved to generate Aβ monomers, which assemble into dimers, soluble oligomers that interact with synapses, then protofibrils, fibrils, and finally extracellular Aβ plaques. Adapted from Ref. [14] under the Creative Commons CC BY 4.0 license. **C** Tau pathway. Stress-activated kinases such as MAPK, GSK-3β, and CDK5, triggered by mitochondrial and calcium-related stress, induce tau hyperphosphorylation, reduce its microtubule binding, and promote aggregation into neurofibrillary tangles in vulnerable neurons. Adapted from Ref. [30,31] under the Creative Commons CC BY 4.0 license. **D** Neurodegeneration pathway. Aβ-induced oxidative stress, aberrant neuronal cell-cycle re-entry, and dysregulated autophagy and phagocytic pathways, mediated through mTOR signaling, P2X7 receptor activation, and JNK-associated mitochondrial dysfunction, converge to drive neuronal injury and death in AD. Adapted from Ref. [39] under the Creative Commons CC BY 4.0 license. (Created with BioRender.com).

procedural complexity, and, in some settings, suboptimal accuracy. Point-of-care testing (POCT) technologies have recently gained attention as a promising approach to addressing this gap [13]. By enabling decentralized, timely, and accessible biomarker assessment without reliance on specialized laboratory infrastructure, POCT offers a feasible and scalable solution to expand diagnostic reach and support large-scale screening efforts. Therefore, there is an urgent need for diagnostic tools that are accurate, rapid, cost-effective, scalable, and user-friendly, as well as for portable or home-testing devices that enable early AD detection and population-level screening, including among older adults and among middle-aged adults over 30 years old.

In this review, we outline the current understanding of AD pathogenesis and progression and summarize existing clinical approaches for early AD detection, highlighting their respective strengths and limitations. The core focus of this review is to systematically examine recent advances in POCT technologies for early diagnosis and large-scale population screening (Fig. 1). We categorize and compare representative POCT platforms with respect to their sensing mechanisms, analytical performance, and translational potential. Finally, we explore future directions in POCT development and present our perspectives on potential strategies to overcome existing barriers and enhance its clinical applicability for early AD diagnosis. The development of POCT technologies for AD has the potential to make a meaningful clinical impact on the aging population and to benefit public health and healthcare systems.

2. Current understanding of AD pathogenesis, disease progression, and conventional clinical diagnostic approaches

AD is characterized by complex and multifactorial pathological processes, and effective diagnosis relies on a clear understanding of the mechanisms underlying disease initiation and progression. Accordingly, this section provides an overview of current knowledge of AD pathogenesis and disease progression, reviews established clinical diagnostic approaches and their limitations, and sets the stage for the discussion of POCT as a promising strategy for early AD diagnosis.

2.1. Current understanding of AD pathogenesis and disease progression

Dementia is a central geriatric syndrome, with AD accounting for more than half of all cases. As illustrated in Fig. 2**A**, AD is a progressive neurodegenerative disorder characterized by a prolonged preclinical phase that can last for 10–15 years or longer [14]. During this stage, individuals typically exhibit no overt cognitive symptoms and maintain normal daily functioning, despite the silent emergence of pathological alterations in key biomarkers, including Aβ and phosphorylated tau (p-tau) [7,15]. Owing to the absence of apparent clinical manifestations, older adults rarely undergo voluntary screening during the preclinical stage, and only a limited number of countries currently offer early AD screening as a public health service, mainly due to practical and economic constraints [16]. As a result, many individuals miss the critical window for timely intervention, thereby diminishing the potential effectiveness of emerging therapies and contributing to escalating medical, social, and economic burdens worldwide. These challenges underscore the urgent need for reliable and accessible strategies for early AD diagnosis and population-level screening. Molecular diagnostics represent a particularly promising approach for this purpose [17]. However, AD pathophysiology is highly complex, and its biomarkers are dynamically interrelated. Their expression patterns and quantitative changes convey distinct biological and clinical meanings across the disease continuum and are commonly interpreted within the AT(N) framework [18,19]. In this subsection, we review the molecular pathogenesis and progression of AD to clarify the relevance and diagnostic value of AD biomarkers in molecular-based detection strategies.

Aβ-centered pathogenic pathway (A). Amyloid precursor protein (APP) is a type I transmembrane protein physiologically expressed on neuronal membranes. Upon sequential cleavage by α-secretase and γ-secretase, APP is processed through the non-amyloidogenic pathway, generating products with important neurotrophic and signaling functions. However, under the influence of genetic factors, aging, and other risk modifiers, β-site-dependent processing is enhanced. Together with subsequent γ-secretase cleavage, this shift increases total Aβ production, while age- and risk-related impairments in clearance preferentially reduce the removal of Aβ42. The high hydrophobicity of Aβ42 promotes its self-assembly into soluble oligomers, followed by the formation of fibrils and extracellular plaques in the brain. As shown in Fig. 2**B**, these molecular events are collectively referred to as the amyloidogenic pathway [4,14]. Accumulating evidence indicates that Aβ42 oligomers represent the most neurotoxic Aβ species [20]. By engaging neuronal surface receptors, these oligomers bias synaptic plasticity toward weakening, impairing learning and memory processes. The accumulation of Aβ42 oligomers also activates microglia and astrocytes. Although these glial cells initially contribute to oligomer clearance, persistent exposure drives them toward maladaptive activation states, thereby amplifying complement-mediated synapse loss and neurotoxicity [21]. In addition, Aβ42 oligomers disrupt neuronal Ca^{2+} homeostasis, inducing oxidative stress and triggering a cascade of pathological events, including mitochondrial dysfunction, lipid peroxidation, and synaptic loss. Overall, this amyloid-driven phase is widely regarded as an upstream trigger for multiple downstream pathological cascades [22,23]. At the biomarker level, this stage is characterized by a decreased Aβ42/Aβ40 ratio in CSF or plasma, together with amyloid PET positivity.

Tau-centered pathogenic pathway (T). Tau is a microtubule-associated protein that stabilizes the neuronal cytoskeleton and supports axonal transport [24]. Soluble Aβ assemblies, including oligomers and protofibrils, engage synaptic receptor complexes and aberrantly activate pathogenic kinases, notably GSK-3β and Cdk5/p25, thereby driving tau phosphorylation at key epitopes, including pThr181, pThr217, and pThr231 [25]. As shown in Fig. 2**C**, pro-inflammatory cytokines, reactive oxygen species, and other mediators released by activated microglia and astrocytes further enhance kinase activity while suppressing phosphatase function, thereby promoting tau hyperphosphorylation. Phosphorylated tau (p-tau) subsequently dissociates from microtubules, leading to microtubule destabilization, impaired axonal transport, and inefficient delivery of organelles and cargo [26,27]. Like Aβ, p-tau readily assembles into soluble oligomers, which subsequently elongate into paired helical and straight filaments, ultimately forming neurofibrillary tangles (NFTs) [28]. While NFTs burden strongly correlates with neuronal dysfunction and loss, soluble tau oligomers are widely considered the most synaptotoxic species [29]. Fig. 2**C** also illustrates that these oligomers bind neuronal surface receptors and cofactors, including the low-density lipoprotein receptor-related protein 1 (LRP1) and heparan sulfate proteoglycans, thereby triggering deleterious signaling and homeostatic disruption, such as enhanced Fyn kinase-N-methyl-D-aspartate receptor (Fyn-NMDAR) activity and Ca^{2+} dysregulation [30,31]. Importantly, p-tau oligomers can exhibit prion-like behavior, functioning as seeds that template the misfolding and aberrant modification of endogenous tau in recipient cells [32]. They can be released via exosomes and activity-dependent secretion and taken up by neighboring neurons, enabling transcellular propagation along connected neural networks consistent with Braak staging. Overall, this tau-driven phase is closely associated with clinical disease progression. At the biomarker level, this stage is characterized by elevated levels of p-tau species in CSF or plasma, notably p-tau181, p-tau217, and p-tau231, as well as tau PET positivity.

Neurodegeneration-centered pathogenic pathway (N). In the central nervous system, two major types of glial cells, microglia and astrocytes, play essential roles in immune surveillance and inflammatory responses in the brain [33]. At the early stages of disease, pattern-recognition receptors on the microglial surface detect Aβ

oligomers and initiate phagocytic clearance of toxic species. During this phase, microglia release anti-inflammatory mediators that support neuronal survival, while astrocytes contribute to Aβ degradation through apolipoprotein E (ApoE)-dependent pathways [34]. However, with prolonged exposure to Aβ and p-tau species, both microglia and astrocytes transition from protective to maladaptive activation states [35]. Activated microglia chronically release pro-inflammatory mediators that induce oxidative stress, synaptic injury, and neuronal death, whereas astrocytes adopt a reactive phenotype characterized by the secretion of inflammatory molecules, excessive glutamate release, and disruption of blood-brain barrier integrity. These processes act in concert to form a self-reinforcing pathological network that accelerates synaptic dysfunction and loss [36]. Furthermore, multiple neurotransmitter systems, including cholinergic, glutamatergic, serotonergic, and noradrenergic pathways, are highly vulnerable to these insults. Because these neurotransmitters play critical roles in cognition, memory, and emotional regulation, their dysfunction directly contributes to the neurological and behavioral symptoms of AD [37]. Together, these interconnected mechanisms define the neurodegeneration-centered pathogenic pathway of AD, linking glial dysfunction, synaptic loss, and neurotransmitter imbalance to progressive cognitive impairment (Fig. 2**D**) [38].

Given the complexity of AD pathogenesis and progression, the following provides a concise integrative overview. With advancing age and increasing genetic susceptibility, the delicate balance between Aβ production and clearance becomes disrupted, leading to the progressive accumulation of Aβ42 monomers into soluble oligomers, protofibrils, and ultimately insoluble plaques. This aggregation process promotes tau hyperphosphorylation and the formation of p-tau oligomers with prion-like properties, thereby accelerating pathological spread across vulnerable brain regions. Although activated microglia and astrocytes initially attempt to eliminate these toxic aggregates, prolonged exposure drives their transition toward maladaptive inflammatory states, resulting in chronic neuroinflammation that further exacerbates disease progression. Collectively, these interconnected pathological events culminate in cytoskeletal destabilization, synaptic dysfunction, widespread neuronal loss, and failure of key neurotransmitter systems. At the macroscopic level, these changes manifest as progressive atrophy of the cerebral cortex and hippocampus, which clinically presents as memory impairment and global cognitive decline. Additional mechanistic details are available in the literature [14,18,39,40–42].

2.2. Conventional clinical approaches for early AD diagnosis and their limitations

Current clinical approaches for early AD diagnosis are commonly grouped into four categories: genetic testing, cognitive and neuropsychological assessment, neuroimaging techniques, and biofluid biomarker analysis. Each modality has distinct strengths and a well-established role in clinical practice. However, limitations in sensitivity at preclinical and prodromal stages, specificity for Alzheimer's pathology, cost and invasiveness, accessibility, and the lack of harmonized standards continue to restrict broad adoption and population-level implementation [43]. This subsection provides an overview of these conventional approaches and summarizes their key strengths and limitations for early AD diagnosis.

Genetic testing for early risk assessment of AD. Familial early-onset AD is primarily driven by pathogenic mutations in APP, PSEN1, PSEN2, and several other genes [44]. Using modern genetic testing technologies, including DNA sequencing, microarray-based assays, and allele-specific PCR, a single blood sample can be used to assess an individual's lifelong genetic risk in a convenient and informative manner. Although this approach is highly effective for identifying familial forms of AD, these cases account for only a small proportion of the overall disease burden. In contrast, for sporadic AD, which represents the vast majority of cases, the predictive power of genetic testing remains limited [1]. Nevertheless, ApoE genotyping provides valuable information for population-level risk stratification. When integrated with neuroimaging or biofluid biomarker data, ApoE genotyping can support more personalized follow-up strategies and risk-informed clinical management.

Cognitive and neuropsychological assessment for early detection of AD. Cognitive and neuropsychological assessments employ standardized screening instruments such as the Mini-Mental State Examination (MMSE), the Montreal Cognitive Assessment (MoCA), and the Clinical Dementia Rating Scale-Sum of Boxes (CDR-SB), global cognitive scales such as the Alzheimer's Disease Assessment Scale-Cognitive Subscale (ADAS-Cog), and structured test batteries including the Repeatable Battery for the Assessment of Neuropsychological Status (RBANS) to quantify core cognitive domains, including episodic memory, language, attention, processing speed, executive function, and visuospatial ability [45]. Changes detected on these instruments document cognitive impairment and inform clinical triage, disease staging, and longitudinal follow-up. The principal advantages of these assessments include low cost, scalability, suitability for repeated administration, and rapid turnaround. These attributes make them well-suited for initial screening in primary care and community-based settings. With the development of digital platforms, remote administration and, in selected contexts, unsupervised home-based testing have become feasible for validated instruments [46]. However, important limitations remain. Performance is influenced by education, language, and cultural background, mood, and comorbid conditions, while reliability depends on examiner training and standardization [47]. Sensitivity is limited at the preclinical stage because neuropathological changes often accumulate for years before symptoms become detectable on cognitive assessments, potentially missing a critical window for early intervention. Practice effects can further complicate longitudinal interpretation unless alternate test forms and appropriate assessment intervals are used [48]. Consequently, cognitive and neuropsychological assessment results should be interpreted alongside neuroimaging or biofluid biomarkers when early AD diagnosis is required.

Neuroimaging techniques for early AD diagnosis. Neuroimaging approaches for AD primarily include PET and MRI. Within the AT(N) framework, neuroimaging is mainly used in etiologic confirmation and biological subtyping. Aβ PET employs radiotracers that bind fibrillar cortical Aβ plaques to quantify amyloid burden, enabling detection of amyloid deposition years before the onset of clinical symptoms [49]. Tau PET visualizes aggregated tau with regionally specific patterns that track Braak staging, thereby improving etiologic certainty and phenotypic staging [50]. FDG-PET measures regional cerebral glucose metabolism as a surrogate for synaptic and neuronal activity; characteristic hypometabolism in the temporoparietal association cortex and posterior cingulate supports the presence of neurodegeneration, although FDG-PET is less pathology-specific than Aβ or tau PET. MRI provides complementary structural, diffusion, perfusion, and functional information [51]. MRI is sensitive to hippocampal and medial temporal lobe atrophy, white-matter abnormalities that often reflect vascular comorbidity, microstructural injury detected by diffusion imaging, and reduced default-mode network connectivity on resting-state functional MRI, thereby indexing neurodegeneration and large-scale network involvement [52]. Because MRI does not directly image Aβ or tau pathology, its specificity at the earliest preclinical stages is limited; therefore, combining MRI with Aβ or tau PET is recommended when etiologic confirmation and biological subtyping are required [53].

Unlike PET, MRI does not involve exposure to ionizing radiation. In practice, access to both imaging modalities is constrained by high capital costs, limited scanner availability, and the need for specialized infrastructure; PET additionally depends on a reliable radiopharmaceutical supply chain. Together, these factors increase time and financial burdens for patients and limit access, particularly in resource-limited settings.

Biofluid biomarker analysis for early diagnosis of AD. Beyond neuroimaging, biofluid biomarkers provide a practical and scalable approach to the biological confirmation of AD. Among available biofluids, CSF remains the reference matrix because it exchanges with brain interstitial fluid and therefore most directly reflects cerebral pathology; it also contains higher concentrations of AD biomarkers than blood, saliva, or urine and is consequently the most widely used specimen in clinical diagnostics [54]. Using high-specificity capture and detection antibodies, CSF biomarkers such as the Aβ42/Aβ40 ratio and p-tau181/217/231 can be quantified with high analytical accuracy using chemiluminescent or electrochemiluminescent (ECL) immunoassay platforms. These results can be mapped to the AT(N) framework, thereby converting symptom-based clinical suspicion into biologically grounded diagnosis and stratification, improving concordance with PET imaging, and informing differential diagnosis, longitudinal follow-up, and treatment decisions [19]. The principal limitation is that lumbar puncture is invasive; although blood and other peripheral matrices are more acceptable to patients, their substantially lower analyte abundances impose stricter requirements on assay sensitivity, precision, and standardization.

2.3. Unmet clinical needs and motivations for POCT in early AD diagnosis

Because the preclinical phase of AD can last 10–20 years and is typically asymptomatic, individuals are often unaware of their potential risk while the underlying pathology continues to progress. By the time patients reach the stage of mild cognitive impairment (MCI), the optimal window for timely management and intervention has often already narrowed or closed [8]. The primary cause of this dilemma is the lack of early diagnostic tools that are simultaneously accurate, accessible, and affordable for use in both primary care settings and by individual users. In some Western countries, reports indicate that individuals may wait several years before receiving appropriate medical assessment and treatment [55]. Therefore, there is an urgent need for early diagnostic approaches that can meet the growing clinical, healthcare, and management demands associated with AD.

In this context, POCT represents one of the most promising strategies to address these unmet needs. With continued advances in highly sensitive, selective, and accurate biomarker detection methods, these assays and reagents can now be seamlessly integrated into compact POCT devices. Such devices are not only portable and user-friendly but are increasingly strengthened by advances in artificial intelligence (AI) and cloud-based data processing. As a result, individuals can collect a sample, load it onto the device, and rapidly obtain reliable, actionable health information [56]. This operating paradigm holds strong potential to address the urgent need for early diagnosis of AD. With the aid of at-home blood collection kits, individuals can self-collect blood samples that can subsequently be analyzed by POCT devices to generate reliable reports and interpretations of AD-related biomarker levels. Such an approach enables regular monitoring with minimal logistical and accessibility barriers. Once alerted to potential risks, individuals can seek timely clinical evaluation and intervention, thereby maximizing the opportunity to act within the therapeutic window. Together, these considerations position POCT as a practical solution to the diagnostic challenges of AD and underscore its growing potential to enable early detection and longitudinal disease management, thereby addressing both the unmet clinical needs and the motivations driving its development.

3. Emerging POCT tools for early detection of AD

3.1. Logical framework of POCT

POCT refers to diagnostic testing performed near the patient across diverse settings, including clinical environments, community sites, pharmacies, and home use. Such testing typically relies on portable, affordable, and user-friendly devices that provide results in a sample-to-answer-out format [57]. Building on the World Health Organization's original ASSURED criteria, the REASSURED framework (R: Real-time connectivity; E: Ease of specimen collection; A: Affordability; S: Sensitivity; S: Specificity; U: User-friendliness; R: Rapidity and Robustness; E: Equipment-free operation; D: Deliverability) defines the essential qualities of effective POCT [13]. The development of a new POCT technology hinges on three core components: analyte recognition (defining the target), detection methodology, and signal transduction with readout (device hardware). Importantly, "POCT readiness" is not determined by analytical performance alone; it is a deployment-driven attribute governed by workflow simplicity (number of user steps), operator skill requirements, instrument dependence, and the feasibility of performing the test across near-patient settings, including clinical environments, primary care clinics, community screening sites, pharmacies, and home use. Here, "POCT readiness" refers specifically to deployment feasibility across these near-patient settings rather than to analytical performance alone.

In target recognition, multiplex assays performed in a single-pot format are preferred over individual tests, although the choice of detection and signal-transduction methods can constrain the number of targets that can be assayed simultaneously. Targets for multiplex panels are chosen based on factors such as co-infection potential, overlapping clinical symptoms, and the need for treatment strategies in regions where multiple pathogens circulate. In AD, combining protein biomarkers such as Aβ40, Aβ42, GFAP, NfL, p-tau231, p-tau181, and total tau within a single sample can improve diagnostic confidence and risk prediction by capturing complementary features across the AT(N) framework. Multiplex panels can also be broadened to support differential diagnosis across neurodegenerative disorders, enabling parallel assessment of AD, Parkinson's disease, frontotemporal dementia, Lewy body dementia, and related conditions. Another important aspect is sample preparation and processing in the pre-analytical or assay-execution stage, where separation, enrichment, and controlled reactions mitigate matrix effects, concentrate targets, and present them in a state that enables specific recognition. This is very important because the complex matrix background of practical samples will severely affect the detection performance and must be taken seriously. In near-patient settings, particularly in home and community deployment, the pre-analytical burden is often the dominant barrier. Centrifugation, multi-step incubation/washing steps should be automated, including lyophilized reagents, which are essential for practical POCT deployment.

After clearly defining the targets, detection methods shall be devised based on the properties of the chosen analytes, which function as the link between targets and detection hardware (signal transduction) [58]. As a systematic engineering issue, the detection method requires careful consideration of various factors to obtain an optimal solution. For example, both isothermal amplification and ultrafast-PCR are potential POCT candidates for nucleic acids test (NAT). However, an isothermal assay is easier to translate into a truly portable POCT platform than ultrafast-PCR, owing to the need for bulk temperature control [59]. POCT detection methods can usually be classified as reagent-based or reagent-free. Reagent-based POCT relies on a supplied kit or cartridge containing recognition molecules that bind or react with targets in the sample via antigen-antibody binding, aptamer-target recognition, receptor-ligand binding, primer-directed nucleotide pairing with enzymes, or enzyme-substrate reactions [60]. These interactions produce a physical signal that the detector measures to generate the diagnostic result. In reagent-based POCT, users add only the sample while the strip

Table 1
POCT platforms for AD detection.

Detection Type	Technology/ Method	Target Biomarker	Type of Sample	Performance Metrics	POCT Friendly	Ref
Electrochemical sensing systems: Immunosensors and aptamer sensors	Portable electrochemical microarray workstation (app-linked)	Aβ40, Aβ42, tau, p-tau181	Serum (10 μL)	T: <1 h; LOD: Aβ42: 0.089 pg mL^{-1}; tau: 0.176 pg mL^{-1}; DR: 0.1-1000 pg mL^{-1}	Yes	[62]
Optical sensing systems: Aptamer-based NAT-free optical sensing	Ultrasound-enhanced AuNP colorimetric LFA	Tau	Human serum, plasma	T: ~21 min (10 min ultrasound pre-treatment + 1 min enrichment + 10 min LFA); LOD: 10.30 pg mL^{-1}; DR: NR	Yes	[66]
Optical sensing systems: Lateral flow and paper-based optical immunoassays	Paper-based LFA	Aβ42 monomer and oligomers	Blood (or CSF)	T: <30 min; LOD: 154 pg mL^{-1}; DR: 625 ng mL^{-1}-154 pg mL^{-1}	Yes	[67]
Optical sensing systems: Aptamer-based NAT-free optical sensing	Shape-coded AuNP LSPR assay	Aβ40, Aβ42, tau protein	Blood (human plasma spiked)	T: ~1 h; LOD: Aβ40: 34.9 fM; Aβ42: 26.6 fM; tau: 23.6 fM; DR: NR	No	[70]
Electrochemical sensing systems: Immunosensors and aptamer sensors	AuNPs-printed electrochemical strip biosensor	miRNA-29a	Buffer/ serum	T: ~3 h; LOD: 0.15 nM (buffer); 0.2 nM (serum); DR: 0.01-500 nM	Yes	[75]
Electrochemical sensing systems: Immunosensors and aptamer sensors	Conductive silk-fibroin composite electrochemical immunosensor array	Aβ40, Aβ42	Serum from triple-transgenic AD mice (3×Tg-AD)	T: NR; LOD: Aβ40: 6.63 pg mL^{-1}; Aβ42: 3.74 pg mL^{-1}; DR: Aβ40: 9-2250 pg mL^{-1}; Aβ42: 22.5-1125 pg mL^{-1}	Yes	[76]
Electrochemical sensing systems: Immunosensors and aptamer sensors	Portable electrochemical aptasensing platform using AuNP-decorated vertical graphene paper electrode with DPV readout	Tau	Human serum (spiked PBS and clinical samples)	T: NR; LOD: 0.034 pg mL^{-1}; DR: 0.1-1 ng mL^{-1}	Yes	[77]
Optical sensing systems: NA-based methods	Hydrogel micropost-based multiplex qPCR	hsa-miR-342-3p, hsa-miR-18b-5p, hsa-miR-30e-5p, hsa-miR-143-3p, hsa-miR-424-5p	Spiked human plasma	T: ≈ 20 min; LOD: 10 ng mL^{-1}; DR: ~4 orders of magnitude	Yes	[87]
Optical sensing systems: NA-based methods	Immunomagnetic exosomal qPCR (iMER)	Aβ40, Aβ42, p-tau396, p-tau404, p-tau181	Plasma exosomes	T: NR; LOD: 10 fg mL^{-1}; DR: NR	Partial	[88]
Optical sensing systems: NA-based methods	NGS miRNA profiling with mL classification	↑brain-miR-112, brain-miR-161, let-7d-3p, miR-5010-3p, miR-26a-5p, miR-1285-5p, miR-151a-3p; ↓miR-103a-3p, miR-107, miR-532-5p, miR-26b-5p, let-7 f-5p	Whole blood	T: NR; LOD: NR; DR: NR (only classification accuracy reported, analytical performance NR)	No	[89]
Optical sensing systems: NA-based methods	RCA-APE1 fluorescence assay	miR-206	Serum	T: ≈1 h; LOD: 1.82 fM; DR: 10 fM-1 nM	Yes	[95]
Optical sensing systems: NA-based methods	CRISPR-Cas12a dual-fluorescence assay	ApoE4 SNP fragments (codons 112/158)	Serum	T: <1 h; LOD: codon 112: 22.4 pM; codon 158: 32.5 pM; DR: 50 pM-25 nM	Yes	[97]
Optical sensing systems: NA-based methods	CRISPR-based fluorescence assay	Aβ40, Aβ42	CSF	T: 60 min; LOD: Aβ40: 1 pg mL^{-1}; Aβ42: 0.1 pg mL^{-1}; DR: NR	Partial	[98]
Optical sensing systems: NA-based methods	16S rRNA amplicon sequencing of gut microbiota with mL prediction (longitudinal mouse study)	Gut microbiota composition (16S rRNA sequencing)	Mouse feces	T: NR; LOD: NR; DR: NR (profiling/classification study, not a quantitative sensor)	No	[102]
Optical sensing systems: NA-based methods	Single-microbead CHA fluorescence	miRNA let-7a	Cell RNA, serum	T: ≈2 h; LOD: 1.09 pM; DR: 5-200 pM	Partial	[103]
Optical sensing systems: NA-based methods	Hydrogel-assisted CHA fluorescence	miR-574-5p	Plasma	T: NR; LOD: 1.29 pM; DR: NR	Yes	[104]
Optical sensing systems: Aptamer-based NAT-free optical sensing	Plasmonic AuNP microcavity SERS	Aβ42, p-tau181	Blood (plasma-like)	T: ~10 min; LOD: 100 fg mL^{-1} (Aβ42 and p-tau181); DR: NR	Partial	[108]
Optical sensing systems: Aptamer-based NAT-free optical sensing	Label-free ratiometric SERS (AuNP-templated)	Aβ40 monomer and fibril	Cultured neurons, mouse brain slices	T: ~50 min; LOD: monomer: 70 pM; fibril: 3.0 nM; DR: monomer: 100-740 pM; fibril: 10-160 pM; DR: NR	No	[109]
Optical sensing systems: NA-based methods	Ratiometric MOF/FRET fluorescence sensor	Presenilin-1 ss-ODN, Aβ, acetylcholine	CSF (spiked & diluted)	T: <10 min (after mixing); LOD: PSEN1: ~0.517 pM; Aβ: ~0.142 nM; ACh: ~0.0323 nM; DR: NR	No	[110]

(*continued on next page*)

Table 1 (*continued*)

Detection Type	Technology/ Method	Target Biomarker	Type of Sample	Performance Metrics	POCT Friendly	Ref
Optical sensing systems: Aptamer-based NAT-free optical sensing	SERS aptasensor (Au nanocube self-assembly)	Aβ42, tau	Serum	T: NR; LOD: Aβ42: 0.041 ng mL^{-1}; tau: 0.0087 ng mL^{-1}; DR: Aβ42: 0.1-10, 000 ng mL^{-1}; tau: 0.01-1000 ng mL^{-1}	No	[111]
Optical sensing systems: Aptamer-based NAT-free optical sensing	Dry-chemistry bipolar ECL immunoassay on a disposable microchip	Alzheimer-associated neuronal thread protein (AD7c-NTP)	Human urine	T: ~6 min; LOD: 0.15 pg mL^{-1}; DR: 1-10^4 pg mL^{-1}	Yes	[112]
Optical sensing systems: Aptamer-based NAT-free optical sensing	Whispering-gallery-mode microresonator	Aβ42	CSF	T: ~6-9 h (prep + run); LOD: NR; DR: NR	No	[113]
Optical sensing systems: Aptamer-based NAT-free optical sensing	Magnetic immunoassay with SIM fluorescence	Aβ42, tau, p-tau181	CSF, serum, saliva, urine	T: ~1 h; LOD: Aβ42: 23 fM; tau: 14 fM; p-tau181: 34 fM; DR: NR	Partial	[114]
Optical sensing systems: Aptamer-based NAT-free optical sensing	Liquid-crystal aptamer sensor	p-tau381	Blood	T: NR; LOD: 2.8, 10.86, 19.31 pg mL^{-1} (matrix-dependent); DR: NR	Yes	[115]
Optical sensing systems: Aptamer-based NAT-free optical sensing	Fluorogenic nanoparticle immunoassay (SNAFIA)	Adenylyl cyclase-associated protein 1 (CAP1)	Human tear fluid	T: ~60 min; LOD: 236 aM; DR: 0.32-1000 fM	Yes	[116]
Optical sensing systems: Aptamer-based NAT-free optical sensing	Nanobody-based colorimetric immunosensor using ITO substrate	ApoE	Human serum (1:10 000 dilution)	T: NR; LOD: 0.42 pg mL^{-1}; DR: 1-10 ng mL^{-1}	Yes	[117]
Optical sensing systems: Lateral flow and paper-based optical immunoassays	AuNP-based colorimetric lateral flow strip	Fetuin B, clusterin	Blood (plasma)	T: ~15 min; LOD: clusterin: 0.12 nM; fetuin B: 0.24 nM; DR: 0.1-100 nM	Yes	[118]
Optical sensing systems: Lateral flow and paper-based optical immunoassays	Entropy-driven catalysis amplified LFA	miRNA-16	Human serum	T: ~45 min; LOD: 1.01 pM; DR: 5-750 pM (tested up to 1 nM)	Yes	[119]
Optical sensing systems: LFA	Dual-readout LFA (colorimetric/SERS)	p-tau396, p-tau404	Human plasma	T: <20 min; LOD: 60 pg mL^{-1} (colorimetric), 3.8 pg mL^{-1} (SERS); DR: NR	Yes	[120]
Optical sensing systems: LFA	SERS-enhanced LFA	Aβ42, Aβ40, tau, NfL	Human blood/plasma	T: NR; LOD: Aβ42: 138.1 fg mL^{-1}; Aβ40: 191.2 fg mL^{-1}; tau: 257.1 fg mL^{-1}; NfL: 309.1 fg mL^{-1}; DR: NR	Partial	[121]
Optical sensing systems: Paper-based immunoassays	Paper-based ELISA (P-ELISA)	Aβ42	Plasma	T: 1.5 h; LOD: 63.04 pg mL^{-1} (buffer), ~100 pg mL^{-1} (plasma); DR: NR	Yes	[122]
Optical sensing systems: Microfluidic and LOC immunoassays	Immunoassay, droplet-based magnetic bead ELISA with LED detection	Aβ peptides (Aβ1-40, Aβ1-42, Aβ2-40, Aβ5-40)	CSF, artificial CSF	T: ~45 min; LOD: ~0.5-1 nM; DR: up to ~10 nM	Yes	[123]
Optical sensing systems: Lateral flow and paper-based optical immunoassays	Digital ELISA (Simoa)	TNF-α	Human serum	T: ~6 h; LOD: ~150 aM; DR: 600 aM-7 fM	No	[124]
Optical sensing systems: Lateral flow and paper-based optical immunoassays	MSD immunoassay (p-tau217) + Simoa immunoassay (p-tau231)	p-tau231, p-tau217	Human plasma	T: NR; LLOQ: 0.04 pg mL^{-1} (p-tau217, MSD); for p-tau231 LOD: NR; DR: NR	No	[125]
Optical sensing systems: LFA	Digital immunoassay with Simoa	p-tau181	Plasma	T: NR; LOD: NR (reported plasma levels ~ 9-33 pg mL^{-1}); DR: NR	No	[126]
Optical sensing systems: Lateral flow and paper-based optical immunoassays	Digital immunoassay with Simoa	Aβ42/Aβ40 ratio, p-tau181, GFAP, NfL	Plasma	T: NR; LOD: Aβ42: 1.51 pg mL^{-1}; p-tau181: 0.338 pg mL^{-1}; GFAP: 11.6 pg mL^{-1}; NfL: 1.6 pg mL^{-1}; DR: NR	No	[127]
Optical sensing systems: Microfluidic and LOC immunoassays	μCHAMP magnetic droplet immunoassay	Aβ oligomers	Buffer/plasma (≤ 10 μL)	T: 15 min (total <1 h); LOD: ~3 pg mL^{-1}; DR: 3-200 pg mL^{-1}	Yes	[128]

(*continued on next page*)

Table 1 (*continued*)

Detection Type	Technology/ Method	Target Biomarker	Type of Sample	Performance Metrics	POCT Friendly	Ref
Optical sensing systems: LFA	Lateral flow sandwich ELISA	NfL	CSF	T: ~2-3 h; LOD: 100 pg mL^{-1} (calibrator); DR: 50-40,000 pg mL^{-1}	No	[129]
Optical sensing systems: Microfluidic and LOC immunoassays	Magnetic-bead droplet microfluidic ELISA	Aβ oligomers	Human serum (10% diluted) and buffer	T: ~40 min; LOD: ~10.7 pg mL^{-1} (buffer), ~20.2 pg mL^{-1} (serum); DR: 12.5-200 pg mL^{-1}	Yes	[130]
Optical sensing systems: Microfluidic and LOC immunoassays	Miniaturized QCM microfluidic device	Aβ42	Serum (male AB plasma)	T: NR; LOD: 100 pM; DR: 0.1-3.2 μM	Yes	[131]
Optical sensing systems: Microfluidic and LOC immunoassays	Integrated immunocapture with PEG-DA hydrogel preconcentration	Aβ peptides (Aβ37, Aβ39, Aβ40, Aβ42)	Human CSF (Spiked & native)	T: <30 min (assay); enrichment in ~5 min; LOD: 0.25 ng μL^{-1}; DR: NR	Partial	[132]
Optical sensing systems: Microfluidic and LOC immunoassays	Smartphone-controlled paper-based ELISA	Aβ42	Artificial plasma	T: <30 min; LOD: 10.07 pg mL^{-1}; DR: 1-1000 pg mL^{-1}	Yes	[135]
Electrochemical sensing systems: Immunosensors and aptamer sensors	Rotary-valve-assisted paper-based ELISA (RAPID)	Aβ42	Artificial plasma	T: ~30 min; LOD: 9.6 pg mL^{-1}; DR: 1-1000 pg mL^{-1}	Yes	[136]
Optical sensing systems: Microfluidic and LOC immunoassays	Smartphone-assisted μPAD (chemiluminescent)	Tau	Artificial plasma	T: ~15 min; LOD: 2.61 pg mL^{-1}; DR: 1-10 ng mL^{-1}	Yes	[137]
Electrochemical sensing systems: Immunosensors	Impedimetric electrochemical immunosensor (EIS)	Aβ Oligomers	Blood (natural, cell-derived)	T: NR; LOD: ~0.5 pM; DR: NR	No	[138]
Electrochemical sensing systems: Immunosensors and aptamer sensors	Superwettable microdroplet electrochemical immunosensor	Aβ40, Aβ42, tau, p-tau181	Serum (5 μL)	T: <1 h; LOD: 0.012-0.064 pg mL^{-1}; DR: 0.1-1000 pg mL^{-1}	Yes	[139]
Electrochemical sensing systems: Immunosensors and aptamer sensors	Hairpin-mediated electrochemical aptamer sensor on gold screen-printed electrode with SWV	Aβ40	Aβ40 spiked in PBS buffer	T: ~30 min; LOD: 7.14 pg mL^{-1}; DR: 20-200 ng mL^{-1}	Yes	[140]
Electrochemical sensing systems: Immunosensors and aptamer sensors	Screen-printed electrochemical sensor (SPES) array with antibody capture and anodic stripping voltammetry readout	Conformationally altered p53 isoform	Peripheral blood (serum; planned)	T: NR; LOD: 2 ng mL^{-1}; DR: 1.25-20 ng mL^{-1}	Yes	[141]
Electrochemical sensing systems: Immunosensors and aptamer sensors	Interdigitated microelectrode immunosensor with SCAP	Aβ42	Mouse plasma (centrifuged from blood); synthetic Aβ spiked in PBS	T: ~20-30 min; LOD: 100 fg mL^{-1}; DR: 0.61 pg mL^{-1}-1 ng mL^{-1}	Partial	[142]
Electrochemical sensing systems: Immunosensors and aptamer sensors	Aptamer-based competitive electrochemical biosensor	Tau	Human plasma	T: <60 min; LOD: 3.21 fM; DR: 10 fM-1 μM	Yes	[143]
Electrochemical sensing systems: Immunosensors and aptamer sensors	On-chip magnetic-bead electrochemical immunoassay	ApoE	Diluted plasma	T: <1 h; LOD: 12.5 ng mL^{-1}; DR: 10-200 ng mL^{-1}	Yes	[144]
Electrochemical sensing systems: MIP-based sensors	Screen-printed rGO/PDA-MIP electrochemical sensor	GFAP	Human plasma	T: ~10 min; LOD: 754.5 fg mL^{-1}; DR: 1-10^6 fg mL^{-1}	Yes	[147]
Electrochemical sensing systems: MIP-based sensors	hPG-functionalized pPy/MIP electrochemical sensor	p-tau 181	Human serum, plasma	T: <10 min; LOD: 498 fg mL^{-1}; DR: 1-16 pg mL^{-1}	Yes	[148]
Electrochemical sensing systems: MIP-based sensors	Cu-Ag BS/GC electrode with PEDOT-MIP electrochemical sensor	Kynurenic acid	FBS and Human Serum	T: ~20 min; LOD: 0.278 fM; DR: 1.0 fM-500 nM	No	[149]
Electronic sensing systems: Aptamer, antibody, and nanostructure-enabled FET	Graphene FET (TDN-G-FET)	Aβ42	Serum	T: <5 min; LOD: ~5 aM; DR: 5 aM-500 pM	Yes	[155]
Electronic sensing systems: Aptamer, antibody, and nanostructure-enabled FET	Aptamer-functionalised carbon-nanotube thin-film FET (CNT-FET)	Aβ42, Aβ40	Undiluted human serum	T: NR (response time: several minutes); LOD: 50 aM; DR: up to ~4 orders of magnitude	Yes	[156]
Electronic sensing systems: Aptamer, antibody, and nanostructure-enabled FET	Label-free solution-gated graphene-oxide composite FET	p-tau217	p-tau217 spiked in PBS and in HSA	T: NR; LOD: 10 fg mL^{-1}; DR: 10 fg mL^{-1}-100 pg mL^{-1}	Yes	[157]

(*continued on next page*)

Table 1 (*continued*)

Detection Type	Technology/ Method	Target Biomarker	Type of Sample	Performance Metrics	POCT Friendly	Ref
Electronic sensing systems: Aptamer, antibody, and nanostructure-enabled FET	Peptide-functionalised extended-gate FET (EG-FET)	c-Abl kinase activity	c-Abl standards in Tris buffer, brain-tissue homogenates from APP/PS1 transgenic	T: NR; LOD: 1 pg mL^{-1}; DR: 1-3.05 μg mL^{-1}	Yes	[158]
Electronic sensing systems: Aptamer, antibody, and nanostructure-enabled FET	AuNP-decorated graphene electrolyte-gated transistor (G-EGT) immunosensor with dual BSA/Tween-20 antifouling strategy	Neuron-derived exosomal Aβ42	Neuron-derived exosomes from human serum (NDE)	T: NR; LOD: 447 ag mL^{-1}; DR: 1.48-148 pg mL^{-1}	No	[159]
Electronic sensing systems: Aptamer, antibody, and nanostructure-enabled FET	Nanoporous-membrane microfluidic electrochemical sensor	Aβ aggregates	1 μL serum	T: ~1 h; LOD: ~2 fM; DR: 2 fM-220 nM	Yes	[160]
Electronic sensing systems: Aptamer, antibody, and nanostructure-enabled FET.	Aptamer-modified solid-state nanopore sensor	Aβ42	Serum	T: <1 min; LOD: 5 pg mL^{-1}; DR: 5-500 pg mL^{-1}	Yes	[161]
Electronic sensing systems: Single-molecule nanopore sensors	Length-encoded aerolysin nanopore-integrated triple-helix molecular switch	p-tau 381, α-1 antitrypsin (AAT), BACE1	Human blood serum	T: NR; LOD: tau: 6.79 fM; AAT: 77.9 fM; BACE1: 86.4 fM; DR: 10 fM-10 nM	Partial	[163]
Electronic sensing systems: Single-molecule nanopore sensors	α-HL biological nanopore	Aβ42, Aβ40, APP (669-711), tau	CSF, serum (mouse and human)	T: NR; LOD: Aβ42: 2.1 pM; APP (669-711): 1.5 pM; Aβ40: 627 fM; DR: NR	Partial	[164]
Electronic sensing systems: Capacitive and magnetic sensors	Polypyrrole (PPy) nanoparticle-based interdigitated microelectrode capacitive immunosensor	Aβ40, Aβ42	Spiked 5% human plasma	T: NR; LOD: Aβ40: 5.71 fg mL^{-1}; Aβ42: 9.09 fg mL^{-1}; DR: 10 fg mL^{-1}-1 μg mL^{-1}	Yes	[171]
Electronic sensing systems: Capacitive and magnetic sensors	Interdigitated capacitive biosensor with Pt-Ti-SiO_2 surface functionalized by aptamer and antibody	Aβ42	Human plasma, including patient plasma	T: ≤5 s; LOD: 0.1 fg mL^{-1}; DR: 0.001-10 μM	Yes	[172]
Electronic sensing systems: Capacitive and magnetic sensors	β-cyclodextrin/reduced graphene oxide (β-CD/RGO) nanohybrid capacitive immunosensor on ITO microdisk	Aβ40	Human serum (HS), diluted 1:100	T: NR; LOD: 0.69 fg mL^{-1} (HS); DR: 10^1-10^5 fg mL^{-1}	Partial	[173]
Electronic sensing systems: Capacitive and magnetic sensors	MEMS micro-fluxgate magnetic immunosensor with sandwich assay on gold film	CRP for AD inflammation	Serum (bovine serum used as matrix)	T: <30 min; LOD: 0.002 μg mL^{-1}; DR: 0.002-10 μg mL^{-1}	Yes	[174]
Optical sensing systems: NA-based methods	Aptamer-HCR-CRISPR fluorescence assay	p-tau181	CSF, serum	T: ≈80 min; LOD: 0.069 pg mL^{-1}; DR: 0.1-10^6 pg mL^{-1}	Yes	[233]
Optical sensing systems: Lateral flow and paper-based optical immunoassays	Sandwich ELISA	NfL	CSF	T: NR; LOD: 31 pg mL^{-1}; DR: 62.5-2000 pgmL^{-1}	No	[234]
Optical sensing systems: Lateral flow and paper-based optical immunoassays	Chemiluminescent sandwich ELISA	Aβ42	Human plasma	T: NR; LOD: 1 pg mL^{-1}; DR: 0.25-500 pg mL^{-1}	No	[235]
Optical sensing systems: NA-based methods	TPET-DNA@Dex-MoS_2 dual-turn-on fluorescence	miR-125b	Brain tissue, PC12 cells	T: ≤1 h; LOD: 1-10 pM; DR: NR	Partial	[236]
Optical sensing systems: Aptamer-based NAT-free optical sensing	3D Au@G SERS substrate	Aβ42, tau	Synthetic proteins (Aβ42, tau)	T: NR; LOD: 100-1 nM (reported working range); DR: NR	No	[237]
Optical sensing systems: Lateral flow and paper-based optical immunoassays	Antibody-aptamer sandwich FRET assay	Aβ oligomers	CSF, serum	T: ~40 min; LOD: 0.22 pg mL^{-1}(≈61 fM); DR: 0.001-10 ng mL^{-1}	Partial	[238]
Optical sensing systems: Aptamer-based NAT-free optical sensing	Electrospun PAN nanofiber aptasensor	Aβ42, human insulin	CSF	T: NR; LOD: Aβ42: 76 aM; human insulin: 26 aM; DR: NR	Partial	[239]
Optical sensing systems: Lateral-flow and paper-based optical immunoassays	Sandwich ELISA	Aβ42, tau, p-tau181	CSF, exosome	T: NR; LOD: 1.56 pg mL^{-1}; DR: NR	Yes	[240]
Optical sensing systems: Microfluidic and LOC immunoassays	Electrochemiluminescence immunoassay (MSD)	p-tau181, p-tau217	Plasma	T: NR; LOD: p-tau181: 0.8 pg mL^{-1}; p-tau217: 0.13 pg mL^{-1}; DR: NR	No	[241]

(*continued on next page*)

Table 1 (*continued*)

Detection Type	Technology/ Method	Target Biomarker	Type of Sample	Performance Metrics	POCT Friendly	Ref
Optical sensing systems: Lateral flow and paper-based optical immunoassays	Fully automated lumipulse immunoassay	p-tau217	Plasma	T: NR; LOD: 0.27 pgmL^{-1} (single cutoff); DR: 0.22-0.34 pg mL^{-1}	Partial	[242]
Electronic sensing systems: Single-molecule nanopore sensors	Resistive-pulse sensing using track-etched PET nanopores	Aβ42 fibrils (well-calibrated lengths)	Synthetic Aβ42 fibrils in buffer (PBS 1× or 1 M NaCl/PBS, pH7.2)	T: NR; LOD: NR; DR: functional detection demonstrated from ~15 nM to 1 μM (fibril concentration; monomer equivalent)	Partial	[243]
Electronic sensing systems: Aptamer, antibody, and nanostructure-enabled FET	Linker-free edge-defect patterned graphene electrolyte-gated FET immunosensor	Tau	Recombinant tau in PBS, serum, human plasma	T: 3 min (incubation after solution exchange, before readout); LOD: 10 fg mL^{-1}; DR: 10 fg mL^{-1} to 1 ng mL^{-1}.	Yes	[244]
Electrochemical sensing: Wearable sensors	Microneedle-integrated electrochemical patch (VG@Au, DPV readout, Bluetooth-enabled)	p-tau181, p-tau217	ISF	T: NR, LOD: p-tau181: 0.058 pg mL^{-1}; p-tau217: 0.079 pg mL^{-1}; DR: 0.1–1000 pg mL^{-1}	Yes	[145]
Electronic sensing: FET	mL-enhanced graphene FET	Aβ42, Aβ40, p-tau217	Clinical plasma	T: ~60 min (RT incubation during detection), LOD: NR; DR: 1 fg mL^{-1}–1.0 × 10^{5} fg mL^{-1}; Accuracy: 98.9–100%	Yes	[213]

Table abbreviations: T: total assay time; LOD: limit of detection; DR: dynamic range; NR: not reported; POCT: point-of-care testing; CSF: cerebrospinal fluid; AuNP: gold nanoparticle; LFA: lateral-flow assay; FET: field-effect transistor; MIP: molecularly imprinted polymer; SERS: surface-enhanced Raman scattering; ELISA: enzyme-linked immunosorbent assay; QCM: quartz crystal microbalance; ↓: Downregulation; ↑: Upregulation; LLOQ: lower limit of quantification.

or cartridge supplies preloaded chemistry, as in hemoglobin photometers with dry-reagent microcuvettes [61], electrochemical strips [62], and blood gas or electrolyte analyzers [63] that run on disposable reagent cartridges [64]. In another example, lateral flow (LF) testing is a scalable, low-cost POCT format. Its architecture is target-agnostic. The same strip design and reader can support different assays by swapping the capture and detector receptors, enabling broad menus at low cost. From a translational perspective, reagent-based formats also allow "cost-of-use" to be driven primarily by standardized consumables (strips/cartridges), whereas reagent-free approaches typically shift cost toward instrument complexity and calibration. Because most prototype studies do not report comparable per-test cost and device amortization, we focus our comparison on workflow steps, instrument dependence, and readiness level rather than direct cost.

In reagent-free methods, signal transduction is achieved by directly probing the physicochemical properties of the target [65–68]. For example, shear-horizontal surface acoustic wave (SH-SAW) sensors offer exceptional sensitivity and specificity, identifying biological agents in liquids by monitoring shifts in resonance frequency induced by changes in mass [69]. Other reagent-free techniques include surface plasmon resonance (SPR) [70], quartz crystal microbalance [71], terahertz spectroscopy [72], magnetic biosensing [73], microwave permittivity sensing [74], electrochemical detection [75–77], NIR spectroscopy [78], and hyperspectral analysis [79]. This approach is cost-effective and user-friendly, but its practical application scope is too narrow due to the considerable technical challenges involved in its development, instrumentation complexity, fabrication challenges, matrix effects, and stability issues [80]. The advantages of reagent-based methods lie in their flexibility within the entire POCT development process [68]. By maintaining a fixed signal output principle for the recognition molecules, the same detection method can accommodate reagent kits designed for different targets, greatly expanding the application scope and effectively reducing costs.

The final part, detection hardware with readout, is the visible part of a POCT system. It contains two modules: signal processing and connectivity [13]. The signal processing module converts target recognition into a measurable signal by selecting a mode matched to property changes in the processed sample, for example, impedance, potentiometric or amperometric sensing, fluorescence, UV or visible absorbance, and pH [75–77,81]. Hardware choices must balance performance, cost, and reusability to keep the device small and affordable. For example, many fluorescence readers use LED illumination instead of a laser to reduce footprint and expense while meeting signal-to-noise requirements [82]. The connectivity module manages computation and data exchange and receives signals from the sensing module, performs preprocessing and quality checks, and then sends data securely to edge or cloud services that apply AI and big data analytics, and results return as values, trends, and alerts in near real time [65,83–85]. Through healthcare Internet of Things (IoT) integration, the device links with wearables, implants, and smart hospital equipment to enable continuous monitoring and remote intervention. The data path is unified and closed loop: sensing, preprocessing, transmission, analysis, reporting, and storage in clinical records [86]. This integration reduces manual steps and improves time to result. Detection hardware should integrate the appropriate sensing modality with practical connectivity while preserving core POCT goals of small size, low cost, and reliable results.

3.2. POCT detection strategies for AD: methods, biomarkers, and POCT readiness

AD diagnostics are evolving from centralized, laboratory-based assays to decentralized, rapid POCT platforms. The growing need for early detection, together with AD biomarker targets spanning both nucleic acids (NA) and proteins, has stimulated the development of diverse sensing approaches. In this review, we organize AD POCT by transduction/readout architecture (optical, electrochemical, and electronic), because the readout principle most directly determines POCT readiness in practice, including workflow complexity, instrument dependence, power/temperature control, and reader requirements. In contrast, biomarker-based (protein vs NA), recognition-element–based (antibody/aptamer/CRISPR), or format-based (e.g., LFA, printed sensors, LOC) classifications substantially overlap across platforms and would fragment the discussion and narrow the scope, particularly established AD POCT biomarkers currently used across studies. Accordingly, and as summarized in Table 1: (1) optical sensing systems, (2) electrochemical

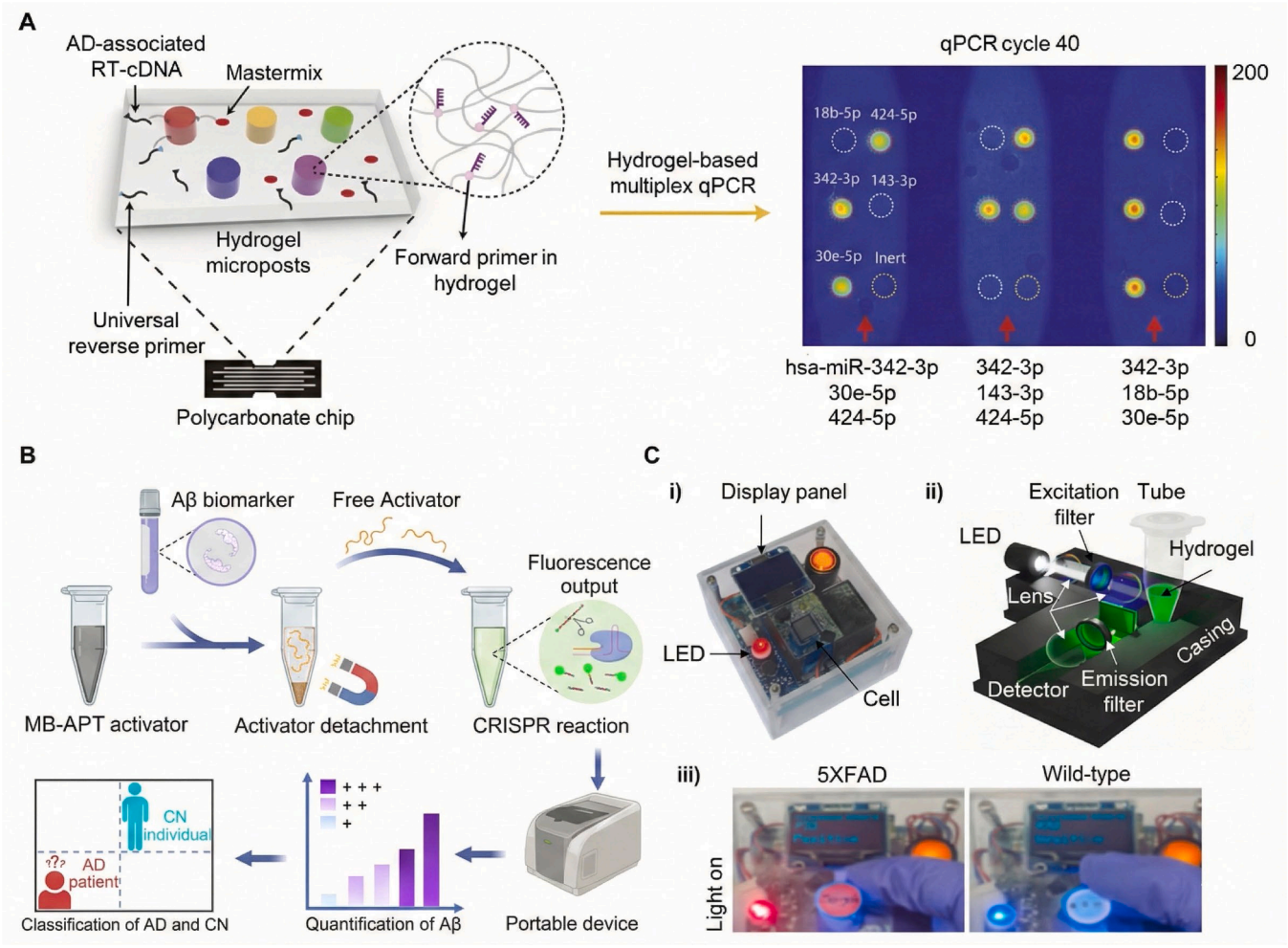

Fig. 3. NAT-based amplification for POC AD diagnosis. A PCR-based multiplex qPCR for sensitive, quantitative profiling of AD-associated plasma microRNAs. Printed with permission from Ref. [87]. Copyright © 2018 Elsevier. **B** CRISPR-Cas fluorescence readout for sequence-specific detection of AD-related targets, often paired with pre-amplification to reach low-abundance levels. Printed with permission from Ref. [98]. Copyright © 2024 American Chemical Society. **C** Enzyme-free amplification via hydrogel-assisted CHA for miRNA sensing using low-power LED fluorescence with picomolar (pM) sensitivity. Printed with permission from Ref. [104]. Copyright © 2022 Elsevier.

sensing platforms, and (3) electronic sensing systems. While these categories overlap in underlying biochemical principles, this classification enables a more precise evaluation of assay performance, sample compatibility, and "POCT readiness". In POCT readiness terms, devices marked "*Yes*" in Table 1 already demonstrate sample-to-answer-out feasibility or noninvasive collection with simple instrumentation, "*Partial*" entries typically require a handheld device that is portable but not yet routine, and "*No*" entries exhibit dependence on microscopes or benchtop analyzers that limit POCT near patients. To address clinical applicability more directly, we additionally compare modalities by parameters that determine where they can realistically be used (home vs. primary care): (i) workflow and user steps (sample handling, incubation/washing, calibration), (ii) instrumentation (reader type, power/temperature control), (iii) sample type and collection (blood/plasma/CSF/saliva), (iv) multiplexing capability (number of biomarkers per run and cross-reactivity control), and (v) analytical performance (biomarker types, LOD and assay time) (iv) system-level pros/cons. We discuss these factors in **Section 3.2** subsections.

3.2.1. *Optical sensing systems*

This subsection reviews optical sensing systems for AD POCT, including NA-based assays (PCR, isothermal amplification, CRISPR, and enzyme-free circuits), amplification-free optical biofluid sensors (colorimetric, fluorescence, plasmonic, ECL, surface-enhanced Raman scattering (SERS), and photonic platforms), and integrated formats such as lateral-flow or paper strips and microfluidic or LOC cartridges with compact readers. It highlights the core translational trade-off between ultrahigh sensitivity and true portability, since many top-performing methods still depend on benchtop optics, whereas emerging sealed, low-power strips and cartridges are closer to near-patient deployment. The clinical significance is that scalable optical POCT platforms could enable earlier community screening.

3.2.1.1. NA-based methods. ***PCR-based NA amplification.*** PCR is a reliable, high-accuracy, and high-sensitivity method for DNA amplification and is considered the 'gold standard' for disease diagnosis. PCR with digital droplet microfluidics is an efficient method for disease detection, ideal for POCT devices. In AD detection using a PCR-based assay, a hydrogel micropost-based multiplex qPCR assay has measured five AD-related plasma miRNAs (Fig. 3**A**) [87]. DNA-barcoded immunoassays that tag exosomal Aβ and tau and qPCR readout have pushed sensitivity to ~10 fg mL^{-1} while illustrating an exosome-targeted liquid-biopsy concept for AD; POCT suitability is also "potential" [88]. The immunomagnetic exosomal polymerase chain reaction (iMEP) platform uses antibodies that are chemically conjugated to short DNA strands. These DNA-antibody conjugates bind specifically to AD proteins (Aβ and

p-tau) captured from blood exosomes by magnetic beads. The attached DNA serves as a unique barcode that is amplified by real-time PCR, converting the protein concentration into a quantifiable NA signal for highly sensitive detection. In the same vein, concrete PCR exemplars include an explicit next-generation sequencing (NGS), reverse transcription quantitative PCR (RT-qPCR) validation, and support vector machine (SVM) classification pipeline that yielded a 12 miRNA whole-blood panel distinguishing AD from controls [89]. A four-plex, exon-specific RT-qPCR targeting CDK2, CDK5RAP3, CDK7, and CDK11B detects elevated transcripts in mouse whole blood and human peripheral blood mononuclear cells, with a turnaround time of under 1 h and potential suitability for POCT [90]. PCR offers strong sensitivity, specificity, and quantitative accuracy; however, precise temperature control, thermal cycling, and optics add to the cost and power burden, making the integration of compact readers into true POCT challenging.

Isothermal NA amplification. Isothermal amplification technologies have emerged as promising alternatives to PCR for decentralized molecular diagnostics, as they eliminate thermal cycling while retaining high analytical sensitivity [91]. These chemistries enable rapid amplification under constant temperatures, reducing instrument complexity and power consumption, offering key advantages for POCT [92]. Among isothermal strategies, several approaches have been developed, including loop-mediated isothermal amplification (LAMP), NA sequence-based amplification (NASBA), strand displacement amplification (SDA), and rolling circle amplification (RCA) [91]. Each method offers benefits but also imposes design or workflow constraints that limit scalability. For example, LAMP requires four to six primers per target and often produces ladder-like by-products that increase false-positive rates [59]. NASBA primarily targets RNA and demands enzyme optimization [93]. SDA involves an initial denaturation step and can yield nonspecific products [94]. Orthogonal to these PCR-like schemes, RCA coupled to apurinic or apyrimidinic endonuclease I (APE I) cleavage has quantified serum miRNA-206 with a 1.82 fM limit of detection (LOD), a 10 fM to 1 nM dynamic range, and a turnaround time of about 1 h, and is explicitly rated POCT-ready [95]. RCA relies on ligation-based circularization and produces concatemeric products, which complicate analysis [96]. In contrast, recombinase polymerase amplification (RPA) offers the best balance of speed and simplicity [59]. At 37–41 °C, RPA amplifies targets in 20–30 min using a single primer pair. Compared with LAMP, RPA generates a single, well-defined amplicon rather than multiple by-products, facilitating downstream interpretation. The reaction also tolerates moderate sequence variability (up to nine base-pair mismatches), allowing detection across viral variants [57]. Modern computational tools, such as PrimedRPA, further enhance primer selection by minimizing cross-dimerization and secondary structure formation in multi-target panels. These features make RPA well-suited for developing rapid, low-power, single-pot assays that simultaneously amplify multiple targets.

CRISPR-Cas diagnostics for sequence-specific readout. In addition to amplification assays, the CRISPR-Cas system, derived from a bacterial defense mechanism, is now a vital tool for sequence-specific detection. It uses engineered crRNA sequences, along with enzymes such as Cas12 and Cas13, to target and cleave specific DNA or RNA sequences, offering high specificity and sensitivity. CRISPR-based fluorescence assays have achieved ultrasensitivity in the low picogram-per-milliliter range. For example, CRISPR fluorescence has been applied to Aβ40 and Aβ42 detection in CSF, while dual-fluorescence Cas12a assays target ApoE4 SNPs in diluted serum (~22–33 pM) within an hour [97]. Their primary advantages are high molecular specificity and compatibility with relatively simple fluorescence optics. However, they often require target pre-amplification to reach low-abundance thresholds [57]. Fig. 3**B** shows the enrichment of Aβ concentration and detection strategy using the POCT device [98]. CRISPR-based multiplexing currently faces limitations, including the need for pre-amplification due to low sensitivity at low viral loads, a limited variety of Cas proteins with distinct substrate preferences, and cross-reactivity with similar targets. However, multiplexed Cas13 detection can be combined with pre-amplification methods such as RPA, enabling simultaneous detection of multiple targets in a single reaction.

miRNA up/downregulation. Apart from DNA/RNA quantification, miRNA quantification, and up- or down-regulation of absolute amounts from healthy individuals to patients, these findings show promising biomarkers for AD [85,99,100]. However, there is no established benchmark workflow for miRNA collection and analysis. For example, measured levels can vary across biofluids and sample types, such as blood and saliva, and are sensitive to pre-analytical factors, including hemolysis, processing time, storage, and platform choice [101]. NAT-based miRNA testing for AD is additionally constrained by variable baseline levels and small effect sizes, strong dependence on contamination control and standardized handling, matrix interference in blood, and the practical need for sealed sample-to-answer-out preparation that often requires complex optical hardware. Consequently, clinical adoption has lagged, in part because protein and imaging biomarkers already benefit from harmonized protocols and well-established analytical performance [102]. In addition, most miRNA detection workflows rely on ligation-based capture followed by amplification using LAMP, PCR, RPA, or RCA, because the short miRNA length of approximately 22 nucleotides complicates primer design and often introduces additional processing steps, thereby increasing system complexity. When expanding beyond blood-based targets, system-level readouts, such as longitudinal 16S rRNA V4 amplicon profiling combined with RT-qPCR host-gene measurements, are feasible but not POCT-ready, limiting their clinical utility.

Catalytic hairpin assembly (CHA). Hydrogel-assisted catalytic hairpin assembly (CHA) provides an enzyme-free route to blood miRNA sensing by localizing hairpin probes within a hydrogel matrix, thereby amplifying fluorescence at room temperature [103,104]. In an early AD demonstration, miR-574–5p was selected using 4-month-old 5XFAD model mice and subsequently quantified with picomolar-level sensitivity (LOD, 1.29 pM), with performance further validated in human patient plasma versus non-AD controls and implemented in a portable fluorometer for POCT feasibility [104]. Fig. 3**C** depicts the hydrogel-embedded CHA scheme, in which target-triggered hairpin opening initiates a cascading strand-displacement reaction that accumulates fluorescent products inside the hydrogel. A key translational limitation is slower reaction kinetics in complex biofluids, but assay speed can be improved through mass-transport and localization strategies, such as acoustic agitation, porous or micro-structured supports, bead or micro-post confinement, and hydrogel mesh tuning, which increase the effective collision frequency between targets and hairpins [105]. Practical designs should co-optimize kinetics, for example, by shortening stems and tuning loop and toehold lengths, and specificity via orthogonal hairpin sets and mismatch-penalizing toeholds to discriminate closely related miRNAs, while maintaining sealed single-pot, low-power optical readout and scalable multiplexing through spectral reporters or spatial barcodes.

Both enzyme-driven and enzyme-free NA assays are viable paths to POCT for AD: the former offers peak sensitivity but requires thermal control and a cold chain; the latter supports simpler, low-power optics, such as color sensors, but requires kinetic and transport engineering. Either can meet clinical thresholds when paired with disciplined pre-analytics, sealed sample prep, external validation, and integration into a single sample-to-answer-out module for robustness.

3.2.1.2. Aptamer-based NAT-free optical sensing. ***Optical sensing.*** NAT-free optical sensing methods for AD span diverse targets and transduction mechanisms, generating direct optical signals without enzymatic amplification. These approaches align well with POCT settings because they combine molecular selectivity with compact, low-power readers [106]. Representative platforms include colorimetric, fluorescent, plasmonic, ECL, and advanced photonic systems.

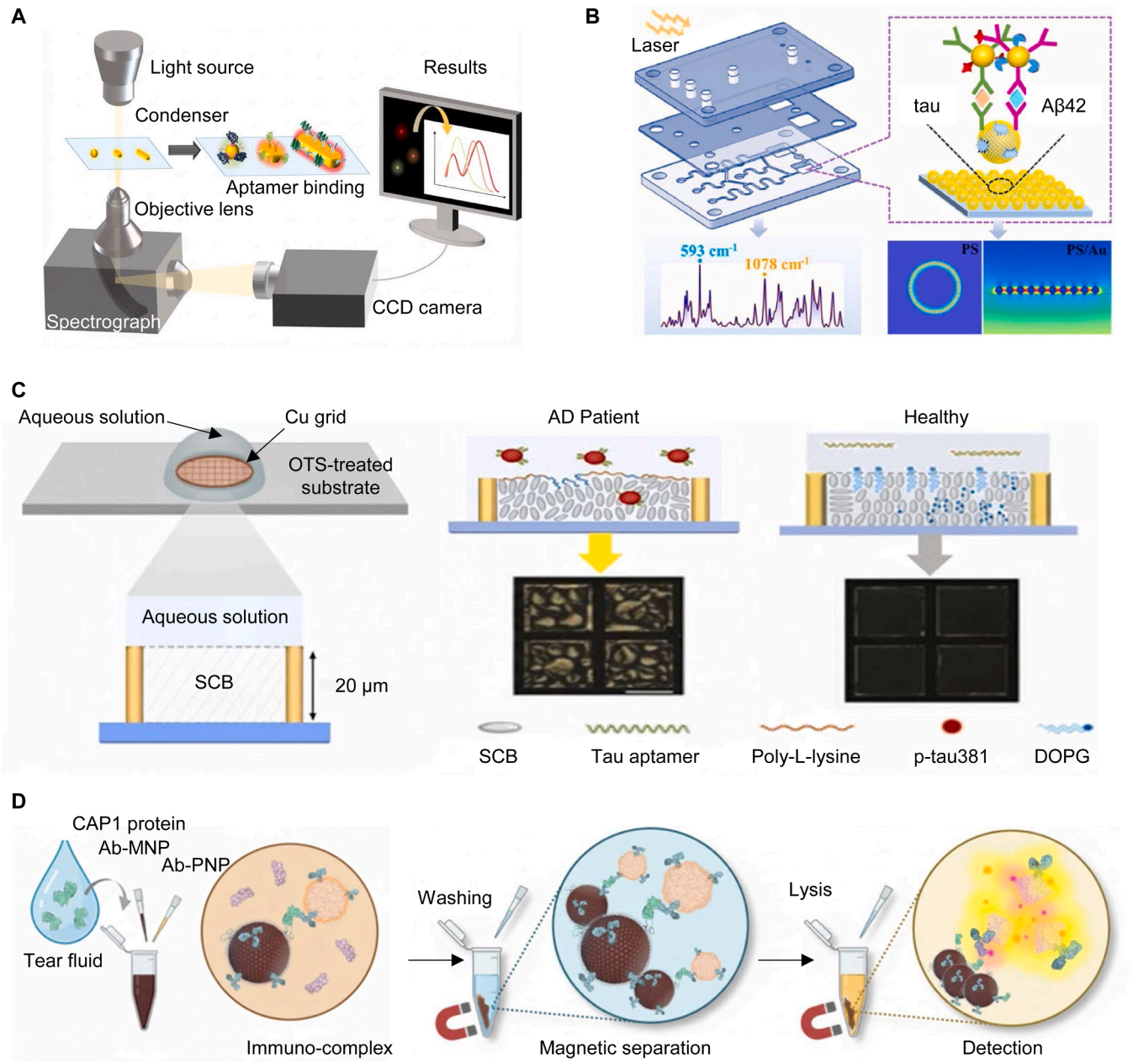

Fig. 4. Aptamer-based NAT-free optical sensing. A Shape-coded AuNPs plasmonic platform enabling multiplex optical discrimination of AD protein biomarkers through LSPR shifts. Printed with permission from Ref. [70]. Copyright © 2018 Elsevier. **B** AuNPs-enabled SERS or microcavity plasmonic chip readout for ultra-sensitive detection, illustrating high analytical performance with instrumentation-dependent workflows. Printed with permission from Ref. [108]. Copyright © 2023 Elsevier. **C** Liquid-crystal aptamer sensor for tau detection that converts target binding into an orientation-based optical signal compatible with simple, portable readout. Printed with permission from Ref. [115]. Copyright © 2025 Elsevier. **D** Fluorogenic nanoparticle-based immunoassay for tear-fluid proteins, supporting a noninvasive sampling route and compact optics suitable for near-patient testing. Printed with permission from Ref. [116] under the Creative Commons CC BY 4.0 license.

Pattern-recognition-based "chemical tongue" arrays convert complex mixtures in plasma, saliva, urine, or tears into multidimensional optical signatures that can be decoded using statistical or machine learning (mL) models [107]. In parallel, colorimetric papers incorporating gold or silver nanoparticles report Aβ aggregation or metal coordination through visible color shifts that are readily quantified by smartphone cameras. Mechanistically related manganese dioxide (MnO_2) nanozyme arrays generate similar strip-like colorimetric outputs via catalytic reactions, supporting faster reaction kinetics, lower LOD, and improved tolerance to matrix interference compared with passive nanoparticle assays. Fluorescent platforms extend sensitivity and multiplexing by exploiting nitrogen-doped carbon dots, conjugated polymer complexes, and metal-organic frameworks (MOF). These materials provide spectrally resolved signatures across multiple emission channels and can detect NA or protein biomarkers in a single cartridge. Shape-coded gold nanoparticles (AuNPs) that exploit shifts in localized surface plasmon resonance (LSPR) enable femtomolar-level detection of Aβ and tau (Fig. 4**A**) [70]. AuNPs-based SERS and microcavity plasmonic chips achieve sub-pg mL^{-1} detection limits in plasma-like matrices (Fig. 4**B**) [108]. However, SERS and shape-coded AuNPs approaches that depend on benchtop microscopes, Raman spectrometers, or charge-coupled device (CCD) cameras remain poorly aligned with true POCT deployment; MOF-based FRET probes and hybrids that combine aggregation-induced emission (AIE) with fluorescence resonance energy

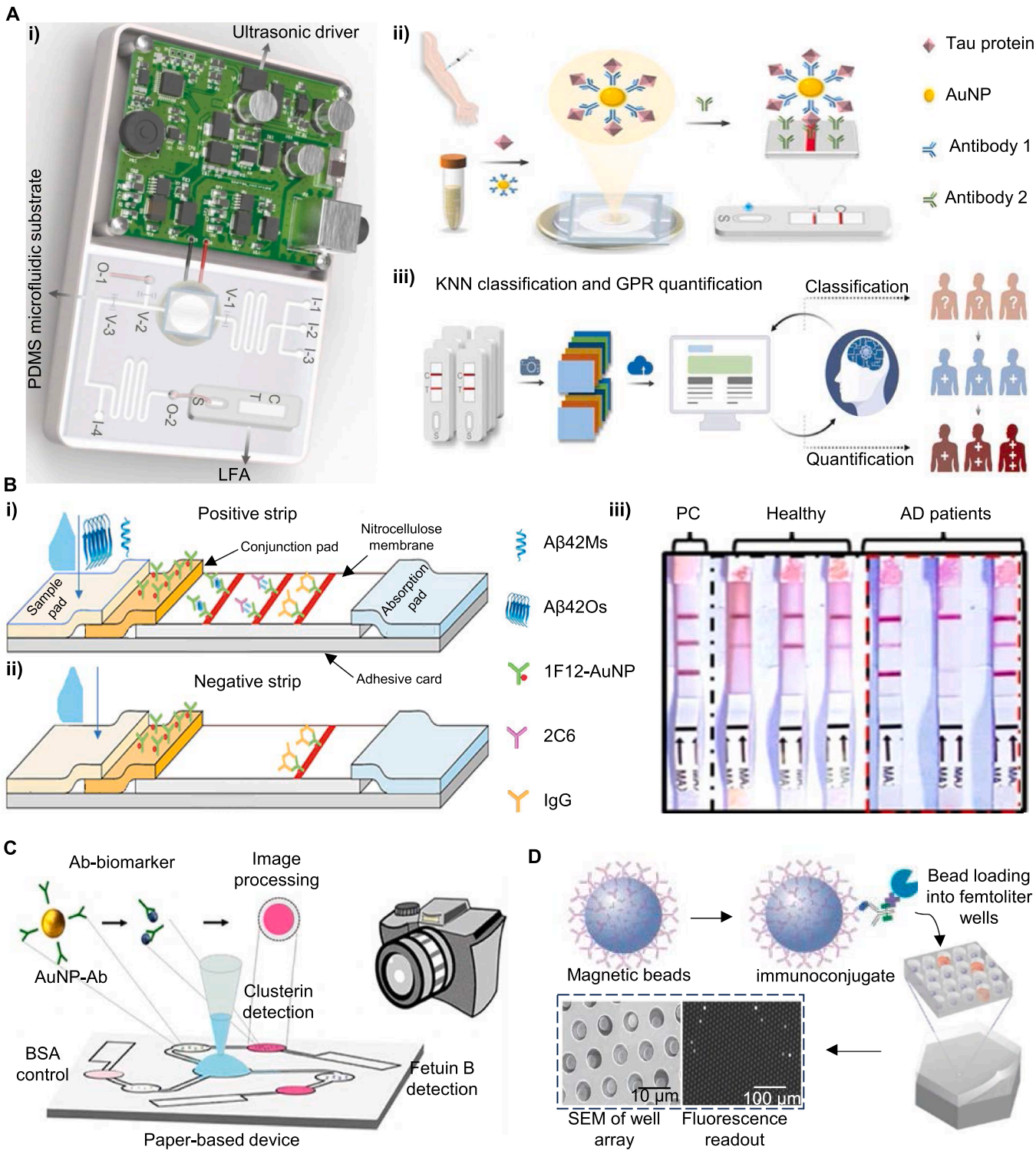

Fig. 5. Lateral-flow and paper-based optical immunoassays. **A** Ultrasound-assisted, mL-optimized AuNPs lateral-flow or microfluidic workflow for tau quantification in serum or plasma with rapid colorimetric readout. Reproduced from Ref. [66] (Printed with permission under the Creative Commons CC BY 4.0 license). **B** Monoclonal antibody LFA for rapid detection of Aβ42 monomers and oligomers. Reproduced from Ref. [67] (Printed with permission under the Creative Commons CC BY 4.0 license). **C** Paper-based AuNPs colorimetric LFA for fast quantification of protein biomarkers such as fetuin B and clusterin. Reproduced from Ref. [118]. Copyright © 2019 American Chemical Society. **D** Digital immunoassay (single-molecule array) for ultrasensitive, multiplex plasma biomarker quantification, serving as a centralized reference benchmark rather than a portable strip format. Reproduced from Ref. [124]. Copyright © 2010 Springer Nature.

transfer (FRET) can achieve comparable analytical sensitivity for NA and protein targets [109–111], but require stringent control of spectral cross-talk and fluorophore photostability, because FRET is a distance-dependent, nonradiative energy transfer from an excited donor to a nearby acceptor.

SERS adds molecular fingerprints and can operate in dual-mode lateral flow cassettes, featuring a rapid color line for screening and a high-sensitivity readout for confirmation. These methods rely on Raman microscopes, lasers, or CCD setups, which limit their compatibility with POCT. Practical urine and serum examples include a handheld ECL

analyzer for AD7c-NTP with a sensitivity of pg mL^{-1}, and a dry-chemistry bipolar ECL sensor on a screen-printed fiber chip that measures AD7c-NTP in approximately 6 min with a few user steps [112]. Resonant photonic and advanced optical systems, such as the "FLOWER resonator, " detect Aβ42 in CSF via whispering-gallery-mode resonance with ultra-sensitivity, though a lab-based setup limits POCT implementation [113]. Magnetic immunoassays with total internal reflection fluorescence (TIRF) or fluorescence readouts can achieve femtomolar-level sensitivity across CSF, serum, saliva, and urine, balancing sensitivity with trade-offs in instrumentation [114]. Liquid crystal aptamer sensors show a clear POCT trajectory for p-tau381, providing orientation-based detection in blood with moderate sensitivity but simple, portable readouts (Fig. 4**C**) [115]. A nanoparticle-based fluorogenic immunoassay (SNAFIA) detects tear-fluid proteins at the attomolar range with 100% specificity, representing a noninvasive, patient-friendly workflow (Fig. 4**D**) [116]. The primary constraints for nanomaterials are optical stability, signal inhibition, spectral crosstalk, and batch control, which necessitate internal controls and temperature compensation. In the near term, these sensors will support triage, rule-in decisions, and therapy monitoring, complementing central lab digital immunoassays that set the clinical benchmark for absolute quantification.

Optical imaging. Optical imaging complements fluid testing by providing a structural and biochemical context, with instruments moving toward clinic-ready footprints. Retinal imaging is the most POCT-friendly approach because the eye is accessible, and changes in the retina mirror neurodegeneration. Optical coherence tomography (OCT) measures the retinal nerve fiber layer and choroidal thickness, and OCT angiography quantifies capillary density and flow. These metrics correlate with cognitive status across many cohorts and can be obtained using compact devices already deployed in community eye clinics. Autofluorescence and fluorescence lifetime ophthalmoscopy add quantitative pigment and lifetime maps that associate with pathology and CSF tau. Together, these tools enable low-burden screening, risk stratification, and follow-up at the POC. Label-free spectroscopic imaging, including infrared and Raman spectroscopy, identifies β-sheet-rich aggregates and lipid chemistry without the need for stains, and coherent Raman or multiphoton imaging tracks plaque dynamics in animal models. While these latter systems are mostly benchtop, they validate biomarkers and train algorithms that can be transferred to lighter clinical devices. Multimodal strategies that integrate OCT metrics with sensor array outputs can enhance specificity, for example, by requiring concordance between vascular loss and elevated plasma or saliva levels before referral. Nanobody-based immunosensors on indium tin oxide (ITO) substrates enable sub-pg mL^{-1} ApoE detection with a colorimetric readout that is compatible with smartphone imaging [117]. Portable carts, teleophthalmology links, and integration with electronic health records enable deployment in primary care settings, memory clinics, and mobile screening units. As costs fall and software matures, POC imaging, combined with a portable device or smartphone, can shift AD assessment from episodic specialty visits to continuous community surveillance, reduce time to treatment, and support personalized monitoring during disease-modifying therapy.

Taken together, NAT-free optical sensing and optical imaging platforms exemplify a trade-off between extreme analytical sensitivity and full portability, because their highest performance still depends on relatively sophisticated, though increasingly compact, instruments. Even so, the accumulated examples above indicate substantial progress toward true POCT readiness across biofluid assays and retinal imaging [112,117]. True multiplexing remains constrained by spectral overlapping and crosstalk, and manufacturing consistency for MOF, AIE, or SERS probes will require tighter control to satisfy regulatory standards. Handheld ECL readers, smartphone-based colorimetry, liquid-crystal aptamer cartridges, and nanobody colorimetric sensors together outline a viable path from laboratory prototypes to field-deployable tests. In practice, near-term deployment will prioritize triage, rule-in confirmation, and longitudinal monitoring rather than stand-alone diagnosis, and mL algorithms can narrow the remaining gap between benchtop performance and field-ready POCT.

3.2.1.3. Lateral flow and paper-based optical immunoassays. Lateral flow and paper-based optical immunoassays now cover most of the core AD biomarkers and are close to practical POC use (Fig. 5). A portable ultrasonic actuator-assisted, mL optimized AuNPs lateral flow and microfluidic system uses ultrasound pre-enrichment followed by colorimetric detection of tau in plasma, achieving a LOD of 10.30 pg mL^{-1} with a total assay time of about 20 min and a dynamic range of 0.02–4 ng mL^{-1} (Fig. 5**A**) [66]. Anti-Aβ42 monoclonal lateral-flow immunoassay (LFI) resolves Aβ42 monomers and oligomers in under 30 min with 154 pg mL^{-1} LOD (Fig. 5**B**) [67]. A paper-based LFI using AuNPs colorimetry enabled the detection of fetuin B and clusterin within ~15 min, with LOD of 0.24 nM and 0.12 nM, respectively (Fig. 5**C**) [118]. An entropy-driven catalysis-enabled LFI achieved a LOD of 1.01 pM for miRNA-16 within a total assay time of ~45 min [119]. These assays use disposable strips, capillary flow, and either visual or smartphone-compatible colorimetric readouts, making them intrinsically compatible with decentralized testing once reagents, sample handling, and calibration are standardized. Dual-readout colorimetric plus SERS strips improve sensitivity for plasma p-tau396 and p-tau404 to 3.8 pg mL^{-1} via SERS, while maintaining a <20 min workflow and visual backup at 60 pg mL^{-1} [120]. SERS-LFA using nanotags can be extended to multiplex panels for Aβ42, Aβ40, tau, and NfL in the fg mL^{-1} regime [121]. In contrast, paper-based ELISA for Aβ42 reports 63.04 pg mL^{-1} in buffer and ~10–100 pg mL^{-1} in plasma within 1.5 h [122]. A droplet microfluidic magnetic immunoassay with optional capillary isoelectric focusing (CIEF) processes CSF in ~45 min for eight replicates with 0.5–1 nM LOD and 10–15 nM dynamic range [123]. Paper-based ELISA for Aβ42, magnetic droplet immunoassays with optional CIEF, and conventional sandwich ELISAs for NfL achieve good analytical performance but remain essentially laboratory methods because they require multi-step pipetting, CSF collection, or benchtop optics and microfluidics. At the same time, amplification-free optical digital immunoassays based on single-molecule arrays provide the current analytical benchmark for blood-based AD panels: multiplex Simoa assays quantify Aβ40, Aβ42, p-tau181, GFAP, and NfL in plasma with LOD of about 4.08, 1.51, 0.338, 11.6, and 1.6 pg mL^{-1}, respectively, while related Simoa HD X assays for p-tau217 and p-tau231 reach LOD near 0.04 pg mL^{-1} and digital ELISA for TNF-α achieves about 150 aM (2.5 fg mL^{-1}) LOD (Fig. 5**D**) [124–128]. These systems deliver fg mL^{-1} sensitivity and automated multiplexing but rely on complex fluidics, multi-hour workflows, and benchtop instruments, so they currently function as centralized reference platforms rather than portable POCT devices.

To convert lateral flow and paper-based optical assays into robust POCT tools, several concrete modifications are required. First, formats that currently depend on CSF or ultrasound pre-treatment should be re-engineered for fingerstick or venous blood, with on-strip plasma separation, chemical release steps, and preconcentration incorporated into a single sealed cartridge. Second, quantitative operation must rely on low-cost readers, for example, smartphone attachments for colorimetry or compact Raman modules for SERS, combined with on-board calibration curves, internal standards, and lot-specific QR codes for strip compensation. Third, multiplex panels for Aβ isoforms, tau species, NfL, and inflammatory markers should use spectral or Raman coding, with physical layouts that minimize cross-talk and fixed mL-based decision thresholds defined before clinical validation [129]. Fourth, manufacturing workflows for AuNPs, SERS nanotags, and antibodies require tight control of size, surface chemistry, and conjugation ratios, along with accelerated stability testing under high-temperature, high--humidity conditions to support ambient shipping and storage. Finally, clinical validation must move beyond buffer-based testing to large, multi-site cohorts using matched serum, plasma, saliva, and urine, and

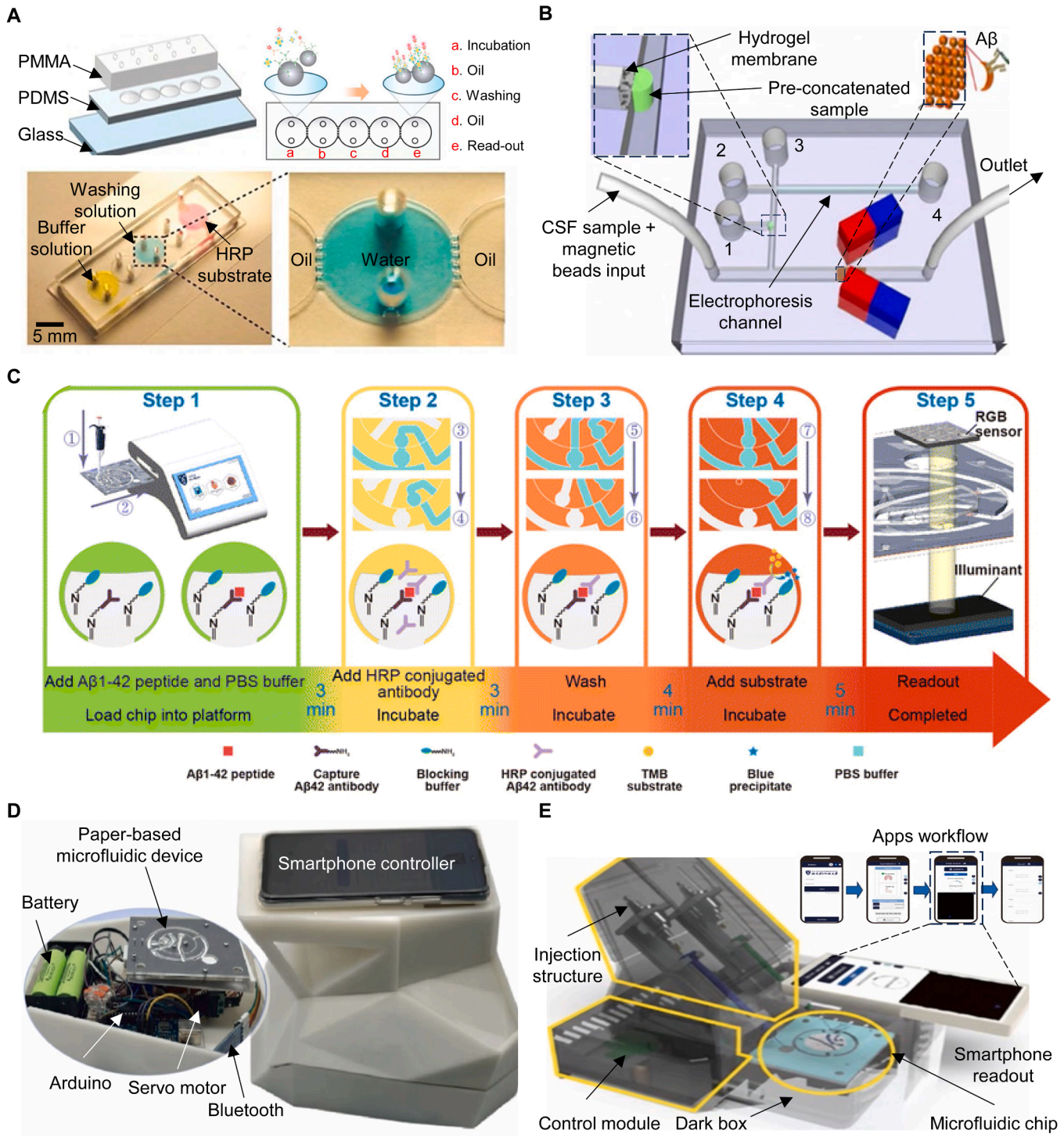

Fig. 6. Microfluidic and LOC optical immunoassays. A Droplet microfluidic magnetic bead immunoassay for Aβ. Printed with permission from Ref. [130]. Copyright © 2015 Elsevier. **B** Integrated immunocapture with hydrogel-based preconcentration in a microchip and fluorescence readout for rapid enrichment and separation of multiple Aβ peptides. Printed with permission from Ref. [132]. Copyright © 2015 AIP Publishing. **C** Smartphone-assisted chemiluminescent paper-based microfluidic ELISA enabling compact imaging and quantitative signal extraction. Printed with permission from Ref. [137]. Copyright © 2025 Elsevier. **D** AI-enhanced smartphone-controlled chemiluminescent microfluidic ELISA for Aβ42 with deep-learning-based image analysis. Printed with permission from Ref. [135]. Copyright © 2024 Elsevier. **E** Rotary-valve or automated paper-based microfluidic ELISA that integrates capture, washing, and imaging steps in a compact cartridge. Printed with permission from Ref. [136]. Copyright © 2025 Royal Society of Chemistry.

harmonize reference ranges with digital immunoassay standards. With these improvements, LFA and paper-strip formats can deliver reliable triage, longitudinal tracking, and rule-in confirmation in clinics and homes. At the same time, advanced optics remain optional for confirmatory sensitivity in centralized settings. Ultrasensitive protein quantification by digital immunoassay provides strong clinical performance

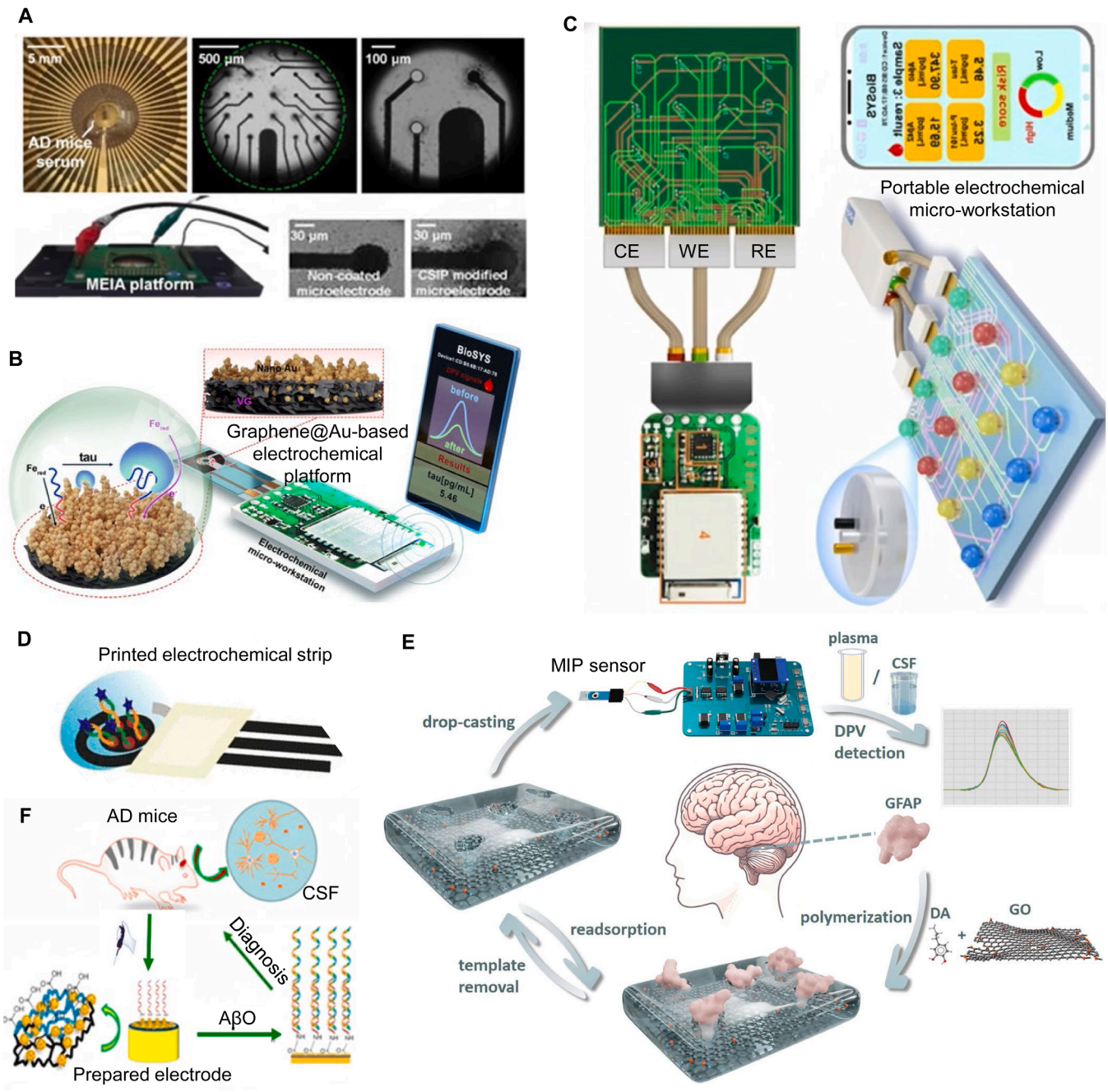

Fig. 7. Electrochemical sensing. A Multichannel microelectrode immunosensor array for serum Aβ40 and Aβ42 quantification with short incubation. Reproduced from Ref. [76]. (Printed with permission under the Creative Commons CC BY 4.0 license). **B** Portable graphene-based paper-electrode aptasensor for tau with an integrated micro-workstation and phone-linked reporting for near-patient readout. Reproduced from Ref. [77] (Printed with permission under the Creative Commons CC BY 4.0 license). **C** Miniaturized electrochemical microarray panel with small serum volumes and app-based output. Reproduced from Ref. [62]. Copyright © 2022 Springer Nature. **D** Printed electrochemical strip format, supporting low-cost disposable testing in buffer and serum. Reproduced from Ref. [75] (Printed with permission under the Creative Commons CC BY 4.0 license). **E** Self-powered enzymatic amperometric platform, exemplified by an acetylcholinesterase-based design that enables low-power plasma testing. Printed with permission from Ref. [147] (Printed with permission under the Creative Commons CC BY 4.0 license). **F** Receptor-protein or whole-cell electrochemical MIP biosensor for selective recognition of GFAP. Printed with permission from Ref. [81]. Copyright © 2019 American Chemical Society.

for plasma p-tau and related biomarkers but relies on benchtop analyzers rather than portable units.

3.2.1.4. Microfluidic and LOC immunoassays. Microfluidic and LOC architecture provides a complementary route to POC AD diagnostics, combining optical readout with automated fluid handling and on-chip preprocessing. Droplet-based magnetic bead ELISA with LED detection has been used to quantify multiple Aβ isoforms (Aβ1–40, Aβ1–42, Aβ2–40, and Aβ5–40) in CSF within about 45 min, with LOD on the order of 0.5–1 nM and dynamic ranges up to about 10 nM [123]. A related magnetic bead droplet microfluidic ELISA resolves oligomeric Aβ in 10% diluted serum in about 40 min, achieving LOD near 10.7 pg mL^{-1} in buffer and 20.2 pg mL^{-1} in serum over a 12.5–200 pg mL^{-1} dynamic range (Fig. 6**A**) [130]. Additional microfluidic formats target Aβ42 in plasma using a PDMS-integrated quartz crystal microbalance with a 100 pM LOD [131], or integrate immunocapture, hydrogel-based

preconcentration, and microchip electrophoresis with fluorescence detection to enrich a panel of Aβ peptides (Aβ37, Aβ39, Aβ40, Aβ42) from CSF in less than 30 min with more than 90% capture efficiency (Fig. 6**B**) [132]. Although not specific to AD, microfluidic gradient generators with paper-based channels and fluorescence readout, and chips that combine Ag or Au nanocomposites with SERS for serum protein detection, illustrate that low-cost disposable microfluidic cartridges can be coupled to colorimetric, fluorescence, or Raman optics for rapid, near-patient analysis [133,134].

Recent AI-enhanced platforms move these concepts closer to deployable POCT systems (Fig. 6**C-E**). Smartphone-controlled sandwich chemiluminescent ELISA on paper-based μPAD, assisted by a YOLOv5 deep learning model for image analysis, detects Aβ42 in artificial plasma in less than 30 min with a 10.07 pg mL^{-1} LOD over a 1–1000 pg mL^{-1} dynamic range [135]. Smartphone-assisted chemiluminescent μPADs and rotary valve paper-based ELISAs provide further examples, delivering tau or Aβ42 readouts from artificial plasma in about 15–30 min with LOD of 26.1 and 9.6 pg mL^{-1}, respectively, while automating capture, washing, and imaging steps in a compact cartridge [136,137]. Collectively, these microfluidic and optics-based systems demonstrate that AD-relevant biomarkers can be measured from small-volume serum, plasma, or CSF with sub-hour turnaround time, integrated sample processing, and digital quantification. To translate them into routine POCT tools, future efforts should prioritize operation with minimally processed fingerstick blood, full integration of plasma separation and preconcentration on chip, robust smartphone or handheld readers for fluorescence, chemiluminescence, or SERS, and clinical validation in multi-site cohorts that benchmark performance against centralized digital immunoassay platforms.

3.2.2. *Electrochemical sensing systems*

Electrochemical sensing platforms for AD biomarkers translate target recognition at an electrode surface into measurable changes in current, impedance, potential, or capacitance. Compared with spectrophotometric assays, electrochemical readouts use low-cost, miniaturizable electronics and can achieve high sensitivity in clinically relevant fluids such as CSF, plasma, and saliva. In this section, we summarize recent advances in electrochemical AD sensing systems, focusing on immunosensors and aptamer sensors, molecularly imprinted polymer sensors, enzymatic electrochemical assays, and whole-cell or receptor-based biosensors, and we organize these examples by their dominant readout mode.

3.2.2.1. Immunosensors and aptamer-based sensors. Electrochemical immunosensors and aptamer-based sensors (aptasensors) are close to POCT devices because they convert molecular recognition (antibody or aptamer recognition) into measurable electrical changes on screen-printed, microarray, or microfluidic electrodes using small sample volumes and short workflows. Screen-printed or microarray electrodes, nanostructured transducers, and aptamer or antibody capture enable detection from pg mL^{-1} to fg mL^{-1} in small serum volumes with short assay times. Across reported AD targets, the most common transduction modes are impedimetric readouts by electrochemical impedance spectroscopy and voltammetric readouts, including differential pulse voltammetry (DPV), square-wave voltammetry (SWV), and stripping voltammetry, whereas potentiometric and capacitive formats are less consistently demonstrated on these platforms. Impedimetric sensing has been applied to Aβ oligomers in blood-derived matrices on printed electrodes with pM-scale sensitivity [138]. For multi-analyte panels, a conductive silk fibroin immunoparticle multichannel microelectrode immunosensor array quantified Aβ40 and Aβ42 in serum with LOD of 6.63 pg mL^{-1} and 3.74 pg mL^{-1} and a 10 min incubation (Fig. 7**A**) [76], while a superwettable vertical graphene (VG@Au) microdroplet immunosensor measured Aβ40, Aβ42, tau, and p-tau181 from 5 μL serum with sub-pg mL^{-1} LODs in about 1 h and demonstrated portability [139]. Portable voltammetric designs further extend sensitivity and connectivity, including a VG@Au paper-electrode aptasensor for tau with LOD 0.034 pg mL^{-1} and phone-linked reporting through a micro-workstation (Fig. 7**B**) [77], a hairpin competitive aptamer sensor for Aβ40 with LOD 7.14 pg mL^{-1} in an approximately 30 min workflow [140], and a mini-pillar electrochemical microarray for Aβ40, Aβ42, tau, and p-tau181 that achieved 0.089–0.176 pg mL^{-1} LOD from 10 μL serum in under 1 h with app-based output (Fig. 7**C**) [62]. Printed platforms support scale and low-cost deployment, including an AuNPs-printed electrochemical strip for miRNA-29a with sub-nanomolar detection in buffer and serum (Fig. 7**D**) [75] and a screen-printed electrochemical sensor array integrated with a custom microprocessor front end, Bluetooth connectivity, and anodic stripping voltammetry readout, validated on IL-8 with a planned transition to early AD blood targets [141]. Additional formats address low-abundance targets and complex matrices, including an interdigitated microelectrode system with signal cancellation and amplification that reached 100 fg mL^{-1} for Aβ42 using medium-change microfluidics [142], a tau aptamer sensor on Au/ITO with femtomolar sensitivity in plasma within 60 min [143], and an on-chip magnetic-bead immunoassay for ApoE with stripping voltammetry that reported quantitative results in under 1 h in a disposable format [144]. In addition to serum-based platforms, wearable electrochemical architectures are beginning to extend AD detection into interstitial fluid (ISF), enabling minimally invasive longitudinal monitoring. A fully integrated wearable electrochemical sensing patch combining a hollow microneedle sampling system with nanogold-modified VG@Au electrodes achieved in situ detection of p-tau181 and p-tau217 in interstitial fluid (ISF) with LOD of 0.058 pg mL^{-1} and 0.079 pg mL^{-1}, respectively, using DPV and a miniaturized on-board electrochemical workstation with Bluetooth transmission [145]. The VG@Au nanostructure enhanced electron transfer kinetics and provided a high surface area for antibody immobilization, enabling a dual-working electrode configuration within a wearable microneedle platform. These findings demonstrate that electrochemical immunosensors can transition from benchtop validation to fully integrated, wearable POCT systems capable of real-time AD biomarker monitoring.

Key barriers remain, and a concrete POCT roadmap specific to electrochemistry needs to be defined. First, matrix effects in serum or plasma, including albumin and lipoproteins, heterophile antibodies, and hemolysis-related species, can cause baseline drift and nonspecific electrochemical signals, necessitating antifouling surface chemistries and cartridge-level sample conditioning to maintain analytical performance. Adopt antifouling chemistries, such as zwitterionic or PEG-like monolayers on gold or carbon, including on-electrode blockers. Incorporate inline dilution or on-electrode depletion to maintain LOD reported in buffer when moving to neat or minimally processed serum [62,76,77]. Second, batch variation of printed electrodes and nanostructured films can limit calibration transfer. Standardize inks and curing, move to roll-to-roll or stencil processes with in-line impedance quality control (QC), and add per-cartridge calibration pads to correct for lot shift at the POC [62,138]. Third, sensitivity improvements often rely on fragile nanomaterial stacks. Favor robust architectures such as vertical graphene with thin Au or Au-decorated carbon that survive drying, shipping, and finger-stick application without reconditioning [77,139]. Fourth, complete the transition for the reader from benchtop potentiostats to sealed palm-sized readers. Integrate amperometry, DPV, and SWV into a single battery device with fixed current ranges, auto-zero routines, and on-board temperature sensing, then pair it with a locked mobile app for guided steps, QC checks, and encrypted results [62,77]. Fifth, design true sample-to-signal cartridges for 10–50 μL capillary blood or 100–500 μL urine that meter sample, route through a single-use cell, and sequester waste, with dried reagents that meet 12-month stability at 25–37 °C. Sixth, improve decision reliability with electrochemical tools only. Use ratiometric outputs, such as dual redox couples or internal reference channels; incorporate duplex or quadplex

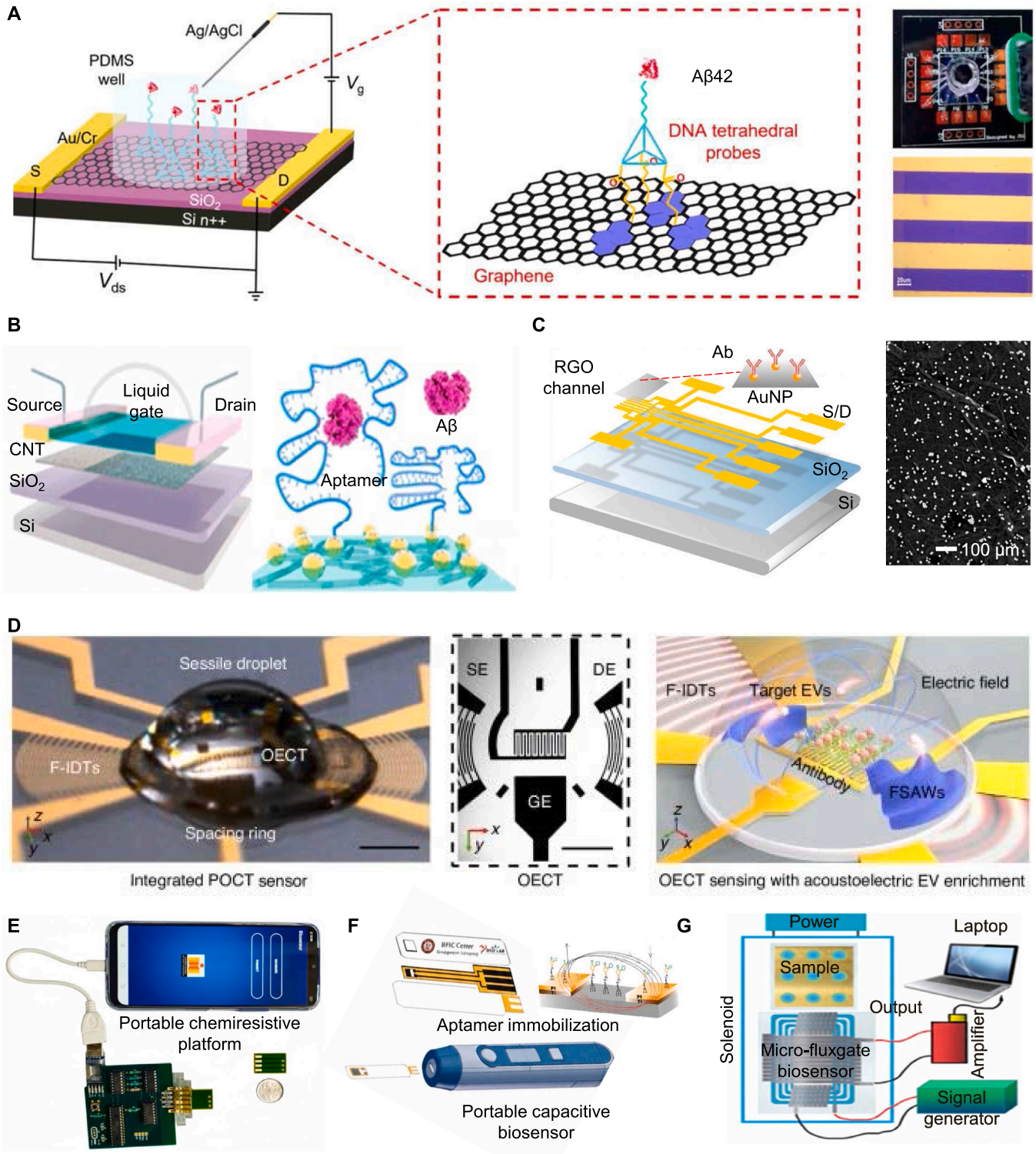

Fig. 8. Electronic sensing. **A** Graphene FET with DNA tetrahedral probes for Aβ42. Reproduced from Ref. [155] (Printed with permission under the Creative Commons CC BY 4.0 license). **B** Liquid-gated CNT-FET with aptamer recognition of Aβ species. Reproduced from Ref. [156]. Copyright © 2022 American Chemical Society. **C** Transistor-based electronic biosensing architecture illustrating device-level integration for label-free signal transduction. Reproduced from Ref. [159]. Copyright © 2023 American Chemical Society. **D** Solution-gated FET for tau quantification. Printed with permission from Ref. [161] (Printed with permission under the Creative Commons CC BY 4.0 license). **E** Portable, smartphone-interfaced electronic reader illustrating user-facing measurement and data acquisition. Printed with permission from Ref. [171]. Copyright © 2021 Elsevier. **F** Interdigitated capacitive aptamer-antibody sensor for Aβ oligomers. Printed with permission from Ref. [172].Copyright © 2022 Elsevier. **G** Compact magnetic bead-tag biosensing workflow for portable detection. Printed with permission from Ref. [174] (Printed with permission under the Creative Commons CC BY 4.0 license).

panels on the same card for Aβ40, Aβ42, or tau forms; and embed on-cartridge positive and negative controls to flag interference [62,76,142]. Finally, execute prospective clinical studies against reference methods with pre-registered cut points, external quality controls, and trans-site validation to support regulatory clearance. Following these sensor-specific steps will convert the current high analytical performance into reliable, affordable, and fully portable electrochemical POCT for AD screening and monitoring.

3.2.2.2. Molecularly imprinted polymer-based sensors. Molecularly imprinted polymers (MIPs) are synthetic polymers that have molecular memory (sometimes referred to as cavities) for a specific target analyte. They are typically synthesized by stoichiometrically mixing the monomers, cross-linkers, and target analyte molecules, followed by polymerization (with trapped analytes) and analyte removal. The cavities, left after analyte removal, act as artificial antibodies, enabling highly selective capture of analyte molecules in electrochemical transducers [146]. Unlike biological probe-based systems, MIPs offer certain advantages, such as long-term stability, high reproducibility, and reusability, making them suitable for POCT implementation. Recently, Li et al. demonstrated a reduced graphene oxide/polydopamine (rGO/PDA) MIP-based POC electrochemical sensor for the detection of GFAP, an astrocytic cytoskeletal protein and a discriminative biomarker for a range of neurological diseases, including AD. The POC sensor was fabricated by functionalizing a carbon-based screen-printed electrode (SPCE, DRP-110, Metrohm) with rGO/PDA MIPs and tested using DPV on a custom analog front-end (Fig. 7**E**). It achieved a sensitivity of 2.13 μA/log (ag mL^{-1}) and a LOD of 754.5 ag mL^{-1} in buffer samples with an assessed imprinting factor of 2.8. The performance of the POC sensor was validated using human plasma and CSF samples [147]. Similarly, another work by Arjun et al. reported the synthesis of a polyphenol red-polypyrrole (pPhR-pPy) composite MIP, its integration onto a highly porous gold (hPG)-coated PCB electrochemical transducer, and a custom-developed wireless handheld potentiostat for the detection and quantification of p-tau181 in plasma. The sensor achieved LOD and sensitivity of 498 fg mL^{-1} and 8.99 μA pg^{-1} mL^{-1}, respectively, in buffer samples with an area under the ROC curve (AUC) of 0.84 in clinical samples. Biofouling, signal instability, and scalability challenges, well-known in electrochemical transducers, were addressed by integrating an hPG electrode, a custom-designed potentiostat, and mL-driven data analytics [148]. More recently, kynurenic acid (KYNA), a newly emerging biomarker for early AD detection, has also been quantified using a PEDOT MIP on a glassy carbon modified transducer with copper-silver bimetallic structures (Cu-Ag BS/GC). The sensor quantified KYNA in a wide linear range of 1.0 fM-500 nM with an LOD of 0.278 fM. It was finally validated with fetal bovine serum (FBS) and human serum samples. It showed a high recovery rate of 100.66±0.57% for the detection of KYNA in human serum, with a relative standard deviation (RSD) of 2.83 across three measurements [149].

Overall, these studies highlight the promise of MIP-based electrochemical platforms for ultrasensitive, label-free POC detection of AD biomarkers, but several challenges remain before widespread clinical translation. Key issues include biofouling and signal drift in complex biofluids, potential cross-reactivity and template leakage that can compromise specificity, and the need for reproducible large-scale fabrication of nanostructured MIP-electrode interfaces on low-cost transducers (SPCEs/PCBs). The integration of highly porous or nanostructured electrodes (rGO/PDA, hPG, PEDOT/Cu-Ag), anti-fouling surface chemistries, and robust custom electronics, as well as mL-assisted signal processing, already points to viable strategies for stabilizing responses and compensating for noise and matrix effects at the POC. Going forward, combining these advances with standardized imprinting protocols, on-chip sample preparation, and multiplexed MIP arrays for simultaneous quantification of panels such as GFAP, p-tau181, and KYNA, along with commonly known Aβ40, Aβ42, and other tau biomarkers, will be crucial to deliver clinically reliable, scalable MIP-based POCT devices for early AD detection.

3.2.2.3. Enzymatic and receptor-based sensors. Enzymatic amperometric biosensors convert a biochemical reaction into a measurable current, typically by using an immobilized enzyme to generate or consume an electroactive species at the electrode, enabling compact electronics and rapid signal transduction for POCT workflows [150,151]. A representative example is a self-powered acetylcholine sensor that integrates an acetylcholinesterase-based anode into a miniature enzymatic fuel cell for on-site plasma testing, illustrating how amperometry can support low-power, portable measurement architectures [150]. However, enzymatic formats often face limitations that are consequential for POCT translation, including enzyme instability during storage and temperature excursions, dependence on cofactors and dissolved oxygen, susceptibility to electroactive interferents in complex biofluids, and calibration drift caused by biofouling or gradual loss of catalytic activity [150,152]. In parallel, receptor-based biosensors and whole-cell-based biosensors aim to improve biochemical selectivity by leveraging biologically evolved binding interfaces, such as receptor domains or disease-relevant binding proteins, and then read out binding-induced changes via potentiometric or impedimetric transduction (Fig. 7**F**) [81]. Receptor-based strategies have demonstrated strong promise for distinguishing toxic Aβ oligomers using cellular prion protein (PrP^{C})-derived probes on impedance platforms, including hydrogel-supported electrodes and highly conductive composite interfaces that amplify changes in charge-transfer resistance [81]. Despite these advances, impedance and potentiometric implementations frequently require stringent control of surface chemistry and matrix effects, and practical studies sometimes rely on pre-processing steps such as medium exchange or aggressive noise cancellation to reach clinically relevant plasma sensitivity, which complicates truly simple POC operation [142,153]. Whole-cell-based biosensors can, in principle, provide functional readouts of receptor engagement in a native membrane context, but their POC deployment is hindered by requirements for cell viability, batch-to-batch variability, biosafety and containment, and limited shelf-stability in low-resource settings [154]. Moving forward, POCT translation will benefit from engineered, stable receptor fragments with oriented immobilization, antifouling, and self-referencing electrode designs that reduce drift, non-faradaic or redox-probe-free impedance strategies when feasible, and cartridge-level integration of sample handling (for example, plasma separation) with disposable electrodes and handheld readers, followed by multi-site clinical validation against standardized reference materials.

3.2.3. Electronic sensing systems

Electronic sensing systems meet this need by converting biomolecular recognition at functionalized transducers into electrical signals that can be measured with compact, low-power instrumentation, enabling rapid, label-free readout in small sample volumes without bulky optics. In this section, we summarize three electronic POC-relevant platform families, including field-effect transistor (FET) and organic electrochemical transistor biosensors using antibody, aptamer, and nanostructure-enabled interfaces, single-molecule nanopore sensors based on ionic current perturbations in biological or solid-state pores, and capacitive and magnetic modalities that quantify binding through interfacial capacitance shifts or magnetic bead tags with portable electronics.

3.2.3.1. Aptamer, antibody, and nanostructure-enabled FET. Electronic sensing systems, such as FETs, already demonstrate POCT-friendly performance for the detection and quantification of AD biomarkers in clinically relevant samples. Graphene and CNT field-effect devices achieve very low LODs in small serum volumes within short assay times.

Fig. 8**A** shows that a tetrahedral DNA nanostructure-modified graphene FET (TDN G-FET) measured Aβ42 in serum in under 5 min at 5 aM with a practical range up to 500 pM [155]. A CNT thin-film FET with floating-gate aptamers detected Aβ42 or Aβ40 in undiluted serum with an LOD of 50 aM and stable device-to-device variation under 10% (Fig. 8**B**) [156]. A label-free solution-gated FET (SGFET) reported a lower LOD of 10 fg mL^{-1} for p-tau217, with a linear response over four orders of magnitude [157]. Extended-gate FETs quantified kinase activity relevant to AD at 1 pg mL^{-1} and across a wide dynamic range [158]. Graphene electrolyte-gated transistors also targeted neuron-derived exosomal Aβ42 at 447 ag mL^{-1} across six orders of magnitude (Fig. 8**C**) [159]. A microfluidic organic electrochemical transistor (OECT) with a charge-repulsion membrane detected Aβ aggregates at ≈ 2 fM from 1 μL of serum [160], and an acoustoelectric OECT enriched EVs to reach a practical limit near 500 particles per mL with saturation in about two minutes (Fig. 8**D**) [161]. These FET and OECT biosensors demonstrate high performance in detecting key AD biomarkers including Aβ42, Aβ40, and tau, with a dynamic operating concentration range, a key aspect for quantifying longitudinal changes in patient samples.

3.2.3.2. Single-molecule nanopore sensors. Nanopore sensors are another emerging class of single-molecule detection devices that can perform highly sensitive detection of biomolecules by measuring disturbances in ionic current as biomolecules pass through nanopores. Biological nanopores, such as α-hemolysin (α-HL) and aerolysin, have been reported for the multiplex screening of AD and related biomarkers, including Aβ40, p-tau381, alpha-1 antitrypsin (AAT), and β-site amyloid precursor protein cleaving enzyme 1 (BACE1) via a length-encoded triple-helix molecular switch with femtomolar limits and six-decade linearity [162,163]. While studies quantifying AD biomarkers using nanopores are limited, the α-HL nanopore has recently been shown to quantify Aβ42, APP(669–711), and Aβ40 at concentrations as low as 2.1 pM, 1.5 pM, and 627 fM, respectively, in serum samples [164]. Unlike FETs, biological nanopore sensors pose challenges for POCT implementation due to the need for specialized expertise and infrastructure, their chemical and mechanical fragility, environmental dependence, and limited shelf life. Solid-state nanopores (SSNs) offer significant advantages over biological nanopores, including high chemical and mechanical resistance. SSNs are being demonstrated for plug-and-play POCT [165]. They have been adapted for the detection of neurotransmitters such as dopamine, histamine, and acetylcholine [166], but they remain largely unexplored for AD biomarker analysis in clinical samples. Recently, stimuli-responsive copolymer (PNI-TP-SA-AQZ)-functionalized glass nanopores have been used to directly detect Aβ monomers and Zn^{2+} in the brains of mice with AD.

Nevertheless, challenges remain in integrating plug-and-play FET or nanopore systems for user-friendly "sample-to-answer-out" POCT workflows. Complex matrices introduce nonspecific adsorption, drift, and pore fouling. These envisioned POCT systems can benefit from robust antifouling and charge-balanced passivation on gates and nanopores, including active washing or buffer-exchange steps that do not require benchtop instruments, with on-device temperature sensing capabilities to reduce baseline drift. Replacing patch-clamp rigs and lab potentiostats with low-noise application-specific integrated circuit (ASIC) front ends and fixed-range current amplifiers inside a sealed palm-sized reader can simplify user operation [167]. Single-use cartridges can be designed to meter 10–50 μL of finger-prick blood or 1 mL saliva, to perform on-cartridge preconcentration if needed, and isolate waste. For nanopore sensors, incorporate anti-clogging mechanisms, reference channels, and ratiometric decision rules to ensure calls remain stable across different batches. Standardize calibration by adding built-in reference features, for example, a reference gate for biosensing FET (arrays) or an internal nanopore reference [165,168–170] and by locking acquisition settings to reduce operator variability [155,158]. Embedding edge analytics for event detection, artifact rejection, and drift correction on the reader or phone, with encrypted reports and QC flags, can further strengthen nanopore-based POCT workflows. Finally, prospective clinical studies against serum reference methods, using pre-specified cut points for Aβ and p-tau, should be conducted to verify lot-to-lot stability for up to 12 months at 25 °C. With these targeted steps, electronic sensors, including nanopore formats, can move from high-performance demonstrations to reliable, low-step POCT for AD screening and monitoring.

3.2.3.3. Capacitive, magnetic, and piezoelectric sensors for antibody and aptamer recognition. Capacitive sensing provides an electrical route to AD POCT by converting biomolecular binding at functionalized electrodes into changes in interfacial capacitance, enabling compact, low-power instrumentation without bulky optics. Across the three studies, blood-accessible amyloid biomarkers are targeted, including plasma Aβ40 and Aβ42 (Fig. 8**E**) [171], as well as Aβ42 oligomers detected in human plasma samples, including those from patients, supporting minimally invasive sampling. An interdigitated capacitive platform integrating Aβ oligomer aptamer and anti-Aβ oligomer antibody reports a rapid, real-time response on the order of seconds. It achieves ultralow LOD with a wide dynamic range (Fig. 8**F**) [172]. In contrast, a non-Faradaic capacitive strategy at an antibody-functionalized nanohybrid interface on an ITO micro-disk electrode eliminates the need for redox probes. It is positioned as POCT compatible with sub-fg mL^{-1} sensitivity in diluted human serum [173]. Portable electronics and smartphone-based interfacing further illustrate a feasible route to user-facing, decentralized readout [171]. At the same time, translation to routine POCT requires managing limitations that are intrinsic to interfacial capacitance measurements, including non-specific adsorption and electrode fouling in complex biofluids, baseline drift and low-frequency noise, sensitivity to ionic strength and temperature, and parasitic capacitances introduced by packaging and wiring that can degrade quantitative reproducibility across devices and over time. Collectively, these studies indicate that scalable electrode geometries, high-affinity aptamer and antibody layers, and portable acquisition can enable capacitive POCT. Still, it will depend on robust anti-fouling surface chemistries, standardized functionalization and regeneration, and calibration strategies that stabilize performance in real clinical matrices [171–173].

Magnetic sensing offers a complementary electrical modality by translating immunorecognition into a bead-tag readout, where antibodies or aptamers capture targets (for example, Aβ or tau), immunomagnetic beads label the complexes, and compact magnetometers (fluxgate, magnetoresistive, Hall, giant magneto-impedance, or SQUID formats) quantify the beads' stray magnetic field so the signal scales with target concentration. A representative micro-MEMS fluxgate example uses a sandwich immunoassay on an Au film substrate with antibody-conjugated magnetic beads as tags, reports a sensor response within 5 s, and completes the full assay in under 30 min, supporting a speed and miniaturization pathway relevant to portable testing (Fig. 8**G**) [174]. Practical constraints, however, include the need for an external magnetizing field and tightly integrated, low-noise readout electronics, because non-integrated signal-conditioning loops can limit true portability, as well as assay-level challenges such as bead handling steps, variability in bead loading or aggregation, and sensitivity to magnetic background and sensor alignment that can impact signal-to-noise and repeatability. In this example, the target is C-reactive protein (CRP), which has been reported to have biological links to amyloid pathology through interactions between altered CRP conformations and Aβ, as well as inflammatory signaling associated with CRP state changes [175]. Yet population-level associations between CRP and cognitive outcomes remain mixed, and Mendelian randomization has reported that higher genetically determined CRP is associated with reduced AD risk, underscoring that magnetic POCT translation depends not only on sensor

integration and workflow simplification but also on careful biomarker selection and clinical interpretation within multi-biomarker panels.

Recent advances in wearable bioelectronic systems demonstrate that miniaturized electronic platforms can extend beyond detection to directly modulate AD-related pathology. A conformal honeycomb-array ultrasonic patch integrating flexible piezoelectric transducers, a miniaturized drive circuit, and wireless control achieved spatiotemporally controllable focused ultrasound delivery across the skull, promoting Aβ depolymerization and improving cognitive function in AD mouse models [176]. The system exhibited stable ultrasonic focusing, targeted energy localization in the hippocampal region, reduction of amyloid plaque burden, and modulation of microglial polarization toward an anti-inflammatory phenotype, while maintaining biosafety and conformal scalp attachment. Although therapeutic rather than diagnostic, this work highlights how compact, wearable electronic architectures evolve toward integrated sensing intervention frameworks for decentralized AD management. Overall, electronic platforms, including FETs, nanopores, capacitive, and magnetic systems, demonstrate that compact, low-power, label-free architectures can achieve ultrasensitive AD biomarker detection. With continued advances in antifouling surface engineering, cartridge-level integration, ASIC-based readout electronics, and prospective clinical validation, these systems are positioned to support scalable, decentralized POCT for early AD screening, longitudinal monitoring, and potentially future closed-loop management strategies.

4. Perspectives and outlook for POCT in early AD diagnosis

POCT-based approaches for early AD diagnosis have advanced substantially in recent years, driven primarily by progress in sensing technologies. Nevertheless, several critical bottlenecks remain, including constraints in analytical sensitivity, challenges in reagent stability, limitations in quantitative accuracy, and restricted multiplexing capability. In this section, we discuss future directions for POCT in early AD diagnosis, focusing on identifying more informative biomarkers, adopting more accessible and scalable sample matrices, and emerging system-level strategies, including representative ongoing efforts from our group.

4.1. Discovery of novel and highly sensitive biomarkers

Although a wide variety of pathological indicators have been proposed for the early diagnosis and population screening of AD, those that are genuinely compatible with POCT technologies remain confined mainly to molecular biomarkers, such as NA, proteins, and metabolites [177]. In CSF, the absolute concentrations of molecular biomarkers, including Aβ42, Aβ40, p-tau231, p-tau181, p-tau217, GFAP, and NfL, as well as derived concentration ratios (e.g., Aβ42/40, p-tau231/Aβ42, p-tau181/Aβ42, and GFAP/p-tau217), have been shown to provide valuable information for diagnosis, disease staging, and treatment monitoring [178]. Emerging and more accessible biofluids, such as blood and saliva, also contain these biomarkers. However, their substantially lower abundance, together with the complexity of sample pre-treatment, makes it challenging for current POCT platforms to achieve reliable and reproducible detection [179]. Therefore, beyond engineering strategies to enhance target enrichment and signal amplification, the discovery of novel biomarkers with higher diagnostic reliability, greater sensitivity to early-stage disease, improved specificity, and lower detection complexity is essential for advancing POCT-based AD diagnostics.

The pathological mechanisms of AD are highly complex, involving multiple interconnected processes, including protein misfolding, autophagy dysfunction, mitochondrial impairment, dysregulated lipid metabolism, and cerebrovascular dysfunction. Consequently, close collaboration with physician-scientists is indispensable. With extensive clinical and research experience, physician-scientists are well-positioned to detect subtle changes in biomarker profiles and concentrations and to integrate these findings with mechanistic insights into AD pathophysiology. Such interdisciplinary efforts can facilitate the identification of candidate biomarkers that offer higher sensitivity, greater abundance, or reduced detection complexity for POCT applications. A representative example is the collaborative work led by Koichi Tanaka and Katsuhiko Yanagisawa. Using immunoprecipitation, they isolated a long-overlooked plasma peptide, APP669–711, which can serve as an internal reference [180]. By calculating the concentration ratio of APP669–711 to Aβ42 and quantifying it using mass spectrometry, they achieved diagnostic performance comparable to that of PET imaging. This advance substantially improved the feasibility of early AD screening using small blood volumes.

4.2. Alternative and easily collectible sample sources

The types and concentrations of biomarkers present in the human body directly reflect underlying physiological and pathological states [181]. Accordingly, monitoring these biomarkers is critical for early disease diagnosis and screening, treatment evaluation, and prognosis prediction. Importantly, for the same disease and biomarker, measured concentrations can vary substantially across biological sample sources. Such variation is determined by the intrinsic characteristics of physiological transport, distribution, and clearance processes [182]. For example, in the diagnosis of AD, CSF is considered the gold-standard sample source. As a neurodegenerative disorder, AD is closely associated with pathological changes in brain tissue, and CSF is in direct contact with the brain microenvironment. As a result, AD-related biomarkers can be detected in the CSF, where they are present at relatively high concentrations, making them easier to detect [183]. However, CSF sampling requires lumbar puncture, an invasive and technically demanding procedure that causes patient discomfort and is therefore unsuitable for POCT applications. In contrast, blood sampling is considerably simpler and less invasive. Blood also contains many of the same AD-related biomarkers found in CSF, making it an attractive sample source for POCT applications [184]. However, due to the presence of the blood-brain barrier, the abundance of these biomarkers in blood is substantially lower than in CSF. In addition, these biomarkers are subject to degradation and peripheral clearance, which significantly increases the difficulty of reliable detection [185].

POCT technologies must satisfy two fundamental requirements: ease of sample collection and high reliability of analytical results [57]. Accordingly, if AD biomarkers can be reliably detected in easily accessible fluids such as saliva, tears, urine, earwax, or nasal secretions, POCT for early AD diagnosis and large-scale screening could be substantially advanced. Recent studies have shown that, in individuals in the early stages of AD, saliva exhibits abnormalities in Aβ, tau, and miRNA levels, as well as a marked decrease in lactoferrin [186–189]. Urine has been reported to contain elevated levels of biomarkers such as AD7c-NTP, formic acid, and 8-OHdG [190–192]. Tears have also been reported to exhibit abnormal Aβ and tau species [193]. Earwax has been found to accumulate volatile organic compounds (VOCs), lipid oxidation products, and stress hormones, which may serve as indicators of AD risk [194]. Additionally, nasal secretions have been reported to contain Aβ and p-tau [195]. Although these alternative matrices may involve more variable sample composition, additional pre-analytical handling, and often lower analyte abundance than CSF, they nonetheless open new avenues for non-invasive AD assessment, particularly when coupled with robust sample preparation and highly sensitive sensing strategies.

From a POCT translation perspective, it is critical to assess whether these emerging, non-traditional biomarkers in accessible matrices have progressed beyond preliminary association studies toward functional POCT or POCT-oriented prototypes. We therefore compare their analytical sensitivity, clinical validation, and POCT readiness in Table 3. As summarized therein, POCT studies on these emerging biomarkers remain at an early stage, yet they suggest practical features that could

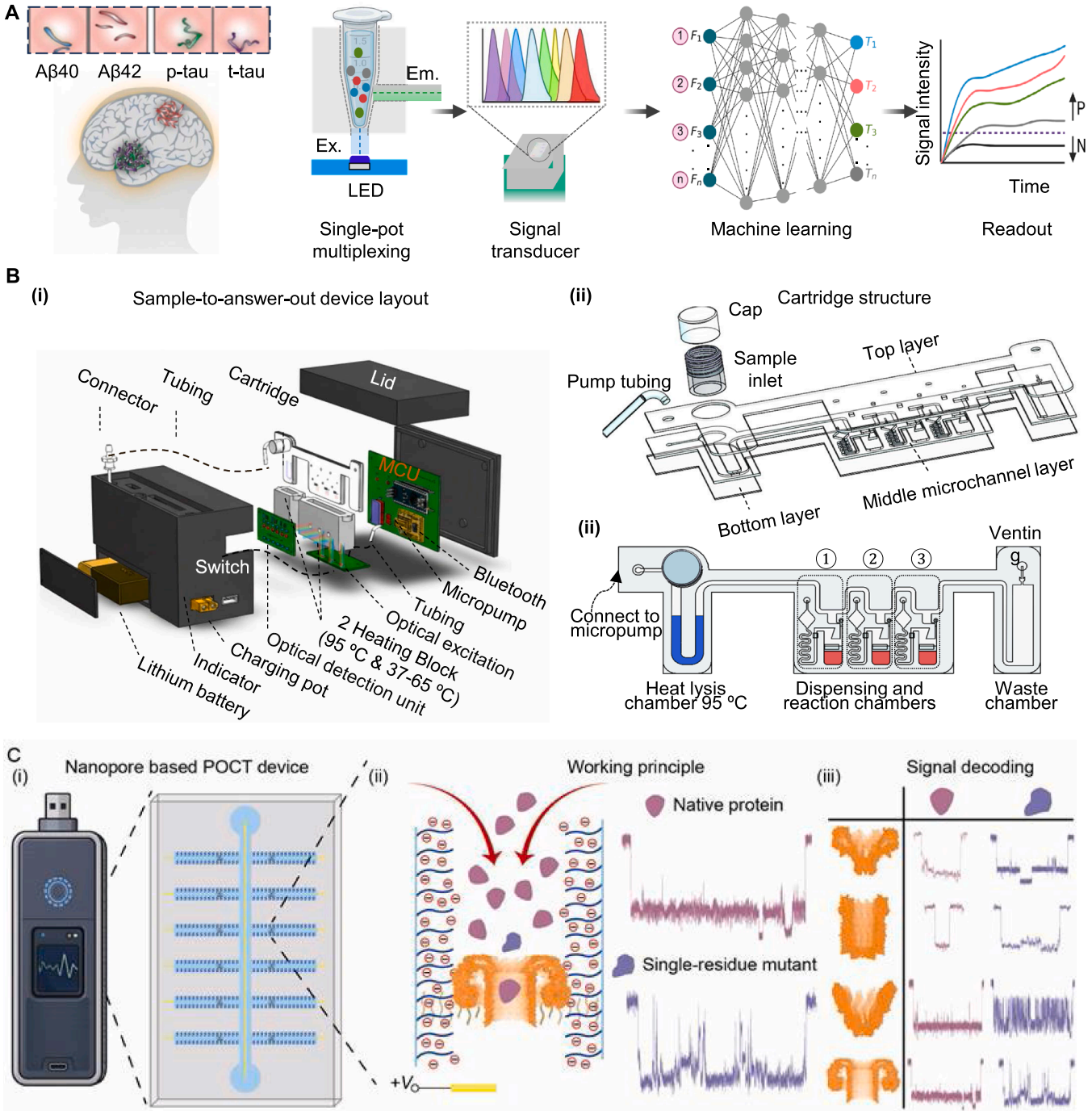

Fig. 9. Engineering roadmap for scalable, multiplex POC diagnostics for AD. A Single assay multiplex readout and AI interpretation. Multiple targets are measured in a single reaction; the signal is detected using optics, and the results are mapped into a compact multi-feature signal space. Afterward, a trained model outputs per-target probabilities and a final positive, negative, or indeterminate call. **B** Integrated sample-to-answer-out device architecture. A portable reader and disposable microfluidic cartridge automate sample handling, reagent delivery, timing, and signal acquisition in a closed workflow, reducing user steps and contamination risk. Printed with permission from Ref. [64]. Copyright © 2023 American Chemical Society. **C** Schematic of a portable nanopore-based POCT platform. A microfluidic chip integrating four structurally distinct biological nanopores is used to enhance target capture via electroosmotic flow and generate characteristic single-molecule current signatures. Cross-validation across multiple nanopores enables reliable discrimination of protein heterogeneity, including native proteins and single-residue mutants.

complement conventional Aβ and tau assays. Many reported prototypes focus on small molecules or redox-active species, which are naturally suited to electrochemical readouts. These formats are compact and low-cost, and in some cases, can avoid the most demanding biorecognition and ultralow-concentration quantification requirements often associated with Aβ and p-tau measurements in peripheral matrices. For example, KYNA has been measured using both competitive displacement amperometric immunosensing and direct oxidation voltammetry, achieving pg mL^{-1} sensitivity in CSF and serum or nM sensitivity in saliva, with proof-of-concept testing in small clinical sample sets [196, 197]. Along similar lines, oxidative-stress-related biomarkers in urine, such as 8-OHdG, have been implemented via direct electrochemical

oxidation and competitive lateral flow immunostrips, reporting nM-level LODs together with initial measurements in human urine [198, 199]. Beyond analytical feasibility, these targets may provide information that is not captured by the Aβ or tau axis, while leveraging accessible matrices such as saliva, urine, and breath that are well-suited for frequent, low-burden sampling. In parallel, proteins outside the canonical AD panel have begun to appear in POCT-oriented devices, including salivary lactoferrin, α-amylase and urinary AD7c-NTP; however, most reports still rely on spiked matrices or limited cohorts, highlighting the need for larger and better-characterized clinical validation [112,200, 201,202]. Synthetic recognition approaches may further ease assay development by reducing dependence on biological reagents, as illustrated by a MIP-based electrochemical sensor for formic acid [203]. At present, this example has only been evaluated in a model buffer, underscoring matrix transferability as a key bottleneck for several metabolite readouts. For VOC-based AD sensing, exhaled breath analysis has been implemented using portable metal-oxide-semiconductor (MOS) sensor arrays that enable real-time, broad-range VOC fingerprint profiling. Proof-of-concept testing in human cohorts (AD, n = 15; controls, n = 44) demonstrated the feasibility of noninvasive patient discrimination. However, because these approaches rely on pattern recognition rather than molecule-specific quantification, analytical metrics such as LOD and linear range are typically not reported, and clinical validation remains preliminary [204]. Collectively, these early demonstrations suggest that non-traditional targets could broaden AD POCT beyond Aβ and tau by enabling simpler assay chemistries, more flexible sampling, and complementary pathophysiological readouts. Their translation will ultimately depend on standardized sample handling, systematic evaluation and mitigation of matrix interferences, and appropriately powered clinical studies.

4.3. Enhancing single-pot multiplex readout

Accurate and timely molecular diagnostics are central to modern disease control; however, most current platforms remain single-target and laboratory-bound [205]. These limitations create a persistent gap between laboratory-grade testing and the need for rapid, multi-target detection at the POC [13]. Multiplex assays that interrogate several targets in a single reaction represent a crucial step toward closing this gap (Fig. 9**a**) [206], since they can identify multiple analytes in parallel, reduce sample volume, shorten turnaround time, and streamline clinical workflows and public health response [207]. In the context of AD, multiplex biomarker detection is critical because no single marker can capture the heterogeneous and multistage biology of the disease. Alzheimer's pathology involves interacting processes that include amyloid and tau deposition, neurodegeneration, synaptic dysfunction, inflammation, and vascular injury, and many patients present with mixed dementias. Measuring several biomarkers in parallel from one small sample improves diagnostic sensitivity and specificity, helps distinguish AD from other dementias, supports staging and prognosis, and enables monitoring of treatment response, while also reducing sample volume, assay time, and cost at the POC. However, existing diagnostic pathways remain constrained by practical and biological limitations. Clinical rating scales are subjective and relatively insensitive to early or mild disease, requiring specialist interpretation. Structural MRI typically reveals cortical atrophy only after substantial neurodegeneration and does not, on its own, distinguish AD from other dementias. PET imaging, including amyloid and tau tracers, provides pathology-specific readouts but requires radiotracers and specialized infrastructure, incurs high cost and radiation exposure, and is primarily restricted to tertiary centers. FDG-PET reflects altered brain metabolism but lacks specificity for AD, can be confounded by comorbid conditions, and is not suitable for large-scale screening or frequent longitudinal monitoring. Therefore, there is an urgent need for simplified, scalable molecular technologies that enable the detection of multiple Alzheimer's biomarkers in a single assay at the POC. Future improvements are likely to include high-throughput panels that jointly quantify amyloid, tau, synaptic injury, inflammation, and vascular damage within a single assay, ideally from non-invasive or minimally invasive samples such as saliva, tears, or comparable biofluids, thereby supporting repeated, longitudinal testing in both clinical and community settings.

4.4. Integrated sample-to-answer-out optical platform

Sample preparation and analyte concentration remain major bottlenecks for POCT. Sensitive and reproducible detection at the POC requires workflows that preserve sample integrity, minimize manual handling, and reduce operational complexity for non-expert users. Conventional platforms typically involve multiple manual steps, including collection, lysis, biomarker extraction, reagent loading, and transfer between separate modules, which increase variability, contamination risk, and training requirements. A user-friendly instrumentation platform that standardizes these operations within a closed, automated format is therefore essential for broader adoption in decentralized settings. Autonomous microfluidic chip operation, including on-chip, in-house reagent actuation and reaction control without an external controller, could further increase efficiency and reliability in the sample-to-answer-out workflow [208]. Such self-contained cartridges reduce system complexity, lower power demand, and minimize user steps, which is particularly important for home and community deployment. Fig. 9**B** illustrates a fully integrated saliva-based self--testing platform that follows the sample-to-answer-out concept, in which an integrated micro-pump delivers reagents to a detection chamber containing the target. The disposable microfluidic cartridge accepts an unprocessed saliva sample for an NA assay. It automates the thermal lysis of viral particles at approximately 95 °C, followed by sample metering and distribution, NA amplification using isothermal chemistries such as RT-LAMP, RCA, or RPA at 37–65 °C, and real-time optical readout using integrated colorimetric or fluorescence sensors. A companion reader module controls temperature and timing, performs on-board signal acquisition and digitization, and interfaces with a smartphone application that interprets results and reports them. The cartridge, which can be fabricated from low-cost laminated PMMA or similar thermoplastics, remains closed throughout the assay, contains the waste stream, and requires only a few minutes of hands-on time. The same design principles apply directly to multiplex AD testing, whether the targeted biomarkers are NA- or protein-based. For saliva-based panels, preconcentration and matrix conditioning can often be integrated into the same cartridge architecture. When biomarker panels are extended to blood or serum, additional front-end operations become essential, including plasma separation and the efficient extraction of low-abundance NAs and proteins from complex matrices. These steps can be implemented using antibody- or aptamer-functionalized magnetic beads or nanostructured capture surfaces, followed by automated washing and controlled elution into downstream reaction chambers. In magnet-based designs, a programmable robot magnet translates bead clusters through spatially separated reservoirs to perform capture, washing, and elution. In pump-based designs, integrated peristaltic or diaphragm pumps route samples and reagents across fixed capture zones patterned within the cartridge. In addition to micro-pump and magnet guided architectures, liquid handling in integrated AD cartridges can be implemented using capillary driven (using burst valves and siphon valves, porous polymer membranes), blister actuated reagent pouches, pneumatic membrane valves, or centrifugal disc formats which together provide a broad design space for automated sample routing, metering, and mixing across both NAT and immunoassay workflows. In all formats, the extraction module can be positioned upstream of AD assays to maintain high recovery and compatibility. Parallel detection chambers can then interrogate multiple biomarkers and internal controls within a single run. Multi-wavelength fluorescence or multiplex colorimetric detection, combined with on-board or edge mL, can resolve partially overlapping emission spectra, compensate for matrix effects, and

convert raw signals into per-analyte qualitative or quantitative calls with associated confidence metrics and indeterminate zones. By integrating these functions into a compact, closed-cartridge reader system, future sample-to-answer-out platforms for AD can preserve sample integrity, reduce the need for skilled personnel, and enable high-throughput, decentralized molecular and immunological testing across outpatient clinics, primary care settings, and home-monitoring environments.

4.5. Development of a nanopore-based POCT platform

Increasing evidence suggests that AD-related protein biomarkers, such as Aβ and p-tau species, can undergo substantial conformational changes when the chirality of specific amino acid residues is altered [209]. These conformationally modified molecules may act as seed species, influencing the aggregation behavior of related molecular populations and ultimately driving the progressive formation of amyloid plaques and NFTs that underline AD pathology [4,14,28]. The ability to detect such seed molecules at an extremely early stage would therefore be of great significance for the early diagnosis of AD. However, the absolute abundance of these seed molecules is exceedingly low [210]. In conventional bulk measurement techniques, such as NMR, circular dichroism spectroscopy, or cryo-electron microscopy (cryo-EM), the signals from non-seed molecules are completely overshadowed. They may even fall below the system noise level, rendering detection and identification extremely challenging [211].

Nanopore single-molecule technology offers a compelling solution to this challenge. Much like a high-resolution camera, nanopore sensing can provide detailed structural information at the single-molecule level. At the same time, statistical analysis of large numbers of translocation events reveals the proportion of molecules in distinct conformational states, making it an ideal tool for probing molecular heterogeneity [212]. Furthermore, the inherent working principle of nanopores enables tight integration of molecular sensing and signal readout within palm-sized, portable devices, making this technology particularly well-suited for POCT applications. Nevertheless, the reliable detection of extremely rare seed molecules using nanopores remains a formidable challenge.

Our ongoing work addresses this challenge by integrating four structurally distinct biological nanopores into a single microfluidic chip, thereby constructing an orthogonal nanopore-target sensing matrix (Fig. 9**C**). As a fundamental principle of physics, structure dictates function, and nanopores exploit this relationship for molecular recognition. Accordingly, the same molecule produces distinct signal patterns in different nanopores, while different molecules generate distinct patterns within the same nanopore. The use of a nanopore sensing matrix, therefore, dramatically expands the overall event dataset while enabling intrinsic cross-validation among translocation events. When coupled with mL-based signal classification, this approach is expected to enable reliable identification and observation of rare seed molecules. To further enhance molecular capture rates and thereby improve overall system sensitivity, we have functionalized the microfluidic channels supporting the nanopores with a high density of charged polymer chains. Under an applied electric field, this modification generates strong electroosmotic flow, thereby facilitating molecular capture by the nanopores. Compared with established ultrasensitive immunoassay platforms such as Simoa and Elecsys, as well as LFA, which rely on antibody-mediated target recognition and downstream signal readout, our nanopore approach follows a different principle. It interrogates individual molecules through physicochemical interactions with the nanopore and, therefore, can be sensitive to structural heterogeneity and conformational variants without requiring a pre-existing, conformation-specific antibody. This feature is particularly relevant for seed-like species whose pathogenic forms may not be fully characterized, where immunoassays remain highly sensitive for known targets but may offer limited discrimination unless dedicated reagents are developed. We anticipate that this platform could serve as a complementary pillar for early AD diagnosis, particularly in the context of single-molecule POCT and population screening.

4.6. Integration with digital health technologies

Digital health technologies are now central to AD research and care for screening, diagnosis, and longitudinal monitoring. Ambient, wearable, and app-based platforms capture cognition, daily function, mobility, sleep, language, and behavior, often through multimodal sensor networks that stream data to secure cloud platforms. Experience with COVID-19 and Mpox has shown that mobile apps, connected sensors, cloud databases, and AI analytics can be combined to build end-to-end digital surveillance pipelines at a national scale. Similar architecture can integrate cognitive, behavioral, physiological, and molecular data for AD, allowing portable devices in clinics, community sites, pharmacies, and homes to upload multiplex assay readouts and metadata for remote review, longitudinal tracking, and population-level analysis, while enabling secure software and algorithm updates. Key limitations include dependence on stable power and network infrastructure and the challenge of managing data volume, storage, and analytics.

AI provides the control-and-interpretation layer for these systems. mL models can denoise and validate raw sensor streams, enforce device-specific quality thresholds, trigger recalibration or repeat measurement when quality degrades, and fuse multimodal data from wearables, ambient sensors, and imaging into feature sets suitable for diagnosis and monitoring. Ultra-sensitive platforms such as graphene FETs and wearable electrochemical patches often exhibit device-to-device variability that can obscure biological signals [213]. mL models, including neural networks (NN), can extract invariant features directly from raw sensor outputs, reducing the need for extensive device-specific calibration and improving robustness across hardware batches. Beyond signal correction, AI enables multi-biomarker integration. Because individual blood biomarkers such as Aβ40, Aβ42, p-tau181, or p-tau217 may show limited diagnostic performance in isolation, backpropagation NN, convolutional NN, and related architectures can analyze combined biomarker panels to improve accuracy, precision, and recall. Studies have shown that integrating multiple molecular features within an AI framework significantly enhances classification performance compared with single marker thresholds [214]. AI models further support staging and grading of disease across clinically relevant categories, including health control, subjective cognitive decline, MCI, and AD. Multi-biomarker NN models have reported diagnostic accuracy exceeding 90% for multi-class grading, demonstrating feasibility for early risk stratification in decentralized settings. Importantly, explainable AI approaches such as SHAP (SHapley Additive exPlanations) analysis reveal that models often leverage subtle, previously underutilized regions of full sensor response curves rather than relying solely on peak amplitude or single time point metrics [213]. This full curve exploitation improves performance while offering mechanistic insight into biosensor behavior under clinical conditions. For lightweight neuroimaging modalities such as electroencephalography, functional near-infrared spectroscopy, retinal imaging, and portable ultrasound, AI can enable point-of-care deployment by reconstructing low-signal data, segmenting neural or retinal structures, quantifying atrophy or perfusion, and stratifying early AD risk. Computer vision models applied to images or video can convert raw pixels, for example, of gait or facial expression, into standardized quantitative metrics that support reproducible and regulatory-grade evidence. Embedded processors or edge modules can perform real-time classification and quantification, then generate a plain-language report and a visual display with color-coded classes, calibrated analyte thresholds, confidence indicators, and an indeterminate zone, which shortens the path from measurement to clinical decision.

Table 2
Representative stability benchmarks for POCT-relevant AD detection platforms.

Platform Type	Reagent Format	Storage Condition	Shelf Life/Stability	Performance Retention	Ref
Cartridge PCR (e.g., GeneXpert)	Lyophilized beads	2-28 °C	≥12 months	No loss in amplification	[218, 219]
RT-LAMP	Freeze-dried enzymes	37 °C (30 days)	>95% activity retained	C_t shift <0.5	[221]
RT-LAMP	Lyophilized (Microfluidic)	Ambient (Point-of-need)	6 months	Sensitivity (0.42 parasites/μL) matches benchtop	[222]
CRISPR	Freeze-dried enzymes	25-30 °C	>95% activity (4 weeks)	concordance >99% vs. fresh	[220]
LFI	Dried (Nitrocellulose)	25-30 °C	12-24 months	<10% signal reduction	[223, 224]

4.7. Field readiness and deployability

Field readiness refers to consistent analytical and operational performance in realistic care settings. In contrast, deployability refers to the practical ability to place a system in clinics, community sites, or homes with reliable operation, maintenance, and service. A significant constraint on both is reliance on a cold chain for the storage and transport of enzymes and buffers that require very low temperatures to remain stable. In NAT systems, enzymes and buffers are vulnerable to hydrolysis and thermal inactivation. In protein-based immunoassays targeting Aβ and tau, antibodies and enzymatic reporters such as horseradish peroxidase (HRP) or alkaline phosphatase (AP) are similarly prone to denaturation during liquid storage, when stored in liquid at room temperature or 4 °C due to aggregation and surface adsorption [215,216]. Electrochemical and chemiluminescent platforms face additional risks from oxidation and moisture exposure [217].

Several NAT assay components are already commercially available as lyophilized powders, partially alleviating this requirement. Building on this concept, our goal is to develop an in-house lyophilized formulation that combines primers, enzymes, and reaction buffers into a single stable, ready-to-use reagent for field deployment. Reagent stability, particularly for enzyme- and luminol-based chemistries, often requires on-cartridge drying, robust oxygen barriers, and a verified shelf life of at least 12 months at 25–37 °C. Stabilizing excipients, such as trehalose, will be incorporated to preserve enzyme activity during freeze-drying. Cartridge-based PCR platforms such as Cepheid GeneXpert employ lyophilized reagent beads validated for storage at 2 to 28 °C, thereby eliminating strict cold-chain requirements [218,219]. Lyophilized CRISPR-Cas12 and RT-LAMP assays report retention of greater than 95% enzymatic activity after 30 days at 37 °C and stability for 3 to 6 months at ambient temperatures [220–222]. Comparative analyses show that lyophilization typically produces less than 5% variation in amplification efficiency relative to fresh liquid reagents, with Ct (time to cross threshold) shifts below 0.5 cycles when stabilizers such as trehalose or sucrose are incorporated. In protein-based systems, dried LFA routinely achieves 12 to 24 months' shelf lives at 25 °C, with less than 10% reduction in binding affinity or signal intensity under desiccated packaging [223,224]. Plasma Aβ42 has been reported to decrease by more than 15% within 6 to 24 h at room temperature, increasing the risk of false negative results if pre-analytical handling is not tightly controlled [215,225]. Therefore, reagent stabilization is not merely a logistical improvement but a technical requirement to ensure analytical reliability in decentralized settings. These representative stability benchmarks across NAT, CRISPR-based systems, and LFI are summarized in Table 2, highlighting the temperature tolerance, shelf life, and performance retention achieved by current POCT-relevant platforms.

The lyophilization protocol will begin with controlled freezing at +4 °C, followed by gradual cooling to −45 °C to promote uniform ice crystal formation. Primary drying will be performed at −40 °C under vacuum to sublimate ice, and secondary drying at +25 °C will remove residual moisture while maintaining enzymatic function. The resulting lyophilized product will be stored at −20 °C and reconstituted with nuclease-free water immediately before use. This strategy is expected to increase portability, reduce dependence on cold-chain logistics, and improve the operational readiness of the multiplex AD assay for on-site diagnostics [226]. Building on these precedents, future AD POCT platforms should target validated shelf lives of at least 12 months at 25 to 30 °C (Zone IVb climatic conditions) [227]. To achieve this goal, standard internal reference reagents for Aβ peptides require a specialized lyophilization protocol. Because Aβ peptides are prone to self-aggregation during the freezing interface, the protocol must employ flash freezing (e.g., using liquid nitrogen or pre-cooled blocks at −196 °C) rather than slow shelf freezing to minimise ice crystal size and prevent freeze-concentration-induced oligomerisation [228]. The formulation must incorporate stabilizing excipients tailored to the physicochemical properties of each biomarker. Lyoprotectants such as trehalose or sucrose should be used at optimized molar ratios (typically >300:1 sugar-to-protein) to replace water molecules and preserve native structure through hydrogen bonding during drying [229]. For Aβ standard internal reference reagents, pre-treatment with high-pH solvents (e.g., NaOH) or hexafluoroisopropanol (HFIP) prior to lyophilization is necessary to maintain monomeric peptide states and reduce aggregation risk [230]. For tau and p-tau standard internal reference reagents, inclusion of reducing agents such as dithiothreitol (DTT) or Tris(2-carboxyethyl)phosphine (TCEP) helps prevent disulfide-linked dimerization during storage. In general, for protein lyophilization, the lyophilization cycle should include primary drying at −40 °C under vacuum (<100 mTorr) to sublimate ice, followed by secondary drying at approximately +25 °C to reduce residual moisture content below 2% [227,231]. Maintaining low residual moisture is essential to achieve a polymer glass transition temperature (T_g) above 50 °C, thereby preserving stability under elevated ambient temperatures [231,232]. Final products should be packaged in moisture-barrier materials with desiccants to support field deployment and minimize cold-chain dependence. In parallel, consumables should be supplied as sealed, traceable units with integrated controls. The end-to-end workflow should require only a few steps, from fingerstick blood or saliva collection to result generation, within 15 to 20 min. For deployment at scale, robust service logistics, secure remote software updates, and clear instructions for use are required, together with a predefined plan for algorithm updates that preserves validated clinical claims.

4.8. Engineering roadmap toward regulatory-ready AD POCT

To translate AD detection into practical, scalable POCT platforms, four parallel workstreams should be prioritized. First, develop true sample-to-answer-out cartridges that accept 10–50 μL of fingerstick blood, urine, or saliva, rely on capillary-driven flow, use blister pouches and passive valving, and incorporate on-chip plasma separation when required. Second, implement sealed dried-reagent architecture supported by desiccants and trehalose-based stabilization, together with an integrated waste chamber, enabling shipment and storage without reliance on a cold chain. Third, standardize embedded electronics around a single low-cost reader, replacing cameras with fixed optics and photodiodes where feasible, or, for smartphone-based imaging, enforcing controlled illumination with a white-balance reference target. For

Table 3
Emerging non-traditional AD biomarkers: detection strategies, analytical performance, and translational readiness for POCT.

Biomarker	Sample Source	Detection Modality	Analytical Sensitivity	Clinical Validation Status	POCT Development Status	Ref
KYNA	CSF, serum	Amperometric electrochemical immunosensor (competitive displacement)	LOD: 9 pg mL^{-1} (CSF); 62 pg mL^{-1} (serum); LR: 1.4-1.1×10^{4} ng mL^{-1}	Proof-of-concept validation in 6 clinical CSF samples	POCT-oriented prototype	[196]
KYNA	Saliva, serum	Voltammetric electrochemical sensor (direct oxidation of KYNA)	LOD: 3 nM; LR: 0.01-500 μM	Proof-of-concept validation in 10 human saliva samples	POCT-oriented prototype	[197]
Lactoferrin	Artificial saliva	Voltammetric electrochemical aptasensor (binding-induced signal change)	LOD: 0.7 ng mL^{-1}; LR: 0.001-500 μg mL^{-1}	Proof-of-concept validation in spiked artificial saliva samples	Early-stage analytical prototype	[200]
Lactoferrin	Saliva	Voltammetric electrochemical immunosensor (binding-induced signal suppression)	LOD: 25 ng mL^{-1}; LR: 0.005-100 μg mL^{-1}	Proof-of-concept validation in spiked human saliva samples	POCT-oriented prototype	[201]
AD7c-NTP	Urine	Bipolar ECL immunoassay device (self-enhanced ECL emission)	LOD: 0.15 pg mL^{-1}; LR: 1-10^{4} pg mL^{-1}	Proof-of-concept validation in spiked human urine samples	POCT-oriented prototype	[112]
Formic acid	Spiked PBS buffer (model solution)	Voltammetric electrochemical sensor (MIP recognition)	LOD: 0.65 μM; LR: 1-80 μM	Proof-of-concept validation in spiked PBS buffer only	Early-stage analytical prototype	[203]
8-OHdG	Human urine	Voltammetric electrochemical sensor (DPV, direct oxidation of 8-OHdG)	LOD: 0.63 nM; LR: 0.005-2.56 μM and 2.56-20.48 μM	Proof-of-concept validation in human urine samples	POCT-oriented prototype	[198]
8-OHdG	Human urine	Fluorometric LFI (competitive immunostrip, upconversion nanoparticle label)	LOD: 0.05 nM; LR: 0.10-10 nM	Proof-of-concept validation in 4 human urine samples	POCT-oriented prototype	[199]
VOCs	Exhaled breath	MOS-based breath VOC sensor (real-time broad-range VOC profiling)	LOD: NR; LR: NR	Proof-of-concept validation in human breath samples (AD: n = 15; controls: n = 44)	Early-stage analytical prototype	[204]
α-amylase	Saliva	Colorimetric enzymatic biosensor (photometric reflectance readout)	LOD: NR; LR: 10-230 U mL^{-1}	Proof-of-concept validation in 20 human saliva samples	POCT-oriented prototype	[202]

Table abbreviations: LR: linear range; NR: not reported^

electrochemical formats, integrate amperometry or differential pulse voltammetry, and, where enrichment is essential, package ultrasound or surface acoustic wave (SAW) drivers on a compact PCB. Fourth, deploy on-device AI with quantized models, built-in calibration using reference zones, and algorithmic safeguards to reduce lot-to-lot and matrix-driven variability. Each cartridge should include internal positive and negative controls, demonstrate matrix equivalency against matched plasma, and support cloud-optional data reporting. Finally, translation should be completed through prospective clinical studies benchmarked against established comparators, such as Simoa or CLIA-certified immunoassays, with pre-specified cutoffs for Aβ42/Aβ40 and relevant p-tau species, together with external quality control programs. Following this roadmap, the sensitivity and speed demonstrated in μPAD ELISA, mL-optimized LFA, and portable electrochemical sensors can be translated into robust, regulatory-ready POCT platforms for AD screening and longitudinal monitoring, while maintaining low cost and minimal user steps..

5. Conclusion

AD is a chronic and progressive neurodegenerative disorder for which therapeutic options remain limited once clinical symptoms have emerged. Consequently, diagnostic strategies that enable identification of biological risk during preclinical and prodromal stages are central to improving clinical management, risk stratification, and enrolment into preventive trials. This review summarizes recent advances in POCT technologies for early AD detection, spanning optical, electrochemical, NA-based, microfluidic, and single-molecule sensing platforms. Collectively, these approaches demonstrate that clinically relevant sensitivity and specificity can increasingly be achieved in formats compatible with decentralized testing. However, translation remains constrained by challenges in sample handling, biomarker multiplexing, reagent stability, calibration robustness, and large-scale clinical validation. Future progress will depend less on incremental gains in analytical sensitivity and more on system-level integration, including sealed sample-to-answer-out workflows, cold-chain-independent reagents, low-cost readers, and embedded quality control and decision-support algorithms. Addressing these factors will be critical for moving POCT platforms beyond proof-of-concept demonstrations toward reliable tools for population screening and longitudinal monitoring in real-world settings. While this review focuses on AD, the principles discussed are broadly applicable to other chronic and complex diseases, underscoring the potential of POCT to support a shift toward earlier, more accessible, and patient-centered diagnostic paradigms aligned with the future of intelligent and data-driven healthcare systems.

CRediT authorship contribution statement

Weihua Guan: Writing – review & editing, Supervision, Formal analysis, Conceptualization. **Feng Guo:** Writing – review & editing. **Tathagata Pal:** Writing – review & editing, Validation. **Muhammad Asad Ullah Khalid:** Writing – review & editing, Writing – original draft. **Bingyuan Guo:** Writing – review & editing, Writing – original draft, Supervision, Project administration, Methodology, Formal analysis, Conceptualization. **Md. Ahasan Ahamed:** Writing – review & editing, Writing – original draft, Validation, Investigation, Formal analysis, Conceptualization.

Declaration of Generative AI and AI-assisted technologies in the writing process

The authors used generative AI (ChatGPT) to refine the grammar and improve sentence structure for clarity in the original draft.

Declaration of Competing Interest

The authors declare that they have no known competing financial interests or personal relationships that could have appeared to influence the work reported in this paper.

Acknowledgements

This work was partially supported by the National Institutes of Health (R33AI147419) and the National Science Foundation (2528103, 2319913). Any opinions, findings, conclusions, or recommendations expressed in this work are those of the authors and do not necessarily reflect the views of the National Science Foundation and National Institutes of Health.

Data availability

Data will be made available on request.

References

[1] P. Scheltens, B. De Strooper, M. Kivipelto, H. Holstege, G. Chételat, C. E. Teunissen, J. Cummings, W.M. Van Der Flier, Alzheimer's disease, The Lancet 397 (2021) 1577–1590, https://doi.org/10.1016/S0140-6736(20)32205-4.
[2] 2024 Alzheimer's disease facts and figures, Alzheimers Dement. 20 (2024) 3708–3821. https://doi.org/10.1002/alz.13809.
[3] Dementia statistics, Alzheimers Dis. Int. (n.d.). ⟨https://www.alzint.org/about/dementia-facts-figures/dementia-statistics/⟩ (accessed February 27, 2026).
[4] D.J. Selkoe, J. Hardy, The amyloid hypothesis of Alzheimer's disease at 25 years, EMBO Mol. Med. 8 (2016) 595–608, https://doi.org/10.15252/emmm.201606210.
[5] J. Zhang, Y. Zhang, J. Wang, Y. Xia, J. Zhang, L. Chen, Recent advances in Alzheimer's disease: mechanisms, clinical trials and new drug development strategies, Signal Transduct. Target. Ther 9 (2024) 211, https://doi.org/10.1038/s41392-024-01911-3.
[6] R. Lefort, Reversing synapse loss in Alzheimer's disease: rho-guanosine triphosphatases and insights from other brain disorders, Neurotherapeutics 12 (2015) 19–28, https://doi.org/10.1007/s13311-014-0328-4.
[7] J.M. Chandler, W. Ye, X. Mi, E.G. Doty, J.A. Johnston, Potential impact of slowing disease progression in early symptomatic Alzheimer's Disease on patient quality of life, caregiver time, and total societal costs: estimates based on findings from GERAS-US study, J. Alzheimers Dis. 100 (2024) 563–578, https://doi.org/10.3233/JAD-231166.
[8] T.E. Golde, S.T. DeKosky, D. Galasko, Alzheimer's disease: The right drug, the right time, Science 362 (2018) 1250–1251, https://doi.org/10.1126/science.aau0437.
[9] E. Bellou, E. Baker, G. Leonenko, M. Bracher-Smith, P. Daunt, G. Menzies, J. Williams, V. Escott-Price, Age-dependent effect of APOE and polygenic component on Alzheimer's disease, Neurobiol. Aging 93 (2020) 69–77, https://doi.org/10.1016/j.neurobiolaging.2020.04.024.
[10] L.W. Shaughnessy, S. Weintraub, The role of neuropsychological assessment in the evaluation of patients with cognitive-behavioral change due to suspected Alzheimer's disease and other causes of cognitive impairment and dementia, Alzheimers Dement 21 (2025) e14363, https://doi.org/10.1002/alz.14363.
[11] L. Chouliaras, J.T. O'Brien, The use of neuroimaging techniques in the early and differential diagnosis of dementia, Mol. Psychiatry 28 (2023) 4084–4097, https://doi.org/10.1038/s41380-023-02215-8.
[12] J.H. Kang, M. Korecka, E.B. Lee, K.A.Q. Cousins, T.F. Tropea, A.A. Chen-Plotkin, D.J. Irwin, D. Wolk, M. Brylska, Y. Wan, L.M. Shaw, Alzheimer disease biomarkers: moving from CSF to plasma for reliable detection of amyloid and tau pathology, Clin. Chem 69 (2023) 1247–1259, https://doi.org/10.1093/clinchem/hvad139.
[13] K.J. Land, D.I. Boeras, X.-S. Chen, A.R. Ramsay, R.W. Peeling, REASSURED diagnostics to inform disease control strategies, strengthen health systems and improve patient outcomes, Nat. Microbiol 4 (2018) 46–54, https://doi.org/10.1038/s41564-018-0295-3.
[14] H. Hampel, J. Hardy, K. Blennow, C. Chen, G. Perry, S.H. Kim, V.L. Villemagne, P. Aisen, M. Vendruscolo, T. Iwatsubo, C.L. Masters, M. Cho, L. Lannfelt, J. L. Cummings, A. Vergallo, The Amyloid-β pathway in Alzheimer's disease, Mol. Psychiatry 26 (2021) 5481–5503, https://doi.org/10.1038/s41380-021-01249-0.
[15] R.A. Sperling, P.S. Aisen, L.A. Beckett, D.A. Bennett, S. Craft, A.M. Fagan, T. Iwatsubo, C.R. Jack, J. Kaye, T.J. Montine, D.C. Park, E.M. Reiman, C.C. Rowe, E. Siemers, Y. Stern, K. Yaffe, M.C. Carrillo, B. Thies, M. Morrison-Bogorad, M. V. Wagster, C.H. Phelps, Toward defining the preclinical stages of Alzheimer's disease: recommendations from the National Institute on Aging-Alzheimer's Association workgroups on diagnostic guidelines for Alzheimer's disease, Alzheimers Dement 7 (2011) 280–292, https://doi.org/10.1016/j.jalz.2011.03.003.
[16] A. Dumas, F. Destrebecq, G. Esposito, D. Suchonova, K. Steen Frederiksen, Rethinking the detection and diagnosis of Alzheimer's disease: Outcomes of a European Brain Council project, Aging Brain 4 (2023) 100093, https://doi.org/10.1016/j.nbas.2023.100093.
[17] G. Grande, M. Valletta, D. Rizzuto, X. Xia, C. Qiu, N. Orsini, M. Dale, S. Andersson, C. Fredolini, B. Winblad, E.J. Laukka, L. Fratiglioni, D.L. Vetrano, Blood-based biomarkers of Alzheimer's disease and incident dementia in the community, Nat. Med. 31 (2025) 2027–2035, https://doi.org/10.1038/s41591-025-03605-x.
[18] H.W. Querfurth, F.M. LaFerla, Alzheimer's Disease, N. Engl. J. Med. 362 (2010) 329–344, https://doi.org/10.1056/NEJMra0909142.
[19] C.R. Jack, D.A. Bennett, K. Blennow, M.C. Carrillo, B. Dunn, S.B. Haeberlein, D. M. Holtzman, W. Jagust, F. Jessen, J. Karlawish, E. Liu, J.L. Molinuevo, T. Montine, C. Phelps, K.P. Rankin, C.C. Rowe, P. Scheltens, E. Siemers, H. M. Snyder, R. Sperling, Contributors, C. Elliott, E. Masliah, L. Ryan, N. Silverberg, NIA-AA research framework: toward a biological definition of Alzheimer's disease, Alzheimers Dement 14 (2018) 535–562, https://doi.org/10.1016/j.jalz.2018.02.018.
[20] U. Sengupta, A.N. Nilson, R. Kayed, The role of amyloid-β oligomers in toxicity, propagation, and immunotherapy, EBioMedicine 6 (2016) 42–49, https://doi.org/10.1016/j.ebiom.2016.03.035.
[21] B. De Strooper, E. Karran, The cellular phase of Alzheimer's disease, Cell 164 (2016) 603–615, https://doi.org/10.1016/j.cell.2015.12.056.
[22] C.R. Jack, D.S. Knopman, W.J. Jagust, L.M. Shaw, P.S. Aisen, M.W. Weiner, R. C. Petersen, J.Q. Trojanowski, Hypothetical model of dynamic biomarkers of the Alzheimer's pathological cascade, Lancet Neurol 9 (2010) 119–128, https://doi.org/10.1016/S1474-4422(09)70299-6.
[23] E. Karran, M. Mercken, B.D. Strooper, The amyloid cascade hypothesis for Alzheimer's disease: an appraisal for the development of therapeutics, Nat. Rev. Drug Discov 10 (2011) 698–712, https://doi.org/10.1038/nrd3505.
[24] M.D. Weingarten, A.H. Lockwood, S.Y. Hwo, M.W. Kirschner, A protein factor essential for microtubule assembly, Proc. Natl. Acad. Sci. 72 (1975) 1858–1862, https://doi.org/10.1073/pnas.72.5.1858.
[25] Y. Zhang, H. Chen, R. Li, K. Sterling, W. Song, Amyloid β-based therapy for Alzheimer's disease: challenges, successes and future, Signal Transduct. Target. Ther 8 (2023) 248, https://doi.org/10.1038/s41392-023-01484-7.
[26] M.T. Heneka, M.J. Carson, J.E. Khoury, G.E. Landreth, F. Brosseron, D. L. Feinstein, A.H. Jacobs, T. Wyss-Coray, J. Vitorica, R.M. Ransohoff, K. Herrup, S.A. Frautschy, B. Finsen, G.C. Brown, A. Verkhratsky, K. Yamanaka, J. Koistinaho, E. Latz, A. Halle, G.C. Petzold, T. Town, D. Morgan, M. L. Shinohara, V.H. Perry, C. Holmes, N.G. Bazan, D.J. Brooks, S. Hunot, B. Joseph, N. Deigendesch, O. Garaschuk, E. Boddeke, C.A. Dinarello, J.C. Breitner, G. M. Cole, D.T. Golenbock, M.P. Kummer, Neuroinflammation in Alzheimer's disease, Lancet Neurol 14 (2015) 388–405, https://doi.org/10.1016/S1474-4422(15)70016-5.
[27] Y. Chen, Y. Yu, Tau and neuroinflammation in Alzheimer's disease: interplay mechanisms and clinical translation, J. Neuroinflammation 20 (2023) 165, https://doi.org/10.1186/s12974-023-02853-3.
[28] K. Tepper, J. Biernat, S. Kumar, S. Wegmann, T. Timm, S. Hübschmann, L. Redecke, E.-M. Mandelkow, D.J. Müller, E. Mandelkow, Oligomer Formation of Tau Protein Hyperphosphorylated in Cells, J. Biol. Chem 289 (2014) 34389–34407, https://doi.org/10.1074/jbc.M114.611368.
[29] F. Lo Cascio, S. Park, U. Sengupta, N. Puangmalai, N. Bhatt, N. Shchankin, C. Jerez, N. Moreno, A. Bittar, R. Xavier, Y. Zhao, C. Wang, H. Fu, Q. Ma, M. Montalbano, R. Kayed, Brain-derived tau oligomer polymorphs: distinct aggregations, stability profiles, and biological activities, Commun. Biol 8 (2025) 53, https://doi.org/10.1038/s42003-025-07499-w.
[30] M. Barron, J. Gartlon, L.A. Dawson, P.J. Atkinson, M.-C. Pardon, A state of delirium: deciphering the effect of inflammation on tau pathology in Alzheimer's disease, Exp. Gerontol 94 (2017) 103–107, https://doi.org/10.1016/j.exger.2016.12.006.
[31] S. Kazemeini, A. Nadeem-Tariq, R. Shih, J. Rafanan, N. Ghani, T.A. Vida, From plaques to pathways in Alzheimer's disease: the mitochondrial-neurovascular-metabolic hypothesis, Int. J. Mol. Sci. 25 (2024) 11720, https://doi.org/10.3390/ijms252111720.
[32] J.I. Ayers, B.I. Giasson, D.R. Borchelt, Prion-like spreading in tauopathies, Biol. Psychiatry 83 (2018) 337–346, https://doi.org/10.1016/j.biopsych.2017.04.003.
[33] R.M. Ransohoff, M.A. Brown, Innate immunity in the central nervous system, J. Clin. Invest 122 (2012) 1164–1171, https://doi.org/10.1172/JCI58644.
[34] C.-C. Liu, J. Hu, N. Zhao, J. Wang, N. Wang, J.R. Cirrito, T. Kanekiyo, D. M. Holtzman, G. Bu, Astrocytic LRP1 Mediates Brain Aβ Clearance and Impacts Amyloid Deposition, J. Neurosci 37 (2017) 4023–4031, https://doi.org/10.1523/JNEUROSCI.3442-16.2017.
[35] H. Franklin, B.E. Clarke, R. Patani, Astrocytes and microglia in neurodegenerative diseases: Lessons from human in vitro models, Prog. Neurobiol 200 (2021) 101973, https://doi.org/10.1016/j.pneurobio.2020.101973.
[36] F. Rohden, P.C.L. Ferreira, B. Bellaver, J.P. Ferrari-Souza, C.S. Aguzzoli, C. Soares, S. Abbas, H. Zalzale, G. Povala, F.Z. Lussier, D.T. Leffa, G. Bauer-Negrini, N. Rahmouni, C. Tissot, J. Therriault, S. Servaes, J. Stevenson, A. L. Benedet, N.J. Ashton, T.K. Karikari, D.L. Tudorascu, H. Zetterberg, K. Blennow, E.R. Zimmer, D. Souza, P. Rosa-Neto, T.A. Pascoal, Glial reactivity correlates with synaptic dysfunction across aging and Alzheimer's disease, Nat. Commun 16 (2025) 5653, https://doi.org/10.1038/s41467-025-60806-1.
[37] M. Sharma, P. Pal, S.K. Gupta, The neurotransmitter puzzle of Alzheimer's: dissecting mechanisms and exploring therapeutic horizons, Brain Res 1829 (2024) 148797, https://doi.org/10.1016/j.brainres.2024.148797.
[38] Y. Yu, R. Chen, K. Mao, M. Deng, Z. Li, The role of glial cells in synaptic dysfunction: insights into Alzheimer's disease mechanisms, Aging Dis 15 (2024) 459, https://doi.org/10.14336/AD.2023.0718.
[39] S. Thakur, R. Dhapola, P. Sarma, B. Medhi, D.H. Reddy, Neuroinflammation in Alzheimer's disease: current progress in molecular signaling and therapeutics, Inflammation 46 (2023) 1–17, https://doi.org/10.1007/s10753-022-01721-1.
[40] J. Hardy, D.J. Selkoe, The amyloid hypothesis of Alzheimer's disease: progress and problems on the road to therapeutics, Science 297 (2002) 353–356, https://doi.org/10.1126/science.1072994.

[41] C. Haass, D.J. Selkoe, Soluble protein oligomers in neurodegeneration: lessons from the Alzheimer's amyloid β-peptide, Nat. Rev. Mol. Cell Biol 8 (2007) 101–112, https://doi.org/10.1038/nrm2101.
[42] C.C. Conrad, R.K. Daher, K. Stanford, K.K. Amoako, M. Boissinot, M.G. Bergeron, T. Alexander, S. Cook, B. Ralston, R. Zaheer, Y.D. Niu, T. McAllister, A sensitive and accurate recombinase polymerase amplification assay for detection of the primary bacterial pathogens causing bovine respiratory disease, Front. Vet. Sci. 7 (2020), https://doi.org/10.3389/fvets.2020.00208.
[43] H. Hampel, R. Au, S. Mattke, W.M. Van Der Flier, P. Aisen, L. Apostolova, C. Chen, M. Cho, S. De Santi, P. Gao, A. Iwata, R. Kurzman, A.J. Saykin, S. Teipel, B. Vellas, A. Vergallo, H. Wang, J. Cummings, Designing the next-generation clinical care pathway for Alzheimer's disease, Nat. Aging 2 (2022) 692–703, https://doi.org/10.1038/s43587-022-00269-x.
[44] R. Cacace, K. Sleegers, C. Van Broeckhoven, Molecular genetics of early-onset Alzheimer's disease revisited, Alzheimers Dement 12 (2016) 733–748, https://doi.org/10.1016/j.jalz.2016.01.012.
[45] S. Cohen, J. Cummings, S. Knox, M. Potashman, J. Harrison, Clinical trial endpoints and their clinical meaningfulness in early stages of Alzheimer's disease, J. Prev. Alzheimers Dis. 9 (2022) 507–522, https://doi.org/10.14283/jpad.2022.41.
[46] S.E. Polk, F. Öhman, J. Hassenstab, A. König, K.V. Papp, M. Schöll, D. Berron, A scoping review of remote and unsupervised digital cognitive assessments in preclinical Alzheimer's disease, Npj Digit. Med. 8 (2025) 266, https://doi.org/10.1038/s41746-025-01583-5.
[47] O. Hatahet, F. Roser, M.L. Seghier, Cognitive decline assessment in speakers of understudied languages, Alzheimers Dement. Transl. Res. Clin. Interv 9 (2023) e12432, https://doi.org/10.1002/trc2.12432.
[48] T.E. Goldberg, P.D. Harvey, K.A. Wesnes, P.J. Snyder, L.S. Schneider, Practice effects due to serial cognitive assessment: Implications for preclinical Alzheimer's disease randomized controlled trials, Alzheimers Dement. Diagn. Assess. Dis. Monit 1 (2015) 103–111, https://doi.org/10.1016/j.dadm.2014.11.003.
[49] V.L. Villemagne, Amyloid imaging: past, present and future perspectives, Ageing Res. Rev. 30 (2016) 95–106, https://doi.org/10.1016/j.arr.2016.01.005.
[50] M. Schöll, S.N. Lockhart, D.R. Schonhaut, J.P. O'Neil, M. Janabi, R. Ossenkoppele, S.L. Baker, J.W. Vogel, J. Faria, H.D. Schwimmer, G. D. Rabinovici, W.J. Jagust, PET imaging of tau deposition in the aging human brain, Neuron 89 (2016) 971–982, https://doi.org/10.1016/j.neuron.2016.01.028.
[51] M. Chiara, T. Francesca, R. Andrea, S. Domenico, R. Marco, G. Barbara, L. Marika, R. Dino, P.A. Rosario, M. Nicola, S.I. Amato Antonio, MRI in the clinical management of Alzheimer's disease: from early detection to therapy guidance, Curr. Radiol. Rep. 13 (2025) 4, https://doi.org/10.1007/s40134-025-00435-0.
[52] N. Spotorno, O. Strandberg, E. Stomrud, S. Janelidze, K. Blennow, M. Nilsson, D. Van Westen, O. Hansson, Diffusion MRI tracks cortical microstructural changes during the early stages of Alzheimer's disease, Brain 147 (2024) 961–969, https://doi.org/10.1093/brain/awad428.
[53] B. Yu, Y. Shan, J. Ding, A literature review of MRI techniques used to detect amyloid-beta plaques in Alzheimer's disease patients, Ann. Palliat. Med. 10 (2021) 10062–10074, https://doi.org/10.21037/apm-21-825.
[54] H. Zetterberg, K. Blennow, From cerebrospinal fluid to blood: the third wave of fluid biomarkers for Alzheimer's disease, J. Alzheimers Dis. 64 (2018) S271–S279, https://doi.org/10.3233/JAD-179926.
[55] O. Kusoro, M. Roche, R. Del-Pino-Casado, P. Leung, V. Orgeta, Time to diagnosis in dementia: a systematic review with meta-analysis, Int. J. Geriatr. Psychiatry 40 (2025) e70129, https://doi.org/10.1002/gps.70129.
[56] G.-R. Han, A. Goncharov, M. Eryilmaz, S. Ye, B. Palanisamy, R. Ghosh, F. Lisi, E. Rogers, D. Guzman, D. Yigci, S. Tasoglu, D. Di Carlo, K. Goda, R.A. McKendry, A. Ozcan, Machine learning in point-of-care testing: innovations, challenges, and opportunities, Nat. Commun 16 (2025) 3165, https://doi.org/10.1038/s41467-025-58527-6.
[57] M.A. Ahamed, A.J. Politza, T. Liu, M.A.U. Khalid, H. Zhang, W. Guan, CRISPR-based strategies for sample-to-answer monkeypox detection: current status and emerging opportunities, Nanotechnology 36 (2025) 042001, https://doi.org/10.1088/1361-6528/ad892b.
[58] C. Lino, S. Barrias, R. Chaves, F. Adega, P. Martins-Lopes, J.R. Fernandes, Biosensors as diagnostic tools in clinical applications, Biochim. Biophys. Acta BBA - Rev. Cancer 1877 (2022) 188726, https://doi.org/10.1016/j.bbcan.2022.188726.
[59] Md.A. Ahamed, W. Guan, Opportunities and challenges in implementing CRISPR-based point-of-care testing for Monkeypox detection, BioTechniques 77 (2025) 41–45, https://doi.org/10.1080/07366205.2025.2473827.
[60] L. Guo, Y. Zhao, Q. Huang, J. Huang, Y. Tao, J. Chen, H.-Y. Li, H. Liu, Electrochemical protein biosensors for disease marker detection: progress and opportunities, Microsyst. Nanoeng 10 (2024) 65, https://doi.org/10.1038/s41378-024-00700-w.
[61] N. Taparia, K.C. Platten, K.B. Anderson, N.J. Sniadecki, A microfluidic approach for hemoglobin detection in whole blood, AIP Adv 7 (2017) 105102, https://doi.org/10.1063/1.4997185.
[62] Y. Liu, Z. Huang, Q. Xu, L. Zhang, Q. Liu, T. Xu, Portable electrochemical micro-workstation platform for simultaneous detection of multiple Alzheimer's disease biomarkers, Microchim. Acta 189 (2022) 91, https://doi.org/10.1007/s00604-022-05199-4.
[63] B. Bénéteau-Burnat, P. Pernet, A. Pilon, D. Latour, S. Goujon, A. Feuillu, M. Vaubourdolle, Evaluation of the GEM® Premier™ 4000: a compact blood gas CO-Oximeter and electrolyte analyzer for point-of-care and laboratory testing, Clin. Chem. Lab. Med. 46 (2008), https://doi.org/10.1515/CCLM.2008.043.
[64] Z. Tang, J. Cui, A. Kshirsagar, T. Liu, M. Yon, S.V. Kuchipudi, W. Guan, SLIDE: saliva-based SARS-CoV-2 self-testing with RT-LAMP in a mobile device, ACS Sens 7 (2022) 2370–2378, https://doi.org/10.1021/acssensors.2c01023.
[65] J. Budd, B.S. Miller, N.E. Weckman, D. Cherkaoui, D. Huang, A.T. Decruz, N. Fongwen, G.-R. Han, M. Broto, C.S. Estcourt, J. Gibbs, D. Pillay, P. Sonnenberg, R. Meurant, M.R. Thomas, N. Keegan, M.M. Stevens, E. Nastouli, E.J. Topol, A. M. Johnson, M. Shahmanesh, A. Ozcan, J.J. Collins, M. Fernandez Suarez, B. Rodriguez, R.W. Peeling, R.A. McKendry, Lateral flow test engineering and lessons learned from COVID-19, Nat. Rev. Bioeng 1 (2023) 13–31, https://doi.org/10.1038/s44222-022-00007-3.
[66] S. Wang, Y. Zhu, Z. Zhou, Y. Luo, Y. Huang, Y. Liu, T. Xu, Integrated ultrasound-enrichment and machine learning in colorimetric lateral flow assay for accurate and sensitive clinical alzheimer's biomarker diagnosis, Adv. Sci. 11 (2024) 2406196, https://doi.org/10.1002/advs.202406196.
[67] L. Zhang, X. Du, Y. Su, S. Niu, Y. Li, X. Liang, H. Luo, Quantitative assessment of AD markers using naked eyes: point-of-care testing with paper-based lateral flow immunoassay, J. Nanobiotechnology 19 (2021) 366, https://doi.org/10.1186/s12951-021-01111-z.
[68] J.R. Sempionatto, J.A. Lasalde-Ramírez, K. Mahato, J. Wang, W. Gao, Wearable chemical sensors for biomarker discovery in the omics era, Nat. Rev. Chem 6 (2022) 899–915, https://doi.org/10.1038/s41570-022-00439-w.
[69] W. Huang, Q. Yang, J. Liao, S. Ramadan, X. Fan, S. Hu, X. Liu, J. Luo, R. Tao, C. Fu, Integrated Rayleigh wave streaming-enhanced sensitivity of shear horizontal surface acoustic wave biosensors, Biosens. Bioelectron 247 (2024) 115944, https://doi.org/10.1016/j.bios.2023.115944.
[70] H. Kim, J.U. Lee, S. Song, S. Kim, S.J. Sim, A shape-code nanoplasmonic biosensor for multiplex detection of Alzheimer's disease biomarkers, Biosens. Bioelectron 101 (2018) 96–102, https://doi.org/10.1016/j.bios.2017.10.018.
[71] C. Wabnitz, A. Canavan, W. Chen, M. Reisbeck, R. Bakkour, Quartz crystal microbalance as a holistic detector for quantifying complex organic matrices during liquid chromatography: 1. Coupling, characterization, and validation, Anal. Chem 96 (2024) 7429–7435, https://doi.org/10.1021/acs.analchem.3c05440.
[72] H. Tian, G. Huang, F. Xie, W. Fu, X. Yang, THz biosensing applications for clinical laboratories: Bottlenecks and strategies, TrAC Trends Anal. Chem 163 (2023) 117057, https://doi.org/10.1016/j.trac.2023.117057.
[73] P. G. Saiz, R. Fernández De Luis, A. Lasheras, M.I. Arriortua, A.C. Lopes, Magnetoelastic resonance sensors: principles, applications, and perspectives, ACS Sens 7 (2022) 1248–1268, https://doi.org/10.1021/acssensors.2c00032.
[74] I. Piekarz, S. Górska, A. Razim, J. Sorocki, K. Wincza, M. Drab, S. Gruszczyński, Planar single and dual-resonant microwave biosensors for label-free bacteria detection, Sens. Actuators B Chem 351 (2022) 130899, https://doi.org/10.1016/j.snb.2021.130899.
[75] A. Miglione, A. Raucci, J. Amato, S. Marzano, B. Pagano, T. Raia, M. Lucarelli, A. Fuso, S. Cinti, Printed electrochemical strip for the detection of miRNA-29a: a possible biomarker related to Alzheimer's disease, Anal. Chem 94 (2022) 15558–15563, https://doi.org/10.1021/acs.analchem.2c03542.
[76] T.-C. Liu, Y.-C. Lee, C.-Y. Ko, R.-S. Liu, C.-C. Ke, Y.-C. Lo, P.-S. Hong, C.-Y. Chu, C.-W. Chang, P.-W. Wu, Y.-Y. Chen, S.-Y. Chen, Highly sensitive/selective 3D nanostructured immunoparticle-based interface on a multichannel sensor array for detecting amyloid-beta in Alzheimer's disease, Theranostics 8 (2018) 4210–4225, https://doi.org/10.7150/thno.25625.
[77] Y. Liu, X. Liu, M. Li, Q. Liu, T. Xu, Portable vertical graphene@Au-based electrochemical aptasensing platform for point-of-care testing of tau protein in the blood, Biosensors 12 (2022) 564, https://doi.org/10.3390/bios12080564.
[78] C. Delrue, M. Hofmans, J. Van Dorpe, M. Van Der Linden, Z. Van Gaever, T. Kerre, M.M. Speeckaert, S. De Bruyne, Innovative label-free lymphoma diagnosis using infrared spectroscopy and machine learning on tissue sections, Commun. Biol 7 (2024) 1419, https://doi.org/10.1038/s42003-024-07111-7.
[79] R. Leon, H. Fabelo, S. Ortega, I.A. Cruz-Guerrero, D.U. Campos-Delgado, A. Szolna, J.F. Piñeiro, C. Espino, A.J. O'Shanahan, M. Hernandez, D. Carrera, S. Bisshopp, C. Sosa, F.J. Balea-Fernandez, J. Morera, B. Clavo, G.M. Callico, Hyperspectral imaging benchmark based on machine learning for intraoperative brain tumour detection, Npj Precis. Oncol 7 (2023) 119, https://doi.org/10.1038/s41698-023-00475-9.
[80] A.V. Kabashin, V.G. Kravets, A.N. Grigorenko, Label-free optical biosensing: going beyond the limits, Chem. Soc. Rev. 52 (2023) 6554–6585, https://doi.org/10.1039/D3CS00155E.
[81] J. Qin, M. Cho, Y. Lee, Ultrasensitive detection of amyloid-β using cellular prion protein on the highly conductive au nanoparticles–poly(3,4-ethylene dioxythiophene)–poly(thiophene-3-acetic acid) composite electrode, Anal. Chem 91 (2019) 11259–11265, https://doi.org/10.1021/acs.analchem.9b02266.
[82] P. Nath, K.R. Mahtaba, A. Ray, Fluorescence-based portable assays for detection of biological and chemical analytes, Sensors 23 (2023) 5053, https://doi.org/10.3390/s23115053.
[83] T. Liu, A.J. Politza, M.A. Ahamed, A. Kshirsagar, Y. Zhu, W. Guan, Compact multiplex PCR device for HIV-1 and HIV-2 viral load determination from finger-prick whole blood in resource-limited settings, Biosens. Bioelectron 271 (2025) 116997, https://doi.org/10.1016/j.bios.2024.116997.
[84] T. Liu, A.J. Politza, A. Kshirsagar, M.A. Ahamed, W. Guan, Rapid simultaneous self-testing of HIV and HCV viral loads with integrated RNA extraction and multiplex RT-PCR in under 1 h, Biosens. Bioelectron 288 (2025) 117843, https://doi.org/10.1016/j.bios.2025.117843.
[85] Md.A. Ahamed, Z. Zhang, A. Kshirsagar, A.J. Politza, U. Sethuraman, S. Suresh, S. Hicks, F. Guo, W. Guan, Multiplexed salivary miRNA quantification for predicting severe COVID-19 symptoms in children using ligation-RPA

amplification assay, ACS Sens 10 (2025) 5150–5159, https://doi.org/10.1021/acssensors.5c01275.
[86] C. Rose, J.H. Chen, Learning from the EHR to implement AI in healthcare, Npj Digit. Med. 7 (2024) 330, https://doi.org/10.1038/s41746-024-01340-0.
[87] W. Choi, S.Y. Yeom, J. Kim, S. Jung, S. Jung, T.S. Shim, S.K. Kim, J.Y. Kang, S. H. Lee, I.-J. Cho, J. Choi, N. Choi, Hydrogel micropost-based qPCR for multiplex detection of miRNAs associated with Alzheimer's disease, Biosens. Bioelectron 101 (2018) 235–244, https://doi.org/10.1016/j.bios.2017.10.039.
[88] S. Hu, L. Zhang, Y. Su, X. Liang, J. Yang, Q. Luo, H. Luo, Sensitive detection of multiple blood biomarkers via immunomagnetic exosomal PCR for the diagnosis of Alzheimer's disease, Sci. Adv. 10 (2024) eabm3088, https://doi.org/10.1126/sciadv.abm3088.
[89] P. Leidinger, C. Backes, S. Deutscher, K. Schmitt, S.C. Mueller, K. Frese, J. Haas, K. Ruprecht, F. Paul, C. Stähler, C.J. Lang, B. Meder, T. Bartfai, E. Meese, A. Keller, A blood based 12-miRNA signature of Alzheimer disease patients, Genome Biol 14 (2013) R78, https://doi.org/10.1186/gb-2013-14-7-r78.
[90] K.-H. Lim, S.-H. Kim, S. Yang, S. Chun, J.-Y. Joo, Advances in multiplex PCR for Alzheimer's disease diagnostics targeting CDK genes, Neurosci. Lett 749 (2021) 135715, https://doi.org/10.1016/j.neulet.2021.135715.
[91] B.B. Oliveira, B. Veigas, P.V. Baptista, Isothermal amplification of nucleic acids: the race for the next "gold standard, Front. Sens 2 (2021) 752600, https://doi.org/10.3389/fsens.2021.752600.
[92] J. Reynolds, R.S. Loeffler, P.J. Leigh, H.A. Lopez, J.-Y. Yoon, Recent uses of paper microfluidics in isothermal nucleic acid amplification tests, Biosensors 13 (2023) 885, https://doi.org/10.3390/bios13090885.
[93] M. Wang, H. Liu, J. Ren, Y. Huang, Y. Deng, Y. Liu, Z. Chen, F.W.-N. Chow, P.H.-M. Leung, S. Li, Enzyme-assisted nucleic acid amplification in molecular diagnosis: a review, Biosensors 13 (2023) 160, https://doi.org/10.3390/bios13020160.
[94] M. De Felice, M. De Falco, D. Zappi, A. Antonacci, V. Scognamiglio, Isothermal amplification-assisted diagnostics for COVID-19, Biosens. Bioelectron 205 (2022) 114101, https://doi.org/10.1016/j.bios.2022.114101.
[95] J. Xie, J. Chen, Y. Zhang, C. Li, P. Liu, W.-J. Duan, J.-X. Chen, J. Chen, Z. Dai, M. Li, A dual-signal amplification strategy based on rolling circle amplification and APE1-assisted amplification for highly sensitive and specific miRNA analysis for early diagnosis of alzheimer's disease, Talanta 272 (2024) 125747, https://doi.org/10.1016/j.talanta.2024.125747.
[96] M.M. Ali, F. Li, Z. Zhang, K. Zhang, D.-K. Kang, J.A. Ankrum, X.C. Le, W. Zhao, Rolling circle amplification: a versatile tool for chemical biology, materials science and medicine, Chem. Soc. Rev. 43 (2014) 3324, https://doi.org/10.1039/c3cs60439j.
[97] J. Wang, X. Yan, Y. He, H. Tang, J. Wang, X. Yi, Fluorescence detection of the genetic risk factor ApoE4 gene associate with Alzheimer's disease based on a CRISPR-Cas12a system, Microchem. J. 210 (2025) 112831, https://doi.org/10.1016/j.microc.2025.112831.
[98] Z. Jia, Y. Maghaydah, K. Zdanys, G.A. Kuchel, B.S. Diniz, C. Liu, CRISPR-powered aptasensor for diagnostics of Alzheimer's disease, ACS Sens 9 (2024) 398–405, https://doi.org/10.1021/acssensors.3c02167.
[99] Z. Zhang, Md.A. Ahamed, D. Yang, Biological properties and DNA nanomaterial biosensors of exosomal miRNAs in disease diagnosis, Sens. Diagn 4 (2025) 273–292, https://doi.org/10.1039/D4SD00373J.
[100] Z. Zhang, T. Liu, M. Dong, Md.A. Ahamed, W. Guan, Sample-to-answer salivary miRNA testing: New frontiers in point-of-care diagnostic technologies, WIREs Nanomedicine Nanobiotechnology 16 (2024) e1969, https://doi.org/10.1002/wnan.1969.
[101] S. Liu, T. Park, D.M. Krüger, T. Pena-Centeno, S. Burkhardt, A. Schutz, Y. Huang, T. Rosewood, S. Chaudhuri, M. Cho, S.L. Risacher, Y. Wan, L.M. Shaw, F. Sananbenesi, A.S. Brodsky, H. Lin, A. Krunic, J.K. Blusztajn, A.J. Saykin, I. Delalle, A. Fischer, K. Nho, for the Alzheimer's Disease Neuroimaging Initiative, Plasma miRNAs across the Alzheimer's disease continuum: Relationship to central biomarkers, Alzheimers Dement 20 (2024) 7698–7714, https://doi.org/10.1002/alz.14230.
[102] E.M. Borsom, K. Conn, C.R. Keefe, C. Herman, G.M. Orsini, A.H. Hirsch, M. Palma Avila, G. Testo, S.A. Jaramillo, E. Bolyen, K. Lee, J.G. Caporaso, E.K. Cope, Predicting neurodegenerative disease using prepathology gut microbiota composition: a longitudinal study in mice modeling Alzheimer's disease pathologies, Microbiol. Spectr 11 (2023) e03458-22, https://doi.org/10.1128/spectrum.03458-22.
[103] Y. Qi, J. Yu, M. Lou, Y. Yu, R. Li, Z. Zhang, Y. Dai, K. Lao, M. Cao, X. Gou, Lab on a single microbead: An enzyme-free strategy for the sensitive detection of microRNA via efficient localized catalytic hairpin assembly, Anal. Chim. Acta 1340 (2025) 343659, https://doi.org/10.1016/j.aca.2025.343659.
[104] J. Lim, S. Kim, S.J. Oh, S.M. Han, S.Y. Moon, B. Kang, S.B. Seo, S. Jang, S.U. Son, J. Jung, T. Kang, S.A. Park, M. Moon, E.-K. Lim, miRNA sensing hydrogels capable of self-signal amplification for early diagnosis of Alzheimer's disease, Biosens. Bioelectron 209 (2022) 114279, https://doi.org/10.1016/j.bios.2022.114279.
[105] Y. Luo, J. Chen, J. Liang, Y. Liu, C. Liu, Y. Liu, T. Xu, X. Zhang, Ultrasound-enhanced catalytic hairpin assembly capable of ultrasensitive microRNA biosensing for the early screening of Alzheimer's disease, Biosens. Bioelectron 242 (2023) 115746, https://doi.org/10.1016/j.bios.2023.115746.
[106] F. Li, C. Stewart, S. Yang, F. Shi, W. Cui, S. Zhang, H. Wang, H. Huang, M. Chen, J. Han, Optical sensor array for the early diagnosis of Alzheimer's disease, Front. Chem 10 (2022) 874864, https://doi.org/10.3389/fchem.2022.874864.
[107] S. Tomita, H. Sugai, Chemical tongues as multipurpose bioanalytical tools for the characterization of complex biological samples, Biophys. Physicobiology 21 (2024) n/a, https://doi.org/10.2142/biophysico.bppb-v21.0017.
[108] J. Sun, Z. Shi, L. Wang, X. Zhang, C. Luo, J. Hua, M. Feng, Z. Chen, M. Wang, C. Xu, Construction of a microcavity-based microfluidic chip with simultaneous SERS quantification of dual biomarkers for early diagnosis of Alzheimer's disease, Talanta 261 (2023) 124677, https://doi.org/10.1016/j.talanta.2023.124677.
[109] Y. Zhou, J. Liu, T. Zheng, Y. Tian, Label-Free SERS strategy for In Situ monitoring and real-time imaging of Aβ aggregation process in live neurons and brain tissues, Anal. Chem 92 (2020) 5910–5920, https://doi.org/10.1021/acs.analchem.9b05837.
[110] X.Z. Wang, J. Du, N.N. Xiao, Y. Zhang, L. Fei, J.D. LaCoste, Z. Huang, Q. Wang, X. R. Wang, B. Ding, Driving force to detect Alzheimer's disease biomarkers: application of a thioflavine T@Er-MOF ratiometric fluorescent sensor for smart detection of presenilin 1, amyloid β-protein and acetylcholine, The Analyst 145 (2020) 4646–4663, https://doi.org/10.1039/D0AN00440E.
[111] L. Wang, M. Chang, P. Ma, H. Chen, S. Ma, N. Chen, X. Zhang, Self-assembly of Au nanocubes for ultrasensitive detection of Alzheimer's disease biomarkers by SERS, Anal. Methods 15 (2023) 6385–6393, https://doi.org/10.1039/D3AY01667F.
[112] Y. Liang, K. Xue, Y. Shi, T. Zhan, W. Lai, C. Zhang, Dry chemistry-based bipolar electrochemiluminescence immunoassay device for point-of-care testing of alzheimer-associated neuronal thread protein, Anal. Chem 95 (2023) 3434–3441, https://doi.org/10.1021/acs.analchem.2c05164.
[113] A. Gin, P.-D. Nguyen, G. Serrano, G.E. Alexander, J. Su, Towards early diagnosis and screening of Alzheimer's disease using frequency locked whispering gallery mode microtoroids, Npj Biosensing 1 (2024) 9, https://doi.org/10.1038/s44328-024-00009-8.
[114] H.-N. Chan, D. Xu, S.-L. Ho, M.S. Wong, H.-W. Li, Ultra-sensitive detection of protein biomarkers for diagnosis of Alzheimer's disease, Chem. Sci. 8 (2017) 4012–4018, https://doi.org/10.1039/C6SC05615F.
[115] J.-S. Ahn, C.-H. Jang, Real-time detection of Tau-381 protein using liquid crystal-based sensors for Alzheimer's disease diagnosis, Colloids Surf. B Biointerfaces 245 (2025) 114211, https://doi.org/10.1016/j.colsurfb.2024.114211.
[116] S. Lee, E. Kim, C.-E. Moon, C. Park, J.-W. Lim, M. Baek, M.-K. Shin, J. Ki, H. Cho, Y.W. Ji, S. Haam, Amplified fluorogenic immunoassay for early diagnosis and monitoring of Alzheimer's disease from tear fluid, Nat. Commun 14 (2023) 8153, https://doi.org/10.1038/s41467-023-43995-5.
[117] X. Ren, J. Yan, D. Wu, Q. Wei, Y. Wan, Nanobody-based apolipoprotein E immunosensor for point-of-care testing, ACS Sens 2 (2017) 1267–1271, https://doi.org/10.1021/acssensors.7b00495.
[118] L.C. Brazaca, J.R. Moreto, A. Martín, F. Tehrani, J. Wang, V. Zucolotto, Colorimetric paper-based immunosensor for simultaneous determination of fetuin b and clusterin toward early Alzheimer's diagnosis, ACS Nano 13 (2019) 13325–13332, https://doi.org/10.1021/acsnano.9b06571.
[119] J. Wang, L. Shi, X. Zhu, Q. Tang, M. Wu, B. Li, W. Liu, Y. Jin, Entropy-driven catalysis-based lateral flow assay for sensitive detection of Alzheimer 's-associated MicroRNA, Talanta 271 (2024) 125656, https://doi.org/10.1016/j.talanta.2024.125656.
[120] L. Zhang, Y. Su, X. Liang, K. Cao, Q. Luo, H. Luo, Ultrasensitive and point-of-care detection of plasma phosphorylated tau in Alzheimer's disease using colorimetric and surface-enhanced Raman scattering dual-readout lateral flow assay, Nano Res 16 (2023) 7459–7469, https://doi.org/10.1007/s12274-022-5354-4.
[121] Y. Zhan, R. Fei, Y. Lu, Y. Wan, X. Wu, J. Dong, D. Meng, Q. Ge, X. Zhao, Ultrasensitive detection of multiple Alzheimer's disease biomarkers by SERS-LFA, The Analyst 147 (2022) 4124–4131, https://doi.org/10.1039/D2AN00717G.
[122] W.-H. Sung, J.-T. Hung, Y.-J. Lu, C.-M. Cheng, Paper-based detection device for alzheimer's disease—detecting β-amyloid peptides (1–42) in human plasma, Diagnostics 10 (2020) 272, https://doi.org/10.3390/diagnostics10050272.
[123] T.D. Mai, D. Ferraro, N. Aboud, R. Renault, M. Serra, N.T. Tran, J.-L. Viovy, C. Smadja, S. Descroix, M. Taverna, Single-step immunoassays and microfluidic droplet operation: Towards a versatile approach for detection of amyloid-β peptide-based biomarkers of Alzheimer's disease, Sens. Actuators B Chem 255 (2018) 2126–2135, https://doi.org/10.1016/j.snb.2017.09.003.
[124] D.M. Rissin, C.W. Kan, T.G. Campbell, S.C. Howes, D.R. Fournier, L. Song, T. Piech, P.P. Patel, L. Chang, A.J. Rivnak, E.P. Ferrell, J.D. Randall, G. K. Provuncher, D.R. Walt, D.C. Duffy, Single-molecule enzyme-linked immunosorbent assay detects serum proteins at subfemtomolar concentrations, Nat. Biotechnol 28 (2010) 595–599, https://doi.org/10.1038/nbt.1641.
[125] M. Milà-Alomà, N.J. Ashton, M. Shekari, G. Salvadó, P. Ortiz-Romero, L. Montoliu-Gaya, A.L. Benedet, T.K. Karikari, J. Lantero-Rodriguez, E. Vanmechelen, T.A. Day, A. González-Escalante, G. Sánchez-Benavides, C. Minguillon, K. Fauria, J.L. Molinuevo, J.L. Dage, H. Zetterberg, J.D. Gispert, M. Suárez-Calvet, K. Blennow, Plasma p-tau231 and p-tau217 as state markers of amyloid-β pathology in preclinical Alzheimer's disease, Nat. Med. (2022), https://doi.org/10.1038/s41591-022-01925-w.
[126] A. Lleó, H. Zetterberg, J. Pegueroles, T.K. Karikari, M. Carmona-Iragui, N. J. Ashton, V. Montal, I. Barroeta, J. Lantero-Rodríguez, L. Videla, M. Altuna, B. Benejam, S. Fernandez, S. Valldeneu, D. Garzón, A. Bejanin, M.F. Iulita, V. Camacho, S. Medrano-Martorell, O. Belbin, J. Clarimon, S. Lehmann, D. Alcolea, R. Blesa, K. Blennow, J. Fortea, Phosphorylated tau181 in plasma as a potential biomarker for Alzheimer's disease in adults with Down syndrome, Nat. Commun 12 (2021) 4304, https://doi.org/10.1038/s41467-021-24319-x.
[127] P. Chatterjee, S. Pedrini, J.D. Doecke, R. Thota, V.L. Villemagne, V. Doré, A. K. Singh, P. Wang, S. Rainey-Smith, C. Fowler, K. Taddei, H.R. Sohrabi, M. P. Molloy, D. Ames, P. Maruff, C.C. Rowe, C.L. Masters, R.N. Martins, the AIBL Research Group, Plasma Aβ42/40 ratio, p-tau181, GFAP, and NfL across the Alzheimer's disease continuum: a cross-sectional and longitudinal study in the

AIBL cohort, Alzheimers Dement 19 (2023) 1117–1134, https://doi.org/10.1002/alz.12724.
[128] M.C. Park, M. Kim, G.T. Lim, S.M. Kang, S.S.A. An, T.S. Kim, J.Y. Kang, Droplet-based magnetic bead immunoassay using microchannel-connected multiwell plates (μCHAMPs) for the detection of amyloid beta oligomers, Lab. Chip 16 (2016) 2245–2253, https://doi.org/10.1039/C6LC00013D.
[129] S. Das, N. Dewit, D. Jacobs, Y.A.L. Pijnenburg, S.G.J.G. In, 'T. Veld, S. Coppens, M. Quaglia, C. Hirtz, C.E. Teunissen, E. Vanmechelen, A novel neurofilament light chain ELISA validated in patients with alzheimer's disease, frontotemporal dementia, and subjective cognitive decline, and the evaluation of candidate proteins for immunoassay calibration, Int. J. Mol. Sci. 23 (2022) 7221, https://doi.org/10.3390/ijms23137221.
[130] J.A. Kim, M. Kim, S.M. Kang, K.T. Lim, T.S. Kim, J.Y. Kang, Magnetic bead droplet immunoassay of oligomer amyloid β for the diagnosis of Alzheimer's disease using micro-pillars to enhance the stability of the oil–water interface, Biosens. Bioelectron 67 (2015) 724–732, https://doi.org/10.1016/j.bios.2014.10.042.
[131] W. Tao, Q. Xie, H. Wang, S. Ke, P. Lin, X. Zeng, Integration of a miniature quartz crystal microbalance with a microfluidic chip for amyloid beta-Aβ42 quantitation, Sensors 15 (2015) 25746–25760, https://doi.org/10.3390/s151025746.
[132] R.M. Mohamadi, Z. Svobodova, Z. Bilkova, M. Otto, M. Taverna, S. Descroix, J.-L. Viovy, An integrated microfluidic chip for immunocapture, preconcentration and separation of β-amyloid peptides, Biomicrofluidics 9 (2015) 054117, https://doi.org/10.1063/1.4931394.
[133] X. He, C. Ge, X. Zheng, B. Tang, L. Chen, S. Li, L. Wang, L. Zhang, Y. Xu, Rapid identification of alpha-fetoprotein in serum by a microfluidic SERS chip integrated with Ag/Au Nanocomposites, Sens. Actuators B Chem 317 (2020) 128196, https://doi.org/10.1016/j.snb.2020.128196.
[134] P. Liu, B. Li, L. Fu, Y. Huang, M. Man, J. Qi, X. Sun, Q. Kang, D. Shen, L. Chen, Hybrid three dimensionally printed paper-based microfluidic platform for investigating a cell's apoptosis and intracellular cross-talk, ACS Sens 5 (2020) 464–473, https://doi.org/10.1021/acssensors.9b02205.
[135] S. Duan, T. Cai, F. Liu, Y. Li, H. Yuan, W. Yuan, K. Huang, K. Hoettges, M. Chen, E. G. Lim, C. Zhao, P. Song, Automatic offline-capable smartphone paper-based microfluidic device for efficient biomarker detection of Alzheimer's disease, Anal. Chim. Acta 1308 (2024) 342575, https://doi.org/10.1016/j.aca.2024.342575.
[136] S. Duan, T. Cai, L. Chen, X. Wang, S. Zhang, B. Han, E.G. Lim, K. Hoettges, Y. Hu, P. Song, An integrated paper-based microfluidic platform for screening of early-stage Alzheimer's disease by detecting Aβ42, Lab. Chip 25 (2025) 512–523, https://doi.org/10.1039/D4LC00748D.
[137] J. Sun, S. Duan, W. Xu, W. He, T. Li, S. Liu, K. Hoettges, J. Zhu, M. Leach, P. Song, A fully automated paper-based smartphone-assisted microfluidic chemiluminescence sample to result immunoassay platform, Anal. Chim. Acta 1358 (2025) 344013, https://doi.org/10.1016/j.aca.2025.344013.
[138] J.V. Rushworth, A. Ahmed, H.H. Griffiths, N.M. Pollock, N.M. Hooper, P. A. Millner, A label-free electrical impedimetric biosensor for the specific detection of Alzheimer's amyloid-beta oligomers, Biosens. Bioelectron 56 (2014) 83–90, https://doi.org/10.1016/j.bios.2013.12.036.
[139] Z. Huang, M. Li, L. Zhang, Y. Liu, Electrochemical immunosensor based on superwettable microdroplet array for detecting multiple Alzheimer's disease biomarkers, Front. Bioeng. Biotechnol 10 (2022) 1029428, https://doi.org/10.3389/fbioe.2022.1029428.
[140] C. Luo, T. Yang, Y. Zhang, L. Wu, X. Zhu, Z. Qian, Advancing Alzheimer's biomarker detection: a hairpin aptamer-based competitive electrochemical biosensor for trace amyloid beta 40 analysis, Microchem. J. 205 (2024) 111361, https://doi.org/10.1016/j.microc.2024.111361.
[141] S. Tonello, G. Abate, M. Borghetti, M. Marziano, M. Serpelloni, D.L. Uberti, N. F. Lopomo, M. Memo, E. Sardini, Wireless point-of-care platform with screen-printed sensors for biomarkers detection, IEEE Trans. Instrum. Meas 66 (2017) 2448–2455, https://doi.org/10.1109/TIM.2017.2692308.
[142] Y.K. Yoo, J. Kim, G. Kim, Y.S. Kim, H.Y. Kim, S. Lee, W.W. Cho, S. Kim, S.-M. Lee, B.C. Lee, J.H. Lee, K.S. Hwang, A highly sensitive plasma-based amyloid-β detection system through medium-changing and noise cancellation system for early diagnosis of the Alzheimer's disease, Sci. Rep. 7 (2017) 8882, https://doi.org/10.1038/s41598-017-09370-3.
[143] S.J. Yang, J.U. Lee, M.J. Jeon, S.J. Sim, Highly sensitive surface-enhanced Raman scattering-based immunosensor incorporating half antibody-fragment for quantitative detection of Alzheimer's disease biomarker in blood, Anal. Chim. Acta 1195 (2022) 339445, https://doi.org/10.1016/j.aca.2022.339445.
[144] M. Medina-Sánchez, S. Miserere, E. Morales-Narváez, A. Merkoçi, On-chip magneto-immunoassay for Alzheimer's biomarker electrochemical detection by using quantum dots as labels, Biosens. Bioelectron 54 (2014) 279–284, https://doi.org/10.1016/j.bios.2013.10.069.
[145] X. Sun, G. Zhong, Y. Zeng, T. Xu, Y. Liu, Fully integrated wearable biosensor for multiple in situ phosphorylated tau protein detection, Anal. Chem 97 (2025) 15941–15948, https://doi.org/10.1021/acs.analchem.5c02541.
[146] L. Wang, M. Pagett, W. Zhang, Molecularly imprinted polymer (MIP) based electrochemical sensors and their recent advances in health applications, Sens. Actuators Rep. 5 (2023) 100153, https://doi.org/10.1016/j.snr.2023.100153.
[147] Y. Li, L. Luo, L. Senicar, R. Asrosa, B. Kizilates, K. Xing, E. Torres, L. Xu, D. Li, N. Graham, A. Heslegrave, H. Zetterberg, D.J. Sharp, B. Li, An ultrasensitive molecularly imprinted point-of-care electrochemical sensor for detection of glial fibrillary acidic protein, Adv. Healthc. Mater 13 (2024) 2401966, https://doi.org/10.1002/adhm.202401966.
[148] A.M. Arjun, S. Deshpande, G. Liu, D. Miura, K. Pawlak, T. Takahiko, M. Higuchi, M. Matsumoto, T. Umemura, K. Tsukakoshi, S. Sharma, Low-cost polyphenol–polypyrrole molecularly imprinted sensor for point-of-care Alzheimer's detection, ACS Sens 10 (2025) 8435–8446, https://doi.org/10.1021/acssensors.5c01816.
[149] K. Turan, G. Aydoğdu TiĞ, Fabrication of MIP-based sensors for femtomolar detection of kynurenic acid for early diagnosis of neurodegenerative diseases, ACS Omega 10 (2025) 20907–20921, https://doi.org/10.1021/acsomega.5c02339.
[150] F.T.C. Moreira, M.G.F. Sale, M. Di Lorenzo, Towards timely Alzheimer diagnosis: a self-powered amperometric biosensor for the neurotransmitter acetylcholine, Biosens. Bioelectron 87 (2017) 607–614, https://doi.org/10.1016/j.bios.2016.08.104.
[151] C.A. Razzino, V. Serafín, M. Gamella, M. Pedrero, A. Montero-Calle, R. Barderas, M. Calero, A.O. Lobo, P. Yáñez-Sedeño, S. Campuzano, J.M. Pingarrón, An electrochemical immunosensor using gold nanoparticles-PAMAM-nanostructured screen-printed carbon electrodes for tau protein determination in plasma and brain tissues from Alzheimer patients, Biosens. Bioelectron 163 (2020) 112238, https://doi.org/10.1016/j.bios.2020.112238.
[152] A. Kaushik, R.D. Jayant, S. Tiwari, A. Vashist, M. Nair, Nano-biosensors to detect beta-amyloid for Alzheimer's disease management, Biosens. Bioelectron 80 (2016) 273–287, https://doi.org/10.1016/j.bios.2016.01.065.
[153] M.-V. Tieu, S.H. Choi, H.T.N. Le, S. Cho, Electrochemical impedance-based biosensor for label-free determination of plasma P-tau181 levels for clinically accurate diagnosis of mild cognitive impairment and Alzheimer's disease, Anal. Chim. Acta 1273 (2023) 341535, https://doi.org/10.1016/j.aca.2023.341535.
[154] A. Sharma, L. Angnes, N. Sattarahmady, M. Negahdary, H. Heli, Electrochemical immunosensors developed for amyloid-beta and tau proteins, leading biomarkers of Alzheimer's disease, Biosensors 13 (2023) 742, https://doi.org/10.3390/bios13070742.
[155] Y. Wu, R. Lu, P.-G. Ren, Z. Xie, Rigid DNA frameworks anchored transistor enabled ultrasensitive detection of Aβ-42 in serum, Sensors 25 (2025) 3260, https://doi.org/10.3390/s25113260.
[156] H. Chen, M. Xiao, J. He, Y. Zhang, Y. Liang, H. Liu, Z. Zhang, Aptamer-functionalized carbon nanotube field-effect transistor biosensors for alzheimer's disease serum biomarker detection, ACS Sens 7 (2022) 2075–2083, https://doi.org/10.1021/acssensors.2c00967.
[157] S.-H. Ciou, A.-H. Hsieh, Y.-X. Lin, J.-L. Sei, M. Govindasamy, C.-F. Kuo, C.-H. Huang, Sensitive label-free detection of the biomarker phosphorylated tau−217 protein in Alzheimer's disease using a graphene-based solution-gated field effect transistor, Biosens. Bioelectron 228 (2023) 115174, https://doi.org/10.1016/j.bios.2023.115174.
[158] Q. Peng, M. Zhang, G. Shi, High-performance extended-gate field-effect transistor for kinase sensing in aβ accumulation of alzheimer's disease, Anal. Chem 94 (2022) 1491–1497, https://doi.org/10.1021/acs.analchem.1c05164.
[159] J. Li, W. Ni, D. Jin, Y. Yu, M.-M. Xiao, Z.-Y. Zhang, G.-J. Zhang, Nanosensor-Driven Detection of Neuron-Derived Exosomal $A\beta_{42}$ with Graphene Electrolyte-Gated Transistor for Alzheimer's Disease Diagnosis, Anal. Chem 95 (2023) 5719–5728, https://doi.org/10.1021/acs.analchem.2c05751.
[160] A. Koklu, S. Wustoni, V.-E. Musteata, D. Ohayon, M. Moser, I. McCulloch, S. P. Nunes, S. Inal, Microfluidic Integrated Organic Electrochemical Transistor with a Nanoporous Membrane for Amyloid-β Detection, ACS Nano 15 (2021) 8130–8141, https://doi.org/10.1021/acsnano.0c09893.
[161] X. Li, J. Chen, Y. Yang, H. Cai, Z. Ao, Y. Xing, K. Li, K. Yang, W. Guan, J. Friend, L. P. Lee, N. Wang, F. Guo, Extracellular vesicle-based point-of-care testing for diagnosis and monitoring of Alzheimer's disease, Microsyst. Nanoeng 11 (2025) 65, https://doi.org/10.1038/s41378-025-00916-4.
[162] B. Lenhart, X. Wei, B. Watson, X. Wang, Z. Zhang, C. Li, M. Moss, C. Liu, In vitro biosensing of β-Amyloid peptide aggregation dynamics using a biological nanopore, Sens. Actuators B Chem 338 (2021) 129863, https://doi.org/10.1016/j.snb.2021.129863.
[163] Z. Zou, H. Yang, Q. Yan, P. Qi, Z. Qing, J. Zheng, X. Xu, L. Zhang, F. Feng, R. Yang, Synchronous screening of multiplexed biomarkers of Alzheimer's disease by a length-encoded aerolysin nanopore-integrated triple-helix molecular switch, Chem. Commun 55 (2019) 6433–6436, https://doi.org/10.1039/C9CC02065A.
[164] Q. Liu, Y. Ouyang, Y. Wang, S. Zhou, Y. Zhan, L. Wang, Multianalyte nanopore detection of Alzheimer's disease biomarkers: a label-free platform with improved sensitivity and range, Adv. Healthc. Mater 14 (2025) 2405058, https://doi.org/10.1002/adhm.202405058.
[165] M. Dong, A. Kshirsagar, A.J. Politza, M.A.U. Khalid, M.A. Ahamed, W. Guan, Addressing buffer, size, and clogging challenges in lamp-coupled solid-state nanopores for point-of-care testing, Anal. Chem (2025) acs.analchem.4c06823, https://doi.org/10.1021/acs.analchem.4c06823.
[166] M. Salehirozveh, P. Dehghani, I. Mijakovic, Nanopore-based neurotransmitter detection: advances, challenges, and future perspectives, ACS Nano 19 (2025) 24404–24424, https://doi.org/10.1021/acsnano.5c04662.
[167] Y. Dong, X. Song, X. Wang, S. Wang, Z. He, The early diagnosis of Alzheimer's disease: blood-based panel biomarker discovery by proteomics and metabolomics, CNS Neurosci. Ther 30 (2024) e70060, https://doi.org/10.1111/cns.70060.
[168] M. Charron, K. Briggs, S. King, M. Waugh, V. Tabard-Cossa, Precise DNA concentration measurements with nanopores by controlled counting, Anal. Chem 91 (2019) 12228–12237.
[169] M.A.U. Khalid, Md.A. Ahamed, A.J. Politza, W. Guan, Solid-state nanopore sizing for cfDNA sample quality control in point-of-need sequencing, ACS Sens (2025), https://doi.org/10.1021/acssensors.5c00803.
[170] Ó. Gutiérrez-Sanz, N. Haustein, M. Schroeter, T. Oelschlaegel, M.S. Filipiak, A. Tarasov, Transistor-based immunosensing in human serum samples without on-site calibration, Sens. Actuators B Chem 295 (2019) 153–158, https://doi.org/10.1016/j.snb.2019.05.043.

[171] P. Supraja, S. Tripathy, R. Singh, V. Singh, G. Chaudhury, S.G. Singh, Towards point-of-care diagnosis of Alzheimer's disease: Multi-analyte based portable chemiresistive platform for simultaneous detection of β-amyloid (1–40) and (1–42) in plasma, Biosens. Bioelectron 186 (2021) 113294, https://doi.org/10.1016/j.bios.2021.113294.
[172] P.K. Sharma, E.-S. Kim, S. Mishra, E. Ganbold, R.-S. Seong, Y.M. Kim, G.-H. Jahng, H.Y. Rhee, H.-S. Han, D.H. Kim, S.T. Kim, N.-Y. Kim, Ultrasensitive probeless capacitive biosensor for amyloid beta (Aβ1-42) detection in human plasma using interdigitated electrodes, Biosens. Bioelectron 212 (2022) 114365, https://doi.org/10.1016/j.bios.2022.114365.
[173] H.T.N. Le, D. Kim, L.M.T. Phan, S. Cho, Ultrasensitive capacitance sensor to detect amyloid-beta 1-40 in human serum using supramolecular recognition of β-CD/RGO/ITO micro-disk electrode, Talanta 237 (2022) 122907, https://doi.org/10.1016/j.talanta.2021.122907.
[174] L. Guo, Z. Yang, S. Zhi, Z. Feng, C. Lei, Y. Zhou, A sensitive and innovative detection method for rapid C-reactive proteins analysis based on a micro-fluxgate sensor system, PLOS ONE 13 (2018) e0194631, https://doi.org/10.1371/journal.pone.0194631.
[175] A. Agrawal, A. Pathak, D.N. Ngwa, A. Thirumalai, P.B. Armstrong, S.K. Singh, An evolutionarily conserved function of C-reactive protein is to prevent the formation of amyloid fibrils, Front. Immunol 15 (2024) 1466865, https://doi.org/10.3389/fimmu.2024.1466865.
[176] F. Zou, Y. Liu, Y. Luo, T. Xu, A wearable spatiotemporal controllable ultrasonic device with amyloid-β disaggregation for continuous Alzheimer's disease therapy, Sci. Adv. 11 (2025) eadw1732, https://doi.org/10.1126/sciadv.adw1732.
[177] B.T. Murti, A.D. Putri, Y.-J. Huang, S.-M. Wei, C.-W. Peng, P.-K. Yang, Clinically oriented Alzheimer's biosensors: expanding the horizons towards point-of-care diagnostics and beyond, RSC Adv 11 (2021) 20403–20422, https://doi.org/10.1039/D1RA01553B.
[178] R. Smith, L. Shaw, S. Palmqvist, N. Mattsson-Carlgren, G. Klein, M. Tonietto, for the Alzheimer's Disease Neuroimaging Initiative, C. Quijano-Rubio, C.M. Rank, M. Andreadou, S.C. Burnham, E. Stomrud, Clinical performance of the elecsys CSF pTau181/Aβ42 ratio for concordance with tau-PET in two independent cohorts, Neurol. Ther 14 (2025) 2011–2031, https://doi.org/10.1007/s40120-025-00798-8.
[179] R.L.C. Franco, T.R. Hunter, F.G. De Felice, Blood biomarkers for Alzheimer's disease: key challenges of clinical implementation, Neural Regen. Res. (2025), https://doi.org/10.4103/NRR.NRR-D-25-00569.
[180] A. Nakamura, N. Kaneko, V.L. Villemagne, T. Kato, J. Doecke, V. Doré, C. Fowler, Q.-X. Li, R. Martins, C. Rowe, T. Tomita, K. Matsuzaki, K. Ishii, K. Ishii, Y. Arahata, S. Iwamoto, K. Ito, K. Tanaka, C.L. Masters, K. Yanagisawa, High performance plasma amyloid-β biomarkers for Alzheimer's disease, Nature 554 (2018) 249–254, https://doi.org/10.1038/nature25456.
[181] Biomarkers and surrogate endpoints: Preferred definitions and conceptual framework, Clin. Pharmacol. Ther. 69 (2001) 89–95. https://doi.org/10.1067/mcp.2001.113989.
[182] J.M. Bader, V. Albrecht, M. Mann, MS-based proteomics of body fluids: the end of the beginning, Mol. Cell. Proteomics 22 (2023) 100577, https://doi.org/10.1016/j.mcpro.2023.100577.
[183] R. Spector, S. Robert Snodgrass, C.E. Johanson, A balanced view of the cerebrospinal fluid composition and functions: Focus on adult humans, Exp. Neurol 273 (2015) 57–68, https://doi.org/10.1016/j.expneurol.2015.07.027.
[184] H. Hampel, S.E. O'Bryant, J.L. Molinuevo, H. Zetterberg, C.L. Masters, S. Lista, S. J. Kiddle, R. Batrla, K. Blennow, Blood-based biomarkers for Alzheimer disease: mapping the road to the clinic, Nat. Rev. Neurol 14 (2018) 639–652, https://doi.org/10.1038/s41582-018-0079-7.
[185] H. Lu, X.-C. Zhu, T. Jiang, J.-T. Yu, L. Tan, Body fluid biomarkers in Alzheimer's disease, Ann. Transl. Med. 3 (2015) 70, https://doi.org/10.3978/j.issn.2305-5839.2015.02.13.
[186] I.S. Ryu, D.H. Kim, J.-Y. Ro, B.-G. Park, S.H. Kim, J.-Y. Im, J.-Y. Lee, S.J. Yoon, H. Kang, T. Iwatsubo, C.E. Teunissen, H.-J. Cho, J.-H. Ryu, The microRNA-485-3p concentration in salivary exosome-enriched extracellular vesicles is related to amyloid β deposition in the brain of patients with Alzheimer's disease, Clin. Biochem 118 (2023) 110603, https://doi.org/10.1016/j.clinbiochem.2023.110603.
[187] M.N. Sabbagh, J. Shi, M. Lee, L. Arnold, Y. Al-Hasan, J. Heim, P. McGeer, Salivary beta amyloid protein levels are detectable and differentiate patients with Alzheimer's disease dementia from normal controls: preliminary findings, BMC Neurol 18 (2018) 155, https://doi.org/10.1186/s12883-018-1160-y.
[188] H. Pekeles, H.Y. Qureshi, H.K. Paudel, H.M. Schipper, M. Gornistky, H. Chertkow, Development and validation of a salivary tau biomarker in Alzheimer's disease, Alzheimers Dement. Diagn. Assess. Dis. Monit 10 (2018) 53–60, https://doi.org/10.1016/j.dadm.2018.03.003.
[189] M. González-Sánchez, F. Bartolome, D. Antequera, V. Puertas-Martín, P. González, A. Gómez-Grande, S. Llamas-Velasco, A. Herrero-San Martín, D. Pérez-Martínez, A. Villarejo-Galende, M. Atienza, M. Palomar-Bonet, J. L. Cantero, G. Perry, G. Orive, B. Ibañez, H. Bueno, V. Fuster, E. Carro, Decreased salivary lactoferrin levels are specific to Alzheimer's disease, EBioMedicine 57 (2020) 102834, https://doi.org/10.1016/j.ebiom.2020.102834.
[190] Y. Wang, Y. Wang, J. Zhu, Y. Guan, F. Xie, X. Cai, J. Deng, Y. Wei, R. He, Z. Fang, Q. Guo, Systematic evaluation of urinary formic acid as a new potential biomarker for Alzheimer's disease, Front. Aging Neurosci 14 (2022) 1046066, https://doi.org/10.3389/fnagi.2022.1046066.
[191] Y. Li, S. Guan, H. Jin, H. Liu, M. Kang, X. Wang, C. Sheng, Y. Sun, X. Li, X. Fang, R. Wang, The relationship between urinary Alzheimer-associated neuronal thread protein and blood biochemical indicators in the general population, Aging 12 (2020) 15260–15280, https://doi.org/10.18632/aging.103356.
[192] O. Zengi, A. Karakas, U. Ergun, M. Senes, L. Inan, D. Yucel, Urinary 8-hydroxy-2′-deoxyguanosine level and plasma paraoxonase 1 activity with Alzheimer's disease, Clin. Chem. Lab. Med. 50 (2012), https://doi.org/10.1515/cclm.2011.792.
[193] A. Zaheer, I.B. Anwar, A. Haseeb, A. Yadav, Liquid clues: tear film biomarkers unravelling Alzheimer's mysteries, Ann. Med. Surg 86 (2024) 3499–3502, https://doi.org/10.1097/MS9.0000000000002014.
[194] R. Postrel, Early Stage Detection for Alzheimers and Other Autoimmune Diseases, US 2021/0181212 A1, 2021.
[195] Z. Liu, N. Kameshima, T. Nanjo, A. Shiino, T. Kato, S. Shimizu, T. Shimizu, S. Tanaka, K. Miura, I. Tooyama, Development of a high-sensitivity method for the measurement of human nasal $A\beta_{42}$, tau, and phosphorylated tau, J. Alzheimer's Dis. 62 (2018) 737–744, https://doi.org/10.3233/JAD-170962.
[196] A. Narváez, J. Jiménez, M. Rodríguez-Núñez, M. Torre, E. Carro, M.-P. Marco, E. Domínguez, A Fast Immunosensor Based on Biohybrid Self-Assembled Nanostructures for the Detection of KYNA as a Cerebrospinal Fluid Biomarker for Alzehimer's Disease, ACS Meas. Sci. Au 5 (2025) 242–249, https://doi.org/10.1021/acsmeasuresciau.4c00102.
[197] M.-B. Irimes, M. Tertis, D. Bogdan, V. Diculescu, E. Matei, C. Cristea, R. Oprean, Customized flexible platform - starting point for the development of wearable sensor for the direct electrochemical detection of kynurenic acid in biological samples, Talanta 280 (2024) 126684, https://doi.org/10.1016/j.talanta.2024.126684.
[198] X. Yuan, Y. He, S. Li, X. Wu, Y. Ling, Z. Zhang, High-sensitivity 8-hydroxy-2′-deoxyguanosine micro-electrochemical sensor based on polyvinylpyrrolidone functionalized laser-induced graphene: design, scalable preparation, and field application, Microchem. J. 207 (2024) 111883, https://doi.org/10.1016/j.microc.2024.111883.
[199] N. Wu, Y. Wei, L. Pan, X. Yang, H. Qi, Q. Gao, C. Zhang, Lateral flow immunostrips for the sensitive and rapid determination of 8-hydroxy-2′-deoxyguanosine using upconversion nanoparticles, Microchim. Acta 187 (2020) 377, https://doi.org/10.1007/s00604-020-04349-w.
[200] D. Verma, A. Jeevaraj, B.S. Unnikrishnan, D. Bhimsaria, G. Packirisamy, Electrochemical aptasensor for non-invasive detection of lactoferrin: a potential biomarker for Alzheimer's disease, Sens. Actuators Phys 400 (2026) 117504, https://doi.org/10.1016/j.sna.2026.117504.
[201] G. Rabbani, M. Ehtisham Khan, W. Zakri, M. Vahid Khan, A.H. Bashiri, An electrochemical immunosensor based on AgNPs/Nafion-GCE for detection of salivary lactoferrin: Alzheimer's disease biomarker, Microchem. J. 207 (2024) 112079, https://doi.org/10.1016/j.microc.2024.112079.
[202] V. Shetty, C. Zigler, T.F. Robles, D. Elashoff, M. Yamaguchi, Developmental validation of a point-of-care, salivary α-amylase biosensor, Psychoneuroendocrinology 36 (2011) 193–199, https://doi.org/10.1016/j.psyneuen.2010.07.008.
[203] H. Fatima, S. Ashraf, A. Raza, P. Sajid, A. Habib, A. Afzal, Hard acid doped carbon nitride sensors for detecting Alzheimer's biomarker: Formic acid, Diam. Relat. Mater 153 (2025) 112102, https://doi.org/10.1016/j.diamond.2025.112102.
[204] A. Mazzatenta, M. Pokorski, F. Sartucci, L. Domenici, C. Di Giulio, Volatile organic compounds (VOCs) fingerprint of Alzheimer's disease, Respir. Physiol. Neurobiol 209 (2015) 81–84, https://doi.org/10.1016/j.resp.2014.10.001.
[205] J.A. Otoo, T.S. Schlappi, REASSURED multiplex diagnostics: a critical review and forecast, Biosensors 12 (2022) 124, https://doi.org/10.3390/bios12020124.
[206] W.-G. Luo, H.-Z. Liu, W.-H. Lin, M.H. Kabir, Y. Su, Simultaneous splicing of multiple DNA fragments in one PCR reaction, Biol. Proced. Online 15 (2013) 9, https://doi.org/10.1186/1480-9222-15-9.
[207] P. Akarapipad, E. Bertelson, A. Pessell, T.-H. Wang, K. Hsieh, Emerging multiplex nucleic acid diagnostic tests for combating COVID-19, Biosensors 12 (2022) 978, https://doi.org/10.3390/bios12110978.
[208] Md.A. Ahamed, M. Hasan, Md.E. Kabir, Z. Zhang, Microfluidic hydraulic oscillators: a comprehensive review of emerging biochemical and biomedical applications, Anal. Chim. Acta 1350 (2025) 343793, https://doi.org/10.1016/j.aca.2025.343793.
[209] R.A. Warmack, D.R. Boyer, C.-T. Zee, L.S. Richards, M.R. Sawaya, D. Cascio, T. Gonen, D.S. Eisenberg, S.G. Clarke, Structure of amyloid-β (20-34) with Alzheimer's-associated isomerization at Asp23 reveals a distinct protofilament interface, Nat. Commun 10 (2019) 3357, https://doi.org/10.1038/s41467-019-11183-z.
[210] D. Böken, Y. Wu, Z. Zhang, D. Klenerman, Detecting the Undetectable: Advances in Methods for Identifying Small Tau Aggregates in Neurodegenerative Diseases, ChemBioChem 26 (2025) e202400877, https://doi.org/10.1002/cbic.202400877.
[211] J. Wu, C. Cao, R.A. Loch, A. Tiiman, J. Luo, Single-molecule studies of amyloid proteins: from biophysical properties to diagnostic perspectives, Q. Rev. Biophys 53 (2020) e12, https://doi.org/10.1017/S0033583520000086.
[212] G. Huang, A. Voorspoels, R.C.A. Versloot, N.J. Van Der Heide, E. Carlon, K. Willems, G. Maglia, PlyAB nanopores detect single amino acid differences in folded haemoglobin from blood**, Angew. Chem. Int. Ed. 61 (2022) e202206227 https://doi.org/10.1002/anie.202206227.
[213] Q. Liu, Y. He, Q. Wang, S. Min, H. Geng, Y. Liu, T. Xu, Robust detection of femtogram-level Alzheimer's biomarkers using machine learning-enhanced graphene biosensors, Biosens. Bioelectron 292 (2026) 118074, https://doi.org/10.1016/j.bios.2025.118074.
[214] Y. Liu, Z. Zhou, X. Liu, J. Zeng, Q. Liu, T. Xu, An AI-assisted multiplex fluorescence sensing platform for grading diagnosis of Alzheimer's disease,

J. Mater. Chem. B 13 (2025) 14315–14325, https://doi.org/10.1039/D5TB01103E.
[215] W. Jiang, J. Liu, Y. Wu, J. Li, H. Jin, Z. Cui, X. Chen, T. Lian, H. Lv, B. Han, D. Yu, C. Wang, G. Li, K. Chen, S. Li, L. Wang, W. Zhang, R. Wang, G. Zhang, Establishment and verification of reference intervals for Alzheimer's disease plasma biomarkers based on evaluation of pre-analytical procedures: a multicenter study, Alzheimers Dement. Diagn. Assess. Dis. Monit 17 (2025) e70194, https://doi.org/10.1002/dad2.70194.
[216] E. Manuilova, I. Schrurs, S. Rutz, S. McIlwrick, O. Goldhardt, P. Sommer, T. Grimmer, Elecsys CSF AD immunoassays: sample stability for a new pre-analytical protocol for fresh CSF, Alzheimers Dement 21 (2025) e70797, https://doi.org/10.1002/alz.70797.
[217] S. Kumar, R. Gallagher, J. Bishop, E. Kline, J. Buser, L. Lafleur, K. Shah, B. Lutz, P. Yager, Long-term dry storage of enzyme-based reagents for isothermal nucleic acid amplification in a porous matrix for use in point-of-care diagnostic devices, The Analyst 145 (2020) 6875–6886, https://doi.org/10.1039/D0AN01098G.
[218] D. Helb, M. Jones, E. Story, C. Boehme, E. Wallace, K. Ho, J. Kop, M.R. Owens, R. Rodgers, P. Banada, H. Safi, R. Blakemore, N.T.N. Lan, E.C. Jones-López, M. Levi, M. Burday, I. Ayakaka, R.D. Mugerwa, B. McMillan, E. Winn-Deen, L. Christel, P. Dailey, M.D. Perkins, D.H. Persing, D. Alland, Rapid detection of *Mycobacterium tuberculosis* and rifampin resistance by use of on-demand, near-patient technology, J. Clin. Microbiol 48 (2010) 229–237, https://doi.org/10.1128/JCM.01463-09.
[219] R. Blakemore, E. Story, D. Helb, J. Kop, P. Banada, M.R. Owens, S. Chakravorty, M. Jones, D. Alland, Evaluation of the analytical performance of the xpert MTB/RIF assay, J. Clin. Microbiol 48 (2010) 2495–2501, https://doi.org/10.1128/JCM.00128-10.
[220] L.T. Nguyen, S.R. Rananaware, B.L.M. Pizzano, B.T. Stone, P.K. Jain, Clinical validation of engineered CRISPR/Cas12a for rapid SARS-CoV-2 detection, Commun. Med. 2 (2022) 7, https://doi.org/10.1038/s43856-021-00066-4.
[221] N.O. Prado, A.M. Marin, L.A. Lalli, H.B.S. Sanchuki, D.K. Wosniaki, J.M. Nardin, H.M.P. Morales, L. Blanes, D.L. Zanette, M.N. Aoki, Development and evaluation of a lyophilization protocol for colorimetric RT-LAMP diagnostic assay for COVID-19, Sci. Rep. 14 (2024) 10612, https://doi.org/10.1038/s41598-024-61163-7.
[222] T. Liu, A.J. Politza, A. Kshirsagar, Y. Zhu, W. Guan, Compact point-of-care device for self-administered HIV viral load tests from whole blood, ACS Sens 8 (2023) 4716–4727, https://doi.org/10.1021/acssensors.3c01819.
[223] G. Wu, J. Srivastava, M.H. Zaman, Stability measurements of antibodies stored on paper, Anal. Biochem 449 (2014) 147–154, https://doi.org/10.1016/j.ab.2013.12.012.
[224] Y. Yang, Y. Dai, Q. Zhao, Recent trends and applications of nanoparticle-based lateral flow immunoassays in infectious diseases detection, Microchem. J. 216 (2025) 114797, https://doi.org/10.1016/j.microc.2025.114797.
[225] D.J. Figdore, B.J. Schuder, S. Ashrafzadeh-Kian, T. Gronquist, J.A. Bornhorst, A. Algeciras-Schimnich, Differences in Alzheimer's disease blood biomarker stability: Implications for the use of tau/amyloid ratios, Alzheimers Dement 21 (2025) e70173, https://doi.org/10.1002/alz.70173.
[226] H.-W. Chen, W.-M. Ching, Evaluation of the stability of lyophilized loop-mediated isothermal amplification reagents for the detection of Coxiella burnetii, Heliyon 3 (2017) e00415, https://doi.org/10.1016/j.heliyon.2017.e00415.
[227] J. Lee, E.H. Benke, I.M. White, D.L. DeVoe, Poly(lactic- *co* -glycolic acid) for reagent storage and controlled release in thermoplastic microfluidics, Lab. Chip 26 (2026) 897–905, https://doi.org/10.1039/D5LC00632E.
[228] P. Hortschansky, V. Schroeckh, T. Christopeit, G. Zandomeneghi, M. Fändrich, The aggregation kinetics of Alzheimer's β-amyloid peptide is controlled by stochastic nucleation, Protein Sci 14 (2005) 1753–1759, https://doi.org/10.1110/ps.041266605.
[229] F. Emami, A. Vatanara, E.J. Park, D.H. Na, Drying technologies for the stability and bioavailability of biopharmaceuticals, Pharmaceutics 10 (2018) 131, https://doi.org/10.3390/pharmaceutics10030131.
[230] W.B. Stine, L. Jungbauer, C. Yu, M.J. LaDu, Preparing Synthetic Aβ in Different Aggregation States, in: E.D. Roberson (Ed.), Alzheimers Dis. Front. Dement, Humana Press, Totowa, NJ, 2010, pp. 13–32, https://doi.org/10.1007/978-1-60761-744-0_2.
[231] L. Kumar, K.B. Chandrababu, S.M. Balakrishnan, A. Allmendinger, B. Walters, I. E. Zarraga, D.P. Chang, P. Nayak, E.M. Topp, Optimizing the formulation and lyophilization process for a fragment antigen binding (Fab) protein using solid-state hydrogen–deuterium exchange mass spectrometry (ssHDX-MS), Mol. Pharm 16 (2019) 4485–4495, https://doi.org/10.1021/acs.molpharmaceut.9b00614.
[232] S. Tchessalov, V. Maglio, P. Kazarin, A. Alexeenko, B. Bhatnagar, E. Sahni, E. Shalaev, Practical advice on scientific design of freeze-drying process: 2023 update, Pharm. Res. 40 (2023) 2433–2455, https://doi.org/10.1007/s11095-023-03607-9.
[233] X. Li, B. Chen, Y. Xie, Y. Luo, D. Zhu, L. Wang, S. Su, Polyvalent aptamers structure-mediated fluorescent aptasensor for the early diagnosis of alzheimer's disease by coupling with HCR and CRISPR-Cas system, Anal. Chem 97 (2025) 793–798, https://doi.org/10.1021/acs.analchem.4c05329.
[234] L. Gaetani, K. Höglund, L. Parnetti, F. Pujol-Calderon, B. Becker, P. Eusebi, P. Sarchielli, P. Calabresi, M. Di Filippo, H. Zetterberg, K. Blennow, A new enzyme-linked immunosorbent assay for neurofilament light in cerebrospinal fluid: analytical validation and clinical evaluation, Alzheimers Res. Ther 10 (2018) 8, https://doi.org/10.1186/s13195-018-0339-1.
[235] P.D. Mehta, B.A. Patrick, D.L. Miller, P.K. Coyle, T. Wisniewski, A sensitive and cost-effective chemiluminescence ELISA for measurement of amyloid-β 1-42 peptide in human plasma, J. Alzheimers Dis. 78 (2020) 1237–1244, https://doi.org/10.3233/JAD-200861.
[236] Q. Zhang, B. Yin, Y. Huang, Y. Gu, J. Yan, J. Chen, C. Li, Y. Zhang, S.H.D. Wong, M. Yang, A dual "turn-on" biosensor based on AIE effect and FRET for in situ detection of miR-125b biomarker in early Alzheimer's disease, Biosens. Bioelectron 230 (2023) 115270, https://doi.org/10.1016/j.bios.2023.115270.
[237] H.J. Park, S. Cho, M. Kim, Y.S. Jung, Carboxylic acid-functionalized, graphitic layer-coated three-dimensional SERS substrate for label-free analysis of alzheimer's disease biomarkers, Nano Lett 20 (2020) 2576–2584, https://doi.org/10.1021/acs.nanolett.0c00048.
[238] C. Credi, O. Bibikova, C. Dallari, B. Tiribilli, F. Ratto, S. Centi, R. Pini, V. Artyushenko, R. Cicchi, F.S. Pavone, Fiber-cap biosensors for SERS analysis of liquid samples, J. Mater. Chem. B 8 (2020) 1629–1639, https://doi.org/10.1039/C9TB01866B.
[239] A. Jaiswal, T.K. Naqvi, P.K. Dwivedi, S. Verma, Single-platform, attomolar detection of multiple biomarkers by a flexible SERS sensor, Chem. – Asian J. 18 (2023) e202300441, https://doi.org/10.1002/asia.202300441.
[240] L. Jia, Q. Qiu, H. Zhang, L. Chu, Y. Du, J. Zhang, C. Zhou, F. Liang, S. Shi, S. Wang, W. Qin, Q. Wang, F. Li, Q. Wang, Y. Li, L. Shen, Y. Wei, J. Jia, Concordance between the assessment of Aβ42, T-tau, and P-T181-tau in peripheral blood neuronal-derived exosomes and cerebrospinal fluid, Alzheimers Dement 15 (2019) 1071–1080, https://doi.org/10.1016/j.jalz.2019.05.002.
[241] M.M. Mielke, R.D. Frank, J.L. Dage, A. Jeromin, N.J. Ashton, K. Blennow, T. K. Karikari, E. Vanmechelen, H. Zetterberg, A. Algeciras-Schimnich, D. S. Knopman, V. Lowe, G. Bu, P. Vemuri, J. Graff-Radford, C.R. Jack, R.C. Petersen, Comparison of plasma phosphorylated tau species with amyloid and tau positron emission tomography, neurodegeneration, vascular pathology, and cognitive outcomes, JAMA Neurol 78 (2021) 1108, https://doi.org/10.1001/jamaneurol.2021.2293.
[242] S. Palmqvist, N. Warmenhoven, F. Anastasi, A. Pilotto, S. Janelidze, P. Tideman, E. Stomrud, N. Mattsson-Carlgren, R. Smith, R. Ossenkoppele, K. Tan, A. Dittrich, I. Skoog, H. Zetterberg, V. Quaresima, C. Tolassi, K. Höglund, D. Brugnoni, A. Puig-Pijoan, A. Fernández-Lebrero, J. Contador, A. Padovani, M. Monane, P. B. Verghese, J.B. Braunstein, S. Kern, K. Blennow, N.J. Ashton, M. Suárez-Calvet, O. Hansson, Plasma phospho-tau217 for Alzheimer's disease diagnosis in primary and secondary care using a fully automated platform, Nat. Med. 31 (2025) 2036–2043, https://doi.org/10.1038/s41591-025-03622-w.
[243] N. Meyer, N. Arroyo, J.-M. Janot, M. Lepoitevin, A. Stevenson, I.A. Nemeir, V. Perrier, D. Bougard, M. Belondrade, D. Cot, J. Bentin, F. Picaud, J. Torrent, S. Balme, Detection of amyloid-β fibrils using track-etched nanopores: effect of geometry and crowding, ACS Sens 6 (2021) 3733–3743, https://doi.org/10.1021/acssensors.1c01523.
[244] S.S. Kwon, D. Kim, M. Yun, J.G. Son, S.H. Lee, The role of graphene patterning in field-effect transistor sensors to detect the tau protein for Alzheimer's disease: Simplifying the immobilization process and improving the performance of graphene-based immunosensors, Biosens. Bioelectron 192 (2021) 113519, https://doi.org/10.1016/j.bios.2021.113519.

Md. Ahasan Ahamed received his BSc degree in mechanical engineering from the Bangladesh University of Engineering and Technology (BUET) in 2014. He served as a lecturer and later assistant professor at the Bangladesh University of Textiles (2015–2020). He earned his MS degree in mechanical design and production engineering from Konkuk University in 2022 and is currently pursuing a Ph.D. in electrical engineering at Pennsylvania State University. His research focuses on POCT platforms, microfluidic device fabrication, nanopore-based sensing, and mL-enabled biomedical applications.

Bingyuan Guo received his Ph.D. in bioinorganic chemistry from Institute of High Energy Physics, Chinese Academy of Sciences, in 2018 under the supervision of Prof. Yuliang Zhao. He subsequently joined Institute of Chemistry, CAS (ICCAS), where he served as an assistant professor until December 2024. During this period, his research focused on the design and development of protein nanomachines. After leaving ICCAS, he served as a research director at a scientific startup, where he rapidly established a commercial solid-state nanopore DNA sequencing platform. He is currently a postdoctoral fellow in Prof. Weihua Guan's lab at Indiana University Bloomington.

Muhammad Asad Ullah Khalid is currently a postdoctoral fellow in Prof. Weihua Guan's lab at Indiana University Bloomington. He received his Ph.D. in mechatronics engineering from Jeju National University, South Korea, in 2021. He has extensive experience in developing physical, chemical, and biosensing technologies for wearable, microfluidic, and POC applications. His research focuses on leveraging advanced micro- and nanofabrication techniques and functional materials to develop molecular diagnostic technologies for healthcare applications.

Tathagata Pal is a postdoctoral fellow in Prof. Weihua Guan's lab at Indiana University Bloomington. He holds a B.Sc. in physics (Hons.), an M.Sc. in biophysics, and an M.Tech. in nanotechnology from IIT Roorkee, as well as a Ph.D. in biomedical engineering from IIT Bombay. From 2024 to 2025, he served as a postdoctoral researcher in the Department of Bioengineering at the University of California, Riverside. His research spans CRISPR-based systems, molecular diagnostics, nanopore technologies, multimodal biosensing, and nanobiotechnology, with a focus on developing stable, field-deployable diagnostic platforms.

Dr. Feng Guo is a tenured associate professor in the Department of Intelligent Systems Engineering at Indiana University Bloomington. He received his Ph.D. in engineering science and mechanics from Penn State and completed postdoctoral training at Stanford. His research focuses on intelligent biomedical devices and sensors integrating microfluidics, acoustics, and AI for translational applications in brain disorders and cancer. He has published over 95 papers with more than 9,700 citations in leading journals and is the recipient of the NIH Director's New Innovator Award and multiple institutional honors.

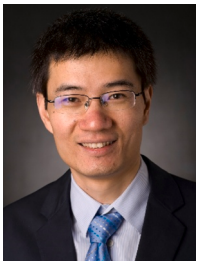

Prof. Weihua Guan is a full professor in the Department of Intelligent Systems Engineering at Indiana University Bloomington. He received his Ph.D. in electrical engineering from Yale University and completed postdoctoral training in biomedical engineering at Johns Hopkins University. His research integrates molecular POCT, nanopore technology, embedded systems, edge computing, and artificial intelligence to develop innovative biomedical sensors and diagnostic platforms. His work has been recognized with honors, including the HHMI International Research Fellowship and the NSF CAREER Award. He is a Senior Member of IEEE and actively serves the scientific community through journal and federal grant review.